Chemical Systematics and Hydrous Melting of the Mantle in Back-Arc Basins

C.H. Langmuir, A. Bézos, S. Escrig, and S.W. Parman[1]

Department of Earth and Planetary Sciences, Harvard University, Cambridge, Massachusetts, USA

This paper explores the chemical systematics of back-arc basins and the physical processes that give rise to them, making use of published data from the Scotia, Mariana, Lau, and Manus Basins. A new low-pressure fractionation model is used to back-correct data with greater than 5.5 wt.% MgO. Even after hydrous correction, back-arc basin basalts (BABB) have low TiO_2 and FeO contents relative to basalts from other ridges. The low TiO_2 both absolutely and relative to Na_2O requires a source depletion followed by a Na enrichment. This signature is critical to evaluate the range of mantle temperature at back-arc basins, which is about 100°C. In addition to a subduction component and wedge depletion, BABB reflect a prevalent enriched component akin to enriched ocean ridge basalts worldwide, despite the absence of mantle plumes. Data from the Mariana Basin suggest this component arises from very recent addition of low-degree (low-F) melts, which may be an important general agent of mantle heterogeneity. Important aspects of the back-arc data are the linear relationships among all major element parameters with each other and with water. Previous models involving isothermal, isobaric melting with increasing water contents do not account for these relationships. A constraint on permissible physical models is that both trace element and major element data show no inherited effects from garnet in back-arc basins, which constrains generation and transport of melts from great depth to the base of the melting regime. Quantitative modeling of the effects of water on mantle melting shows that previous conclusions based on the MELTS thermodynamic approach are not consistent with experimental data for the mantle. Our new models can account for the back-arc systematics by mixing between dry, pooled fractional melts, formed similarly to open ocean ridges, with hydrous melts generated from sources enriched in H_2O, Na_2O, and K_2O that have equilibrated at low pressure. Thus, successful physical models must be able to produce melts by these two different mechanisms. The effects of H_2O in back-arc basin ridges and open ocean ridges contrast markedly. In the open ocean, increased water is associated with lower mean extents of melting, increased TiO_2 contents, and an increased garnet effect. In back-arc basins, increased water is associated with increased extents of melting, lower TiO_2, and no garnet influence. These differ-

Back-Arc Spreading Systems: Geological, Biological, Chemical, and Physical Interactions
Geophysical Monograph Series 166

10.1029/166GM07

[1]Present address: Department of Earth Sciences, Durham University, Durham DH1 3LE, UK.

ences can be accounted for by contrasts in the melting regimes and tectonic setting of the two environments. In the open ocean, deep, low-degree, hydrous melts are produced in the "wings" of the melting regime and combine with higher degree drier melts produced at a range of shallower pressures. At back-arcs, geometrically and thermally, there is no room for "wings" on the arc side of back-arc spreading centers. On the arc side of the spreading center, where water is added, shallow hydrous melting is important, and melt must get to the surface in the context of descending mantle flow. On the back side, dry melting under relatively anhydrous conditions occurs, similar to open ocean ridges. Mixing between melts from the dry side and the wet side should then lead to the characteristic spectra of parental BABB compositions. Both the geometry of melting and the fact of continual rifting of young lithosphere may contribute to the very different water signatures in the open ocean and back-arc settings.

1. INTRODUCTION

Back-arc basins make up a small but significant fraction of the global ocean ridge system and provide a unique and important perspective on problems of igneous petrogenesis. This perspective arises from the fact that back-arc basin basalts contain moderate amounts of water—less than the more hydrous environment of arc volcanism, and more than the drier volcanism of open ocean ridges. Water has long been recognized as pivotal to arc petrogenesis (e.g., *Gill* [1981] and references therein; *Sisson and Grove,* [1993]; *Wallace* [2005]), but the quantitative understanding of melting at convergent margins is not yet mature. Water has also become increasingly recognized as a critical component in normal ocean ridge settings [*Michael and Chase*, 1987; *Hirth and Kohlstedt*, 1996; *Asimow and Langmuir*, 2003; *Cushman et al.*, 2004, and references therein], where the tectonic environment is simpler and quantitative models more developed—but the water contents are low and the effects often subtle. Back-arc basins are an intermediate case. The magmas are wet enough that the influence of water on various petrogenetic processes can be more clearly seen, and back-arc spreading centers have the relative simplicity of a ridge environment, unencumbered by the assimilation and contamination issues so prevalent in discussions of convergent margin volcanism (e.g., *Davidson* [1987]; *Hildreth and Moorbath* [1988]; *Davidson et al.* [1990]; *Chesley et al.* [2002]). Back-arc basins thus provide a useful window to a better understanding of both convergent margin and spreading center volcanism.

There are three principal aspects of the importance of water.

(1) Water profoundly influences the solidus temperature, and therefore the depth at which melting begins and the extent of melting for a given temperature and chemical composition of other elements (e.g., *Burnham and Davis* [1974]; *Hirth and Kohlstedt* [1996]; *Gaetani and Grove* [1998]; *Cushman et al.* [2004]).

(2) Water has an influence on the stability of igneous phases, and suppresses the appearance of plagioclase more than the ferro-magnesian minerals. This significantly influences the path of differentiation (e.g., *Green and Ringwood* [1967]; *Sinton and Fryer* [1987]; *Sisson and Grove* [1993]; *Danyushevsky* [2001]).

(3) Water correlates well with incompatible trace elements. Addition of water to an environment implies the addition of many other elements that accompany water, and hence water contents and source composition are inevitably coupled (e.g., *Schilling et al.* [1980]; *Stolper and Newman* [1994]; *Asimow et al.* [2004]).

These concomitant effects on source composition, melting depth, melting rate, and differentiation path, not to mention physical properties of magmas, make an understanding of hydrous processes central to igneous petrogenesis. Back-arc basins are an invaluable natural laboratory for study of these effects.

This paper explores these various aspects of the influence of water and how they are elucidated by study of back-arc basin magmas. Our approach is to look carefully at the data from back-arc basin basalts (BABB) and to interpret them in light of quantitative models for the effects of water on melting and differentiation. An important aspect of this comparison is the marked contrast between the influence of water on back-arc basin ridges and its influence on ridges far from convergent margins, originally pointed out by *Asimow and Langmuir* [2003].

This paper, which reflects work initially presented at the back-arc basin conference in May 2004, represents the third recent review of back-arc basins. *Taylor and Martinez* [2003]

summarized back-arc basin data, pointed out characteristic correlations between water and major and trace elements, and developed a model of progressive change in wedge composition. *Kelley et al.* [in press], in work developed largely independently and in parallel with the present paper, present similar data systematics but a rather different quantitative interpretation of back-arc data than is presented here. All these papers agree on several major conclusions: BABB differ from open ocean mid-ocean ridge basalts (MORB) in consistent ways; back-arc basins exist over a range of mantle temperatures (as pointed out by *Klein and Langmuir* [1987]); and back-arc basins show striking positive correlations between water contents and extent of melting, as first documented by *Stolper and Newman* [1994]. Both this paper and *Kelley et al.* [in press] emphasize the contrast in melting systematics between open ocean and back-arc ridges. The distinguishing contributions of this paper are (1) a data treatment that takes into account interlaboratory correction factors and fractionation normalization that takes into account the effects of water on phase appearance; (2) a reassessment of the effects of water on melting and the use of quantitative, hydrous melting models to evaluate back-arc data; (3) an emphasis on the constraints from Fe, Na, Ti, and the Dy/Yb ratios on back-arc melting models showing that the inherited effects of water are shallow and not deep.

Kelley et al. [in press], agreeing with the suggestion of *Hirschman et al.* [1999], call upon dF / dC_0^{H2O}, the change in extent of melting with increased water content, as a measure of mantle temperature. They suggest that at higher mantle temperatures, water has an augmented effect on the extent of melting. They also invoke deep melting at the hydrous solidus and compare their data with isobaric, isothermal melting models. The essence of their model and approach is that progressive addition of water to the same melting environment produces a range of extents of melting to produce an array of back-arc data. We suggest that dF / dC_0^{H2O} does not increase appreciably with temperature for temperatures above the dry solidus and show there is no inherited evidence for deep hydrous melts in the BABB data. We also suggest that mixing of two distinct melts, one relatively dry and the other hydrous, generated by distinct melting conditions, is at the root of back-arc basin systematics. These contrasts have important implications for the relationships between mantle flow and melting in the back-arc system.

1.1. Importance of Water on Normal Ocean Ridges

Water has the effect of increasing the extent of melting of mantle peridotite at any given temperature. The more water is added, the greater the extent of melting, up to the point of water saturation. For this reason, it had long been considered that mantle with relatively higher water contents would melt to greater extents than drier mantle. This intuition was supported by early studies of BABB that showed increasing extents of melting with increased water contents [*Stolper and Newman*, 1994].

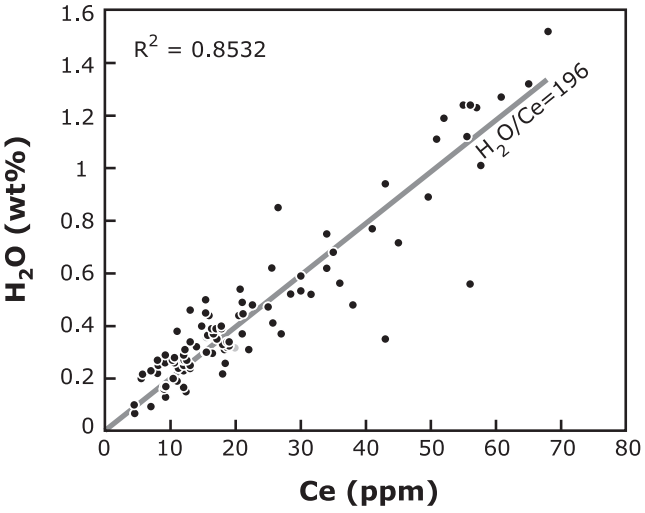

Figure 1. H_2O (wt.%) vs. Ce (ppm) measured in MORB glasses (data from www.petdb.org; Petdb is the Petrological Database of the Ocean Floor) show a relatively constant ratio over a large range of concentrations. Such behavior shows that both elements have the same bulk partition coefficient (D) and allows the D for water to be well-estimated from the abundant data on Ce partitioning.

Another long-standing assumption has been that in the presence of water, the first melt would appear at the water-saturated solidus (e.g., *Grove et al.* [2002]; *Gaetani and Grove* [2003], and references therein), an assumption that may be true in the water-rich setting of convergent margin volcanoes. In this case, the first appearance of melt is independent of the water content in the source, because no matter how little water may be present, that water would form a small amount of water-saturated melt.

Both of these conceptions of the effects of water were overturned in the relatively water-poor ocean ridge environment by the realization that water behaves during melting as a slightly incompatible element, with a finite partition coefficient in nominally anhydrous phases, such as olivine and clinopyroxene. This result was clear from the comparison of water to other incompatible elements. *Michael* [1988] showed that during mantle melting beneath ocean ridges, water had the same geochemical behavior as Ce (Figure 1) and therefore had the same bulk partition coefficient (D) of about 0.01. This result has been substantiated by many further measurements of water contents of MORB (e.g., *Danyushevsky* [2001]; *Dixon et al.* [2002]; *Simons et al.* [2002]), and also has been documented by experimental

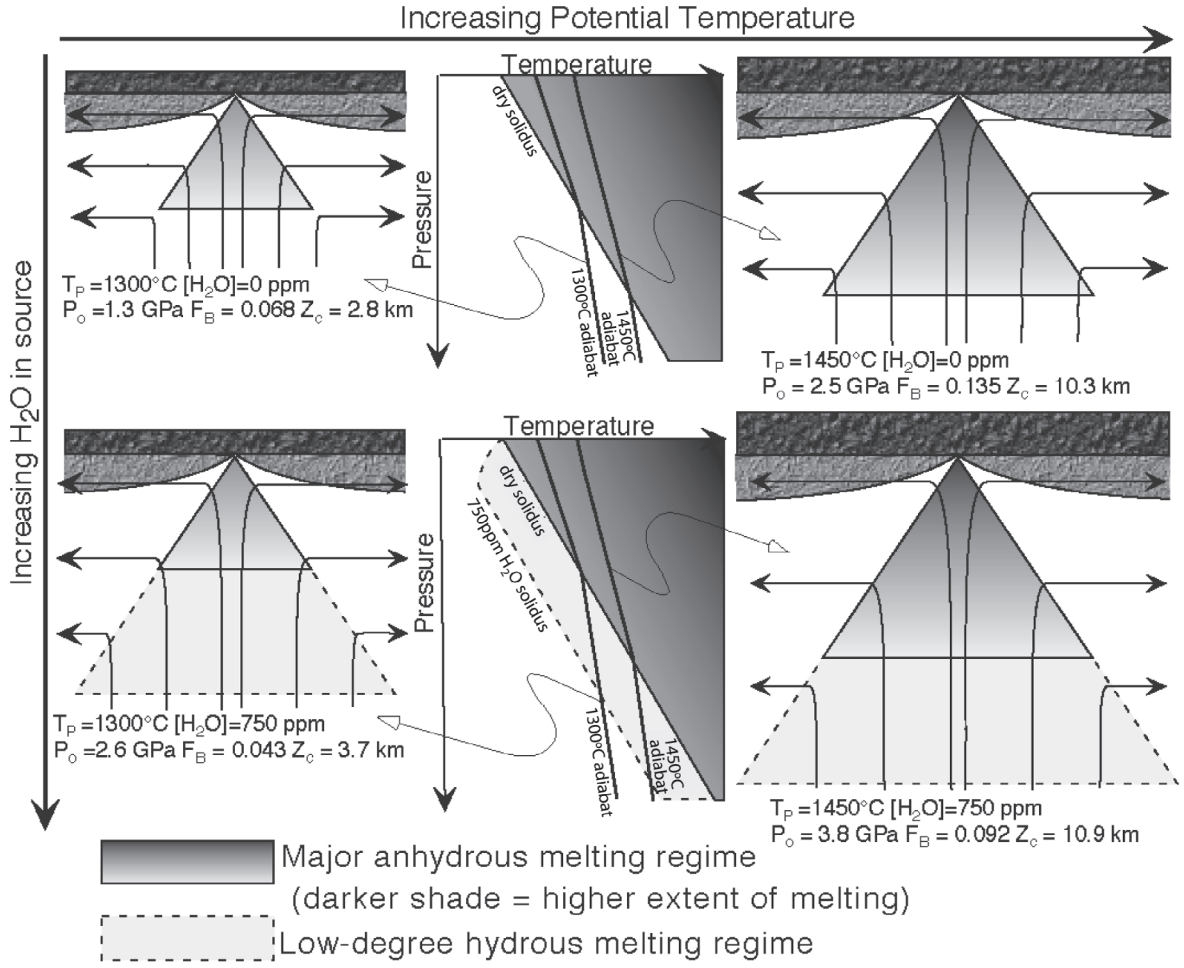

Figure 2. Conceptual models for the effect of various mantle adiabats and source H_2O concentration on mid-ocean-ridge melting regimes (after *Asimow and Langmuir* [2003]). T_p, potential mantle temperature in ˚C; [H_2O], water concentration in the source; P_0, initial pressure of melting; F_B, mean extent of melting [*Plank et al.*, 1995]; Z_c: crustal thickness. Beneath open ocean ridges, increased water leads to a deeper melting regime populated by a large quantity of low-degree melts at depth. This leads to greater crustal thickness and a lower mean extent of melting. This effect is the opposite of what is observed in back-arc basins.

studies of water solubility in nominally anhydrous minerals [*Bell and Rossman*, 1992] and mineral/melt experiments [*Aubaud et al.*, 2004]. During melting, the maximum enrichment of an element is 1/D, and therefore water contents of melts cannot be more than 100 times enriched relative to the source region. This limits the amount of water in the melt and precludes water saturation for most mantle compositions, as also inferred from solubility studies by *Hirth and Kohlsted* [1996]. For example, melt at 20 kb requires some 20% water to be saturated [*Dixon et al.*, 1995; *Mysen and Wheeler*, 2000; *Katz et al.*, 2003], which would not occur for source water contents of less than 2000 ppm, a very high level relative to the 116 ppm of depleted mantle [*Salters and Stracke*, 2004].

The finite D of water in nominally anhydrous phases has profound consequences for the effects of water beneath ocean ridges far from convergent margins. As long as the concentration of water is low enough that liquids are not water-saturated, increased water leads to deeper pressures of intersection of the solidus as mantle ascends beneath an ocean ridge [*Hirth and Kohlstedt*, 1996; *Asimow and Langmuir*, 2003]. For example, 100 ppm water in the source (1% water in the liquid) would lower solidus temperature by about 75°C, while 500 ppm water would lower temperature by 130°C. The effect of water on the solidus beneath a normal ocean ridge is illustrated in Figure 2.

Between the depth of initiation of melting and the dry solidus, the productivity of melting remains low (e.g., *Plank*

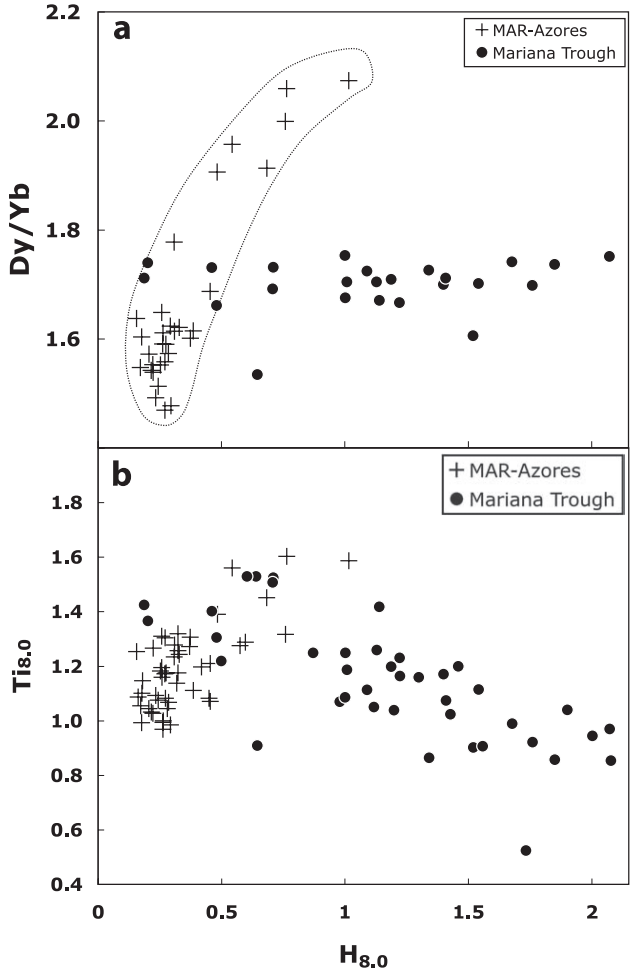

Figure 3. (a) Dy/Yb vs. $H_{8.0}$ for individual samples from the Mariana Trough and the Mid-Atlantic Ridge (MAR; 33˚N–40.5˚N) influenced by the Azores hotspot (MAR-Azores); $H_{8.0}$ is water contents corrected to a value of 8 wt.% MgO. (b) $Ti_{8.0}$ vs. $H_{8.0}$ for MAR 33˚N–40.5˚N samples and individual samples from the Mariana basin. Enrichment in H_2O on mid-oceanic ridge is correlated with the Dy/Yb ratio, caused by increasing contribution of melt from the garnet peridotite stability field (deep low-degree hydrous melting regime [*Asimow and Langmuir*, 2003]). H_2O and TiO_2 are incompatible elements, yet both show orthogonal trends between MAR-Azores and Mariana Trough samples. The water-rich source leads to high $Ti_{8.0}$ in MORBs but is associated with low $Ti_{8.0}$ for the Mariana back-arc samples.

and Langmuir [1992] and references therein). The size of this region increases as water increases in the source, and the volume of mantle undergoing low degree melting increases as water content increases. The increased volume of low degree melt leads to a lower average degree of melting for the entire melting regime for high water contents relative to dry conditions.

These effects then lead to very different results than would be inferred from the earlier assumptions of a water-saturated solidus, of no effect of water contents on the pressure of intersection of the solidus, and of greater extents of melting for higher water contents. Instead, for a normal melting regime beneath an ocean ridge, the pressure of intersection of the solidus depends on water content, and the average extent of melting decreases with increasing water, even as the total volume of melt produced and maximum extent of melting at the top of the melting regime increase.

Another melting parameter that is critically dependent on pressure of melting is the "garnet signature." Garnet is a high-pressure mantle phase, and the increased pressure of melting associated with increased water contents are reflected in an increased garnet influence. Because garnet retains the heavy rare earth elements (HREE), the garnet effect is most clearly represented by either the Dy/Yb or Lu/Hf ratio.

Asimow and Langmuir [2003] illustrated these various effects for normal ocean ridges around the Azores platform, where water contents increase progressively as the Azores are approached (Figure 3). Water contents correlate positively with Ti contents and there are substantial changes in Dy/Yb (and Lu/Hf) with increased water. These characteristics are present around the Galapagos hot spot as well [*Asimow and Langmuir*, 2003; *Cushman et al.*, 2004]. *Cushman et al.* [2004] raise the additional possibility that increased water can lower the viscosity sufficiently that there is active mantle flow in the deep, hydrous part of the melting regime, leading to further augmentation of these effects.

The highest water contents along open ocean ridges occur for ridge segments that are influenced by hot spots, such as the mid-Atlantic Ridge near the Azores [*Schilling*, 1975; *Asimow et al.*, 2004] and the central portions of the Galapagos spreading center [*Schilling et al.*, 1982; *Cushman et al.*, 2004], and it is in these large regions that these effects of water on ridges have been well documented.

1.2. Importance of Water at Back-Arc Basins

Stolper and Newman [1994], in an influential study of basalts from the Mariana back-arc basin, showed a negative correlation between TiO_2 and H_2O (see Figure 3b), from which they inferred a positive correlation between source water content C_0^{H2O} and extent of melting (F) (Figure 4)—the opposite of what has more recently been found on open ocean ridges [*Asimow and Langmuir*, 2003; *Cushman et al.*, 2004; *Kelley et al.*, in press]. The contrasting behavior of water extends to the "garnet influence" as well. As apparent in Figure 3a, there is no

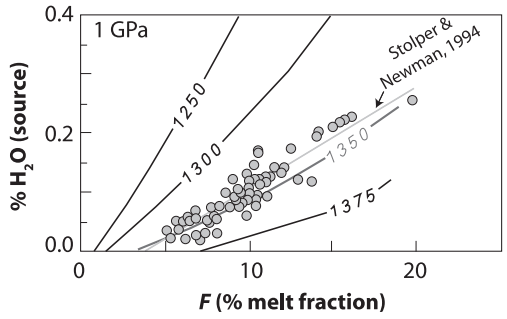

Figure 4. Calculated water contents in the source vs. melt fraction for the Mariana back-arc basin [*Stolper and Newman*, 1994] compared with the MELTS calculation of isobaric and isothermal melting at 1250ºC, 1300ºC, 1350ºC, and 1375ºC. Note the substantial change in slope with increasing temperature in the MELTS calculations. This figure has been modified from Figure 7 of *Hirschmann et al.* [1999].

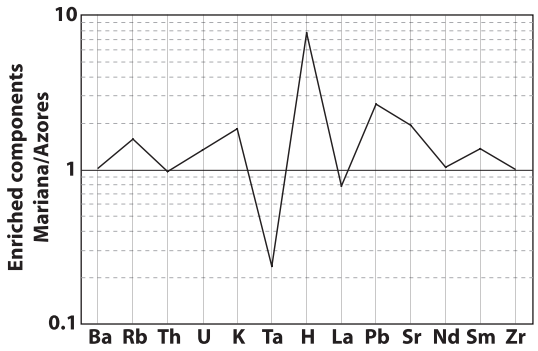

Figure 5. Comparison of the compositions of the hydrous "ocean island basalt (OIB) component" as determined for the Azores [*Asimow et al.*, 2004] and the hydrous "back-arc component" estimated for the Mariana Trough [*Stolper and Newman*, 1994]. Both components are normalized to Zr for comparison purposes. The differences between end member arc and OIB components are probably greater than evident from this figure, because Mariana data contain OIB and arc contributions (see discussion in text, and *Pearce and Stern*, this volume).

increased Dy/Yb ratio with increasing water in the back-arc environment. Since Ti reflects extent of melting, and Dy/Yb reflects the presence of garnet, which is a proxy for the depth of melting, in back-arc basins water appears to increase the extent of melting while having no effect on the depths of melting.

Stolper and Newman [1994] also made use of a spectrum of trace elements in Mariana basalts to estimate the composition of the hydrous component added in this region. While their calculation is model dependent and determines element ratios rather than absolute amounts, the general characteristics are robust and can be compared with the open ocean hydrous component, or "ocean island basalt (OIB) component", as determined for the Azores [*Asimow et al.*, 2004]. The relative compositions of these components are presented in Figure 5. Ratios of water to all other elements are elevated in the Mariana component, and there is relative depletion in Ta (and presumably Nb, which was not determined by *Stolper and Newman* [1994]). Because *Stolper and Newman* [1994] treat TiO_2 as absent from their fluid, the ratio of Ti in the two fluids would be zero, which cannot be shown in the log diagram. In contrast, the OIB-component is an enriching agent for TiO_2.

As we discuss below, it is also possible to have the "OIB component" of water and trace element enrichment present in back-arc basins, and indeed, *Pearce et al.* [2005, and this volume] have noted the presence of such a component in several back-arc basins (for data sources, see the Appendix), and an OIB-like component has been recognized by *Danyushevsky et al.* [1993] and in all papers written on the Scotia basin [*Leat et al.*, 2000; *Fretzdorff et al.*, 2002], and in the Manus Basin [*Sinton et al.*, 2003]. The presence of two distinct water-rich components with contrasting trace element characteristics is one of the challenges to be faced in understanding the role of water in the back-arc setting.

1.3. Testing Hypotheses for the Origin of Back-Arc Basin Basalt Systematics

A central motivation behind this paper is to understand this marked contrast in the apparent influence of water on melting in back-arc basins and along open ocean ridges in the vicinity of hot spots, and to understand the relative roles of the two distinct hydrous components. *Both back-arc and hot spot sources are enriched in water relative to depleted mantle, and the predominant effect on melting in the two environments appears not only to differ, but to be opposite in sign*. This contrast is a profound and fundamental difference between the two tectonic settings, and needs to be well understood in order to obtain a qualitative and quantitative understanding of the differences between two of the major igneous domains of our planet.

The current hypothesis for the origin of the back-arc basin systematics stems from the treatment of *Stolper and Newman* [1994], who were able to successfully account for the data by having different extents of melting of a source with homogeneous TiO_2 contents. The observed negative correlation between TiO_2 and H_2O in the samples (Figure 3b) could then be used to estimate the amount of melting associated with increased water. The melting effects were summarized in a plot of F (the extent of melting) vs. C_0^{H2O} and favorably compared to isobaric, isothermal models of melting with progressively increasing water contents (see Figure 4).

A further aspect of this hypothesis is the suggestion that the effects of water on melting of the mantle have a quasi-linear relationship for a single temperature, and that the

slope of this relationship is temperature dependent, such that the same amount of water leads to greater extents of melting at higher temperatures than at lower temperatures (see Figure 4). In this case, the slope of a data array of F vs. C_0^{H2O}, dF / dC_0^{H2O}, gives temperature information about the mantle source. Such a result could have wide applicability to determination of the temperature structure of the mantle wedge. These aspects are derived from and supported by MELTS modeling [Hirschmann *et al.*, 1999], experimental data [*Hirose and Kushiro*, 1993; *Gaetani and Grove*, 2003] and observations [*Kelley et al.*, in press].

An important and puzzling feature of this hypothesis is that the comparison to MELTS and experiments has been based on isobaric, isothermal data and calculations, even though melt generation beneath spreading centers is understood to be a polybaric process. A first question, then, is whether such a polybaric process can effectively give rise to melt properties that are indistinguishable from the isobaric, isothermal model. Or, perhaps the melt generation process at back-arc basin spreading centers differs fundamentally from that at open ocean ridges. For example, diapiric uprise with complete melt retention would lead to results that were not distinguishable from an isothermal, isobaric model.

There is also an alternative hypothesis, explored in this paper, that the linear arrays of TiO_2 vs. H_2O shown for the Marianas by *Stolper and Newman* [1994] and for other back-arc basins by *Taylor and Martinez* [2003], *Kelley et al.* [in press], and this paper, are mixing arrays between more and less hydrous melts, rather than a continuous series of melts generated by progressively increasing amounts of water in the source. The similarity of the driest back-arc magmas to mid-ocean ridge basalts from the open ocean suggests to us as well as to *Kelley et al.* [in press] the same polybaric, fractional melting process that successfully accounts for these data globally. This suggests an important role for a normal ocean ridge melting regime, with the modification that the underlying slab thermal structure may influence the deepest portions of the melting regime in some cases. Mixing of these melts with a hydrous, subduction-influenced melt could then give rise to the back-arc arrays.

To explore this diversity of issues requires that we address a broad range of subjects. These include:

(1) the role of source heterogeneity in creating back-arc basin systematics;
(2) whether isobaric, isothermal melting produces linear arrays on plots of TiO_2 vs. H_2O;
(3) the effect of temperature on wet melting parameters such as the change in extent of melting with increased water contents, dF / dC_0^{H2O}, in compositions appropriate to the upper mantle;
(4) the apparent pressure requirements of the hydrous melt;
(5) the placement of back-arc data into the geodynamic context of mantle flow and upwelling beneath back-arc spreading centers.

These issues can all be furthered by careful comparison of the back-arc data to quantitative melting models.

2. ANATOMY OF THE EXTENT OF MELTING VS. WATER IN THE SOURCE DIAGRAM

Much of the recent discussion of back-arc data and its comparison to experimental and modeling results has made use of the extent of melting vs. water in the source diagram (Figure 4). The change in extent of melting with water content cannot be directly determined from geochemical data, because F and C_0^{H2O} are not parameters that can be measured. This diagram, therefore, is calculated from the data using assumptions about element partitioning and mantle source. It is useful to understand better how the real data are transformed to the calculated F vs. C_0^{H2O} diagram, and the extent to which model-dependent assumptions influence the transformation. This understanding then can help to guide data presentation and interpretation.

2.1. Algebraic Transformation From the Data to the C_0^{H2O} vs. F Diagram

The extent of melting, F, is determined from the elements that are presumed to be conservative and are not added to the source along with water. The high-field-strength elements (HFSE) Ti, Zr Y, Hf, and Nb are believed to be insoluble in fluids (e.g., *Pearce and Parkinson* [1993]) and therefore reflect the initial source composition and extent of melting. If the partition coefficients and source concentrations are known for these elements, F can be determined from a melting equation. In the simplest case, this is the batch melting equation:

$$C_l = \frac{C_0}{(D\ *(1-F)+F)} \tag{1}$$

where C_l and C_0 are the concentrations in the source and the liquid, and D is the partition coefficient, C_s/C_l. Then, for any parental magma, F can be calculated from

$$F = \frac{C_0 - D*C_l}{C_l - D*C_l} \tag{2}$$

For the incompatible elements such as H_2O with very small D, equation (2) can be simplified to:

$$F = \frac{C_0^{H2O}}{C_l^{H2O}} \quad \Leftrightarrow \quad C_0^{H2O} = F * C_l^{H2O} \tag{3}$$

as long as F >> D. C_l^{H2O} is a measured quantity. The value of F can be estimated from equation (2) by using the conservative elements for known D and C_o. For a highly incompatible element, such as Nb or Ta, the equivalent of equation (3) can be used to estimate F.

$$F = \frac{C_0^{Nb}}{C_l^{Nb}} \tag{4}$$

Substituting (4) into (3),

$$C_0^{H2O} = C_l^{H2O} * \frac{C_0^{Nb}}{C_l^{Nb}} \tag{5}$$

In principle, any one of the conservative elements could be used to calculate F and C_0^{H2O} using equations (2) and (3). These simple relationships then show that for low-D elements the F vs. C_0^{H2O} diagram is A/X vs. A*Y/X, where the constant A is the assumed source concentration of the conservative element, and X and Y are the concentrations of the conservative element and of H_2O, respectively, in the liquid.

Stolper and Newman [1994] showed that the Marianas data have a linear negative correlation between C_l^{Ti} and C_l^{H2O}, and other back-arc basins have a rough negative correlation as well [*Taylor and Martinez*, 2003; *Kelley et al.*, in press]:

$$C_l^{H2O} = m * C_l^{TiO2} + b \tag{6}$$

Combining (6) with (5) for TiO_2 gives:

$$C_0^{H2O} = (m * C_l^{TiO2} + b) * \frac{C_0^{TiO2}}{C_l^{TiO2}} \tag{7}$$

The axes of the F vs. C_0^{H2O} diagram then become

$$\frac{C_0^{TiO2}}{C_l^{TiO2}} \text{ and } m * C_o^{TiO2} + b * \frac{C_0^{TiO2}}{C_l^{TiO2}},$$

the C_l^{TiO2} on both axes being accompanied by different arrangements of constants.

Provided the linear relationship between $C_l^{TiO2}$and C_l^{H2O} holds for a given back-arc basin, then there is simple transformation from the C_l^{TiO2} vs. C_l^{H2O} to the F vs. C_0^{H2O} diagram with the model-dependent assumption of C_0^{TiO2}. The C_l^{TiO2} vs. C_l^{H2O} diagram, which plots the real data, thus has the same information as the C_0^{H2O} vs. F plot, absent the assumption of source.

For TiO_2, D may not be low enough to be neglected. Then the combination of the equations (2), (3), and (6) lead to an expression for the water content in the source as

$$C_0^{H2O} = (m * C_l^{TiO2} + b) * \frac{C_0^{TiO2} - D^{TiO2} * C_l^{TiO2}}{C_l^{TiO2} - D^{TiO2} * C_l^{TiO2}} \tag{8}$$

The slope on the F vs. C_0^{H2O} diagram can be shown to be:

$$(dF / dC_0^{H2O}) = \frac{C_0^{TiO2}}{b * C_0^{TiO2} + m * D^{TiO2} * C_{l2}^{TiO2} * C_{l1}^{TiO2}} \tag{9}$$

Note that when D is small, dF / dC_0^{H2O} = 1/b, that is, the inverse of the intercept of the water axis on the C_l^{TiO2} vs. C_l^{H2O} diagram; for a consistent set of data this intercept should be the same for all incompatible conservative elements plotted with respect to C_l^{H2O}. This is a useful rule of thumb and simple visual hypothesis test.

For the dry system where $C_0^{H2O} = 0$ in the source, then $C_l^{TiO2} = -\frac{b}{m}$ and the extent of melting F_{dry} is

$$F_{dry} = \frac{\frac{-m * C_0^{TiO2}}{b} - D^{TiO2}}{\left(1 - D^{TiO2}\right)} \tag{10}$$

where m and b are the slope and intercept from the C_l^{TiO2} vs. C_l^{H2O} diagram. The only variable in equations (9) and (10) is C_l^{Ti}. Values for Ds and source concentrations are estimated quantities.

Figure 6 shows how dF / dC_0^{H2O} and the F-intercept (F_{dry}) vary with changes in D^{TiO2} and C_0^{TiO2} for m and b from the Mariana data set. It shows how dF / dC_0^{H2O} is sensitive to the values of D^{TiO2} and can increase by 30% over the range of Ds from various experimental data (0.01 – 0.1). For constant D^{TiO2}, dF / dC_0^{H2O} varies by up to 20% with source concentration. The F-intercept is also dependent on both source and D^{TiO2}. Note in Figure 6b that when D is not equal to zero, the C_0^{H2O} vs. F diagram is not a linear transformation of the $C_l^{Ti} - C_l^{H2O}$ data. The curvature is minor, however, for the concentration ranges observed in back-arc basins, and within the error of the analytical data the nonlinearity would not be resolved.

The point of this algebraic exercise is to emphasize the derivative nature of the F vs. C_0^{H2O} diagram, and that the real information behind this diagram is contained in the

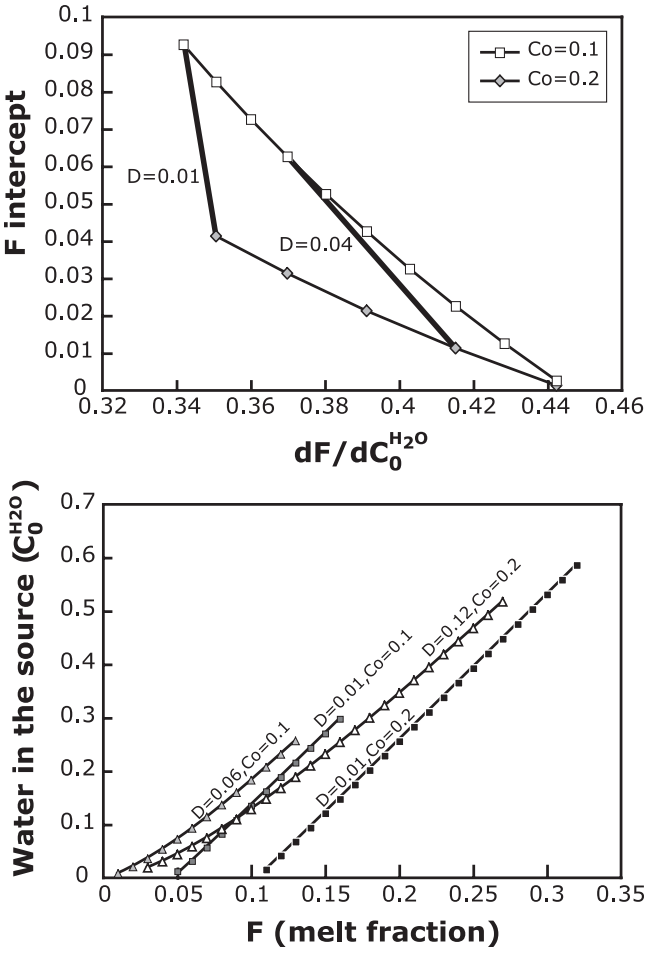

Figure 6. Effects of variations in source concentration and partition coefficient on the transformation from TiO_2 vs. H_2O plots to the F-source water content diagram. Both F and the calculated productivity are influenced by the D that is assumed for TiO_2. The calculated melt fraction is very sensitive to the assumed source content for TiO_2.

C_l^{TiO2} vs. C_l^{H2O} diagram. For any incompatible element X that is not carried in the fluid, the slope on the F vs. C_0^{H2O} diagram is simply the H_2O intercept on the C_l^X vs. C_l^{H2O} diagram, provided D^X / C_0^X is small. When D^X is small, the F-intercept on the F vs. C_0^{H2O} diagram is the ratio of slope and intercept on the C_l^X vs. C_l^{H2O} diagram times the assumed source concentration of X. The importance of this discussion is that all the information we need to investigate the melting systematics can come from plots of the real data (corrected for differentiation), avoiding some of the pitfalls in the transformation from C_l^{TiO2} vs. C_l^{H2O} to F vs. C_0^{H2O}.

2.2. Tests of the Melting Hypothesis for C_l^{TiO2} vs. C_l^{H2O} and F vs. C_0^{H2O} Diagrams

The unstated assumption in this entire approach is that the correlations between TiO_2 and H_2O are produced by different extents of melting of a common source, caused by changes in source water content. This is not necessarily the case. It is not evident a priori that addition of water to a source will produce such a linear relationship. And, there could be differences in the TiO_2 content of the source. For example, the water-rich and water-poor end members could be produced by the same extent of melting of sources that vary in TiO_2. Therefore we need to test the particular melting hypothesis that lies at the root of the calculation and interpretation of the F vs. C_0^{H2O} diagram.

Several tests are possible. The first question is, Does hydrous melting produce linear arrays on the TiO_2–H_2O diagram? Other tests can be applied when data from multiple back-arc basins are considered. Both slope and intercept on the F vs. C_0^{H2O} diagram may be related to temperature for simple melting models. The *x*-intercept F_{dry} is interpreted as the extent of melting that occurs in the absence of water, which would increase with increasing mantle temperature. The slope, dF / dC_0^{H2O}, has been suggested to be sensitive to temperature as discussed above. To be consistent, the slope should increase as the intercept increases, a conclusion reached by *Kelley et al.* [in press] And, since the calculation of the Mariana source component assumes a common background source for all elements, all plots of incompatible conservative elements vs. water should form linear arrays with the same water intercept for each back-arc basin.

Armed with understanding, tests, and questions, we now turn to the data.

3. GENERAL CHARACTERISTICS OF BACK-ARC BASIN BASALTS

Back-arc basin ridges extend over 3000 km of ridge length and encompass a substantial fraction of the global range of depth and spreading rate. Basalts from back-arc basins (BABB) have long been recognized to differ in subtle characteristics from basalts from open ocean ridges. *Sinton and Fryer* [1987] identified the generally low FeO and high Al_2O_3 contents of BABB, based on data from the Mariana back-arc basin, and suggested the important contributing role of water. *Gill* [1976], in an early study of the Lau Basin, predicted high water contents for BABB, which was subsequently confirmed [*Garcia et al.*, 1979; *Muenow et al.*, 1980]. Many others have identified key aspects of BABB (e.g., *Wood et al.*

[1982]; *Frenzel et al.* [1990]; *Hawkins et al.* [1990]; *Volpe et al.* [1990]; *Martinez and Taylor* [2003]). *Klein and Langmuir* [1987] confirmed the low FeO contents of BABB, noting that although back-arc basins plot on the global correlations of $Na_{8.0}$ (Na_2O corrected for differentiation to 8 wt.% MgO) and axial depth for global ridges, they have low FeO contents for a given Na content.

With the larger data set that is now available, it is possible to present large numbers of BABB from around the world and investigate for a large range of elements the differences between these sources and normal ridges. Figure 7 shows maps for the four major back-arc basins investigated in this paper. For more details concerning each basin and the available data sets, see the Appendix. Figure 8 presents

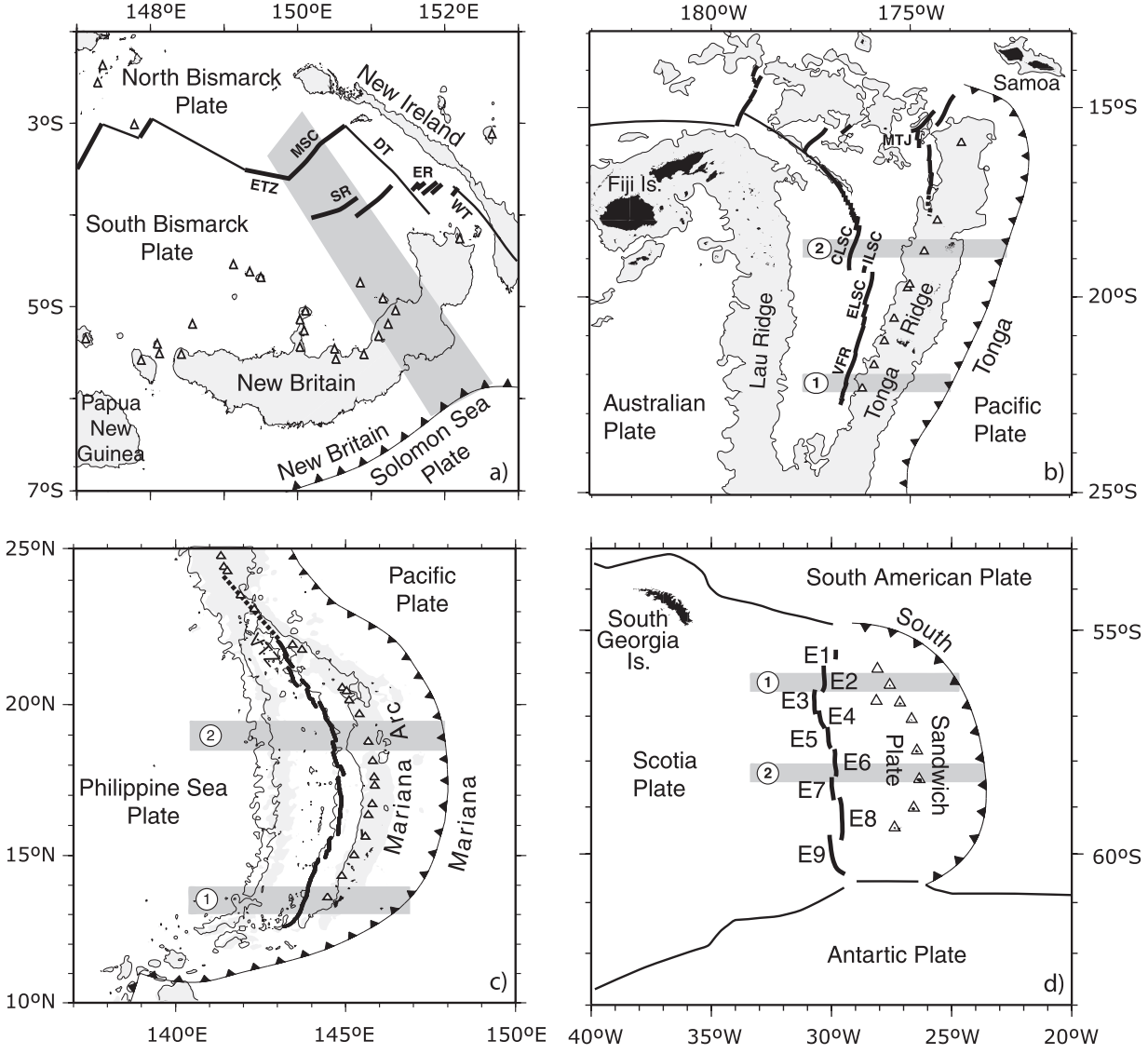

Figure 7. Back-arc basin structural maps (after *Taylor and Martinez* [2003]). Thick lines are spreading centers; dashed lines are rifts; thin lines are transform faults; open triangles are arc volcanoes; lines with filled triangles are trenches. (a) Manus basin: ETZ, extensional transform fault; MSC, Manus spreading center; SR, Southern Rift; ER, Eastern Rift; WT, Weitin Transform; DT, Djaul Transform. (b) Lau Basin: VFR, Valu Fa Ridge; ELSC, Eastern Lau spreading center; ILSC, Intermediate Lau spreading center; CLSC, Central Lau spreading center; MTJ, Mangatolu triple junction. (c) Mariana Trough: VTZ, Volcano Tectonic Zone. (d) East Scotia basin: E1 through E9, segment numbering [*Fretzdorff et al.*, 2002]. Shaded areas are locations of the cross-sections of the distribution of the earthquakes shown in Figure 46.

the distribution of chemical compositions of BABB and compares them with basalts from open ocean ridges and the Mariana arc. The BABB have slightly higher SiO_2, higher Al_2O_3, and lower FeO and TiO_2. These latter characteristics are particularly significant because BABB also have slightly lower average MgO, and FeO and TiO_2 increase and Al_2O_3 decreases with decreasing MgO. Therefore BABB have a distinctive major element signature, a characteristic that should be useful to classify the tectonic environment of ophiolites and other ancient rock suites of uncertain provenance.

To fully investigate the petrogenesis of back-arc basins, an understanding of the systematics of the data and the specifics of the tectonic settings for the different back-arc basins is necessary. In the following sections we explain our approach to correct for shallow level fractionation in this setting, and present and discuss the data from the four major back-arc basins, all of which at this point have significant, albeit still incomplete data sets on numerous samples.

4. DATA TREATMENT

To approach the processes occurring during melting and melt transport in the mantle, it is necessary first to adequately correct for the effects of low-pressure fractionation. For back-arc basins these corrections are particularly important and problematic. Previous work on back-arc basins has also made attempts to back-correct to more primitive compositions. *Stolper and Newman* [1994] adjusted compositions back to equilibrium with Fo_{90} by adding olivine. *Kelley et al.* [in press], in the revised version of their paper, first correct to 8 wt.% MgO, using the constant slope expressions from *Klein and Langmuir* [1987] ($Fe_{8.0}$, $Na_{8.0}$) and *Taylor and Martinez* [2003] ($Ti_{8.0}$ $H_{8.0}$), then correct to MgO of 8.5 wt.% for olivine and plagioclase fractionation, and finally correct the data to a primitive composition by adding olivine until the liquid is in equilibrium with Fo_{90}. Neither of these methods takes into account the important effect of water on the liquid line of descent.

Water suppresses the appearance of plagioclase relative to ferro-magnesian phases (see *Green and Ringwood* [1967]; *Sinton and Fryer* [1987]; *Sisson and Grove* [1993]; *Danyushevsky* [2001]). *Asimow and Langmuir* [2003] showed through quantitative liquid line of descent calculations that plagioclase suppression leads to artificially low $Fe_{8.0}$ and $Ti_{8.0}$ and high Al_2O_3. This effect is important in the interpretation of back-arc data for two reasons. First, as pointed out above, low FeO and TiO_2 and high Al_2O_3 are the characteristic signature of BABB. Is this a characteristic of parental magmas, or a consequence of hydrous fractionation? Second, *Stolper and Newman* [1994] evaluated hydrous melting using the negative correlation between TiO_2 and H_2O. Are the low TiO_2 contents characteristics of parental

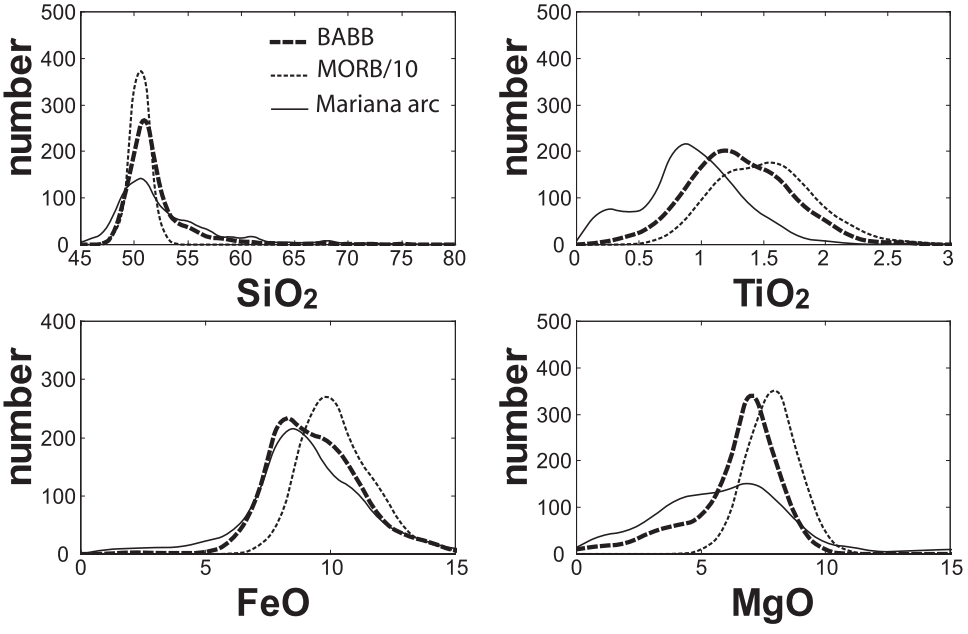

Figure 8. Distribution of the chemical composition for global MORB and BABB data set (from www.petdb.org) compared with the Mariana arc (data from GEOROC: http://www.mpch-mainz.gwdg.de/georoc/). These are raw data from glass and whole rock.

magmas, or artifacts of fractionation correction that does not take water into account?

These questions can be evaluated confidently only by fractionation correction that takes into account the effects of water.

4.1. Data Compilation

Our compilation includes about 850 BABB samples with geochemical and petrological analyses available on the online Petdb database (www.petdb.org). Most of the analyses come from the papers cited in the Appendix. Additional unpublished water analyses were provided by S. Newman (East Scotia). To obtain the most reliable and coherent BABB dataset, analyses performed on fresh glassy material were used when available. When there were no glass data, whole rock data were used. Only H_2O data collected on glasses were used.

To compare data from such a diversity of sources requires attention to problems of interlaboratory bias. Different laboratories use different analytical methods and different standards, which often leads to significant and systematic analytical offset [*Langmuir et al.*, 1992; *Su*, 2002; *Bezos and Humler*, 2005]. More than 90% of the major element data compiled in this study comes from the following laboratories: the Smithsonian Institution of Washington, electron microprobe (EMP) analyses performed by William Melson to produce the "Smithsonian Volcanic glass file"; The University of Hawaii, x-ray florescence (XRF) and electron microprobe (EMP) [*Sinton and Fryer*, 1987; *Sinton et al.*, 2003]; The University of Tasmania, EMP data [*Danyushevsky et al.*, 1993], and The University of Newcastle-Upon-Tyne, atomic absorption spectrometry [*Pearce et al.*, 1995]. The corrections factors determined by *Su* [2002] between these laboratories and the Lamont Doherty Laboratory EMP have been used to correct each individual major element analyses (Table 1). EMP Data from *Fretzdorff et al.* [2002] on East Scotia basin basalts did not need corrections since they were collected using the Lamont Doherty EMP glass standard JDF-D2. Previous studies [*Stolper and Newman*, 1994; *Taylor and Martinez*, 2003; *Kelley et al.*, in press] did not take interlaboratory differences into account.

4.2. Data Selection

Because the aim is to investigate mantle sources and processes, not all data that are available are suitable. Almost all major element analyses come from glasses, but whole-rock trace elements were included. We excluded a few whole rocks with clear evidence of phenocryst accumulation and did not use data for samples with less than 5.5 wt.% MgO. For comparison, *Taylor and Martinez* [2003] used samples with MgO between 6.0 and 8.5 wt.% (in some instances down to 5 wt.% for shallow ridges) and *Kelley et al.* [in press] used MgO > 7 wt.% for all basins except the Manus Basin, where they used samples with MgO > 6.25 wt.%.

Magmatic degassing occurs when the combined abundances of all volatiles in the melt exceed their solubility in the melt defined at a given temperature and pressure [*Dixon et al.*, 1995]. This is best evaluated when both CO_2 and H_2O data are available. Unfortunately, the present compiled data set does not allow a systematic study of the major volatile species to evaluate magmatic degassing. Following *Dixon et al.* [2002], we have calculated the saturation pressure curve at 1150˚C for H_2O using the *Newman and Lowenstern* [2002] VOLATILECALC model (Figure 9) and evaluated the measured water content and the pressure of collection for each sample. All samples that lie to the right of this curve are saturated with respect to H_2O, and their water data were excluded from the dataset. VOLATILECALC calculations account for the strong positive control of SiO_2 on molecular water solubility. We use a curve for 49 wt.% SiO_2, which is lower than almost all BABB data. Higher silica contents

TABLE 1. Correction factors determined from the global PetDB data base by *Su* [2002] on the basis of the same samples analyzed in different laboratories.

Method	Institution	SiO_2	TiO_2	Al_2O_3	FeOt	MgO	CaO	Na_2O
EMP	SMITHSONIAN	0.991	0.960	1.010	0.975	1.080	1.000	1.000
EMP	UNIV. OF HAWAII	0.989	0.967	1.015	0.963	1.089	1.015	1.015
EMP	UNIV. OF TASMANIA	0.983	1.000	1.002	1.022	1.075	0.998	1.048
XRF	UNIV. OF HAWAII	0.987	0.964	1.003	1.017	1.045	1.010	1.045
AAS	UNIV. NEWCASTLE-UPON-TYNE	0.988	0.964	0.998	1.023	1.033	1.014	1.025

Data from each laboratory is multiplied by the correction factor to become consistent with Lamont and Harvard data normalized to probe standards JDFD2 or VE32.

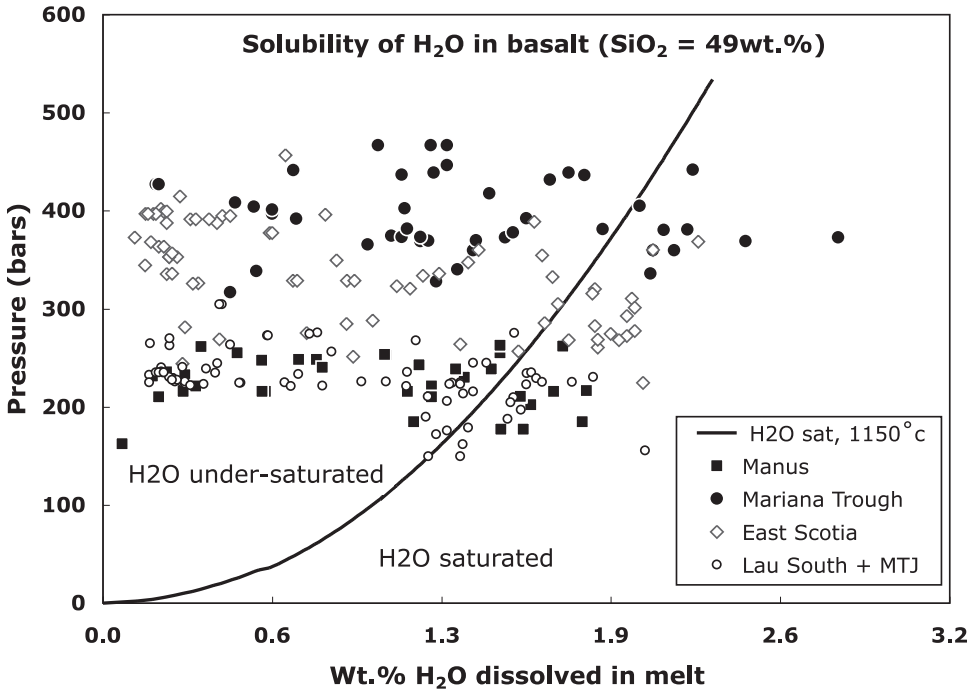

Figure 9. H_2O content vs. pressures of recovery for glass samples. Solid line: H_2O-saturated line for basaltic melts (after *Newman and Lowenstern* [2002]). All samples lying below the curve were supersaturated with gas at the depth where they were recovered, and hence were excluded from the data set due to H_2O-saturation.

lead to higher solubility, so the use of 49 wt.% SiO_2 is conservative. *Kelley et al.* [in press] use a similar screen for their data set.

4.3. Correction for Hydrous Fractionation

To approach the processes occurring during melting and melt transport in the mantle, it is necessary first to adequately correct for the effect of low-pressure fractionation. The data normalization to 8 wt.% MgO, using the constant slopes from *Klein and Langmuir* [1987], is problematic for FeO and TiO_2 in back-arc basins because water has a marked effect on the relative appearance of solidifying phases (e.g., *Sisson and Grove* [1993]; *Danyushevsky* [2001]). Indeed, the suppression of plagioclase crystallization relative to olivine and clinopyroxene in the presence of water, leads, for a given MgO content, to higher Al_2O_3 and lower TiO_2 and FeO content compared with anhydrous crystallization. This has been well known from previous work (e.g., *Michael and Chase* [1987]; *Sinton and Fryer* [1987]; *Danyushevsky* [2001]; *Asimow and Langmuir* [2003]). Hydrous BABB data, therefore, need a correction procedure that takes into account the effects of wet differentiation, a distinguishing aspect of our approach to this problem compared to previous work [*Stolper and Newman*, 1994; *Taylor and Martinez*, 2003; *Kelley et al.*, in press].

As pointed out by *Asimow and Langmuir* [2003], if the effects of water on fractionation are not taken into account, calculated values of $Fe_{8.0}$ and $Ti_{8.0}$ are far too low. Figure 10 illustrates this effect, using calculations from our hydrous fractionation program. As shown in Figure 10a, 1 wt.% H_2O in the primitive liquid can delay the appearance of plagioclase by 1 wt.% MgO. If this delay in plagioclase appearance relative to olivine is not taken into account, the calculated $Fe_{8.0}$ content of a sample with 6 wt.% MgO and 1.0 wt.% H_2O can lead to $Fe_{8.0}$ that is lower than the true value by 1.5 wt.% (Figure 10b). This is a minimum effect. If a constant slope correction were used, the differences would be 2.5% change in $Fe_{8.0}$. The effect also applies to $Ti_{8.0}$ and incompatible elements and generates significant errors compared to the compositional range observed in back-arc basin. This can lead to spurious conclusions concerning pressures and extents of melting or the Fe/Mg ratio and TiO_2 contents of the mantle source. In this paper, $Fe_{8.0}$ and $Ti_{8.0}$ values are corrected by specifically taking into account the effects of water on the liquid line of descent (LLD) and therefore should be much closer to actual parental values.

Fractionation correction for hydrous samples is an imperfect art, in part because for most samples water contents are not available. Our approach to fractionation correction takes

into account both the slope variations with melt composition and the MgO at which plagioclase starts to crystallize. For this purpose, olivine, plagioclase, and clinopyroxene partition coefficients have been calibrated with a recent compilation of anhydrous and hydrous experiments ranging from MORB to BABB-like compositions This new set of partition coefficients is used in combination with the mineral-melt equilibrium model of *Weaver and Langmuir* [1990] to generate theoretical LLDs for BABB compositions with an updated version of the BASALT code, "hBasalt" [*Bezos et al.*, in prep.]. For each basin, the data set has been separated into individual spreading segments, with each segment treated as an independent magmatic system. The theoretical LLDs calculated for the most primitive samples of each segment (using the measured water content) can then be compared to the overall data array to check for consistency and potential variations in parental magma compositions. For most segments, the calculated LLD tracks the trends of the segment data (see examples in Figure 11). For these segments, samples that lie along the LLDs can be related to a common parental liquid and collapse to a fairly homogeneous set of corrected compositions. if corrected with their appropriate computed LLD slopes.

In addition to determining the slope, we also needed to estimate the MgO value for the onset of plagioclase crystallization. For dry MORB compositions, *Klein and Langmuir* [1987] and *Langmuir et al.* [1992] proposed a value of 8.5 wt.% MgO, which is typical of dry liquid lines of descent. For wet BABB compositions, we have calculated the saturation state of all primitive compositions to give bounds for this MgO value (called $MgO_{plag\ in}$). If no water analyses were available on a primitive composition, we first determined the dry saturation state to get an upper limit for the $MgO_{plag\ in}$, then artificially added water to the sample (according to the water content of samples with similar composition, based on TiO_2, FeO, and K_2O) to get the lower bound for $MgO_{plag\ in}$. When possible, this value of $MgO_{plag\ in}$ was compared with the $MgO_{plag\ in}$ that can be estimated from the Eu*/Eu-MgO variation diagrams. Since divalent Eu has a relatively high partition coefficient in plagioclase relative to its neighboring REE (e.g., Sm and Gd) ongoing plagioclase crystallization will lead to increasing negative Eu anomalies in the REE pattern (defined as Eu*/Eu) with decreasing MgO. However, to be able to estimate plagioclase onset within 1 wt. % MgO, this method requires the use of high-precision inductively coupled plasma mass spectroscopy (ICP-MS) data acquired on pristine glass material, which is often lacking. Estimated $MgO_{plag.\ in}$ values range from 7 wt.% MgO from the most water-rich magmatic suite up to 8.5 wt.% MgO for the driest suites. The fractionation

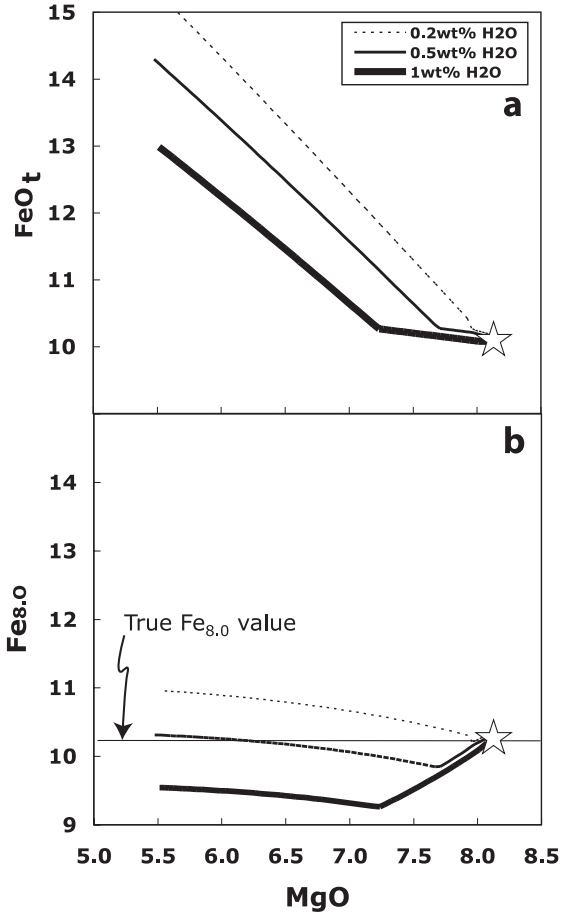

Figure 10. Examples of errors associated with fractionation correction for hydrous samples. (a) FeOt vs. MgO diagram. Star: sample SONO048-G042 (CLSC, Lau basin) with theoretical liquid lines of descent (LLD) from hBasalt code and water content of 0.2 wt.%, 0.5 wt.%, and 1.0wt. %. The kink in the LLD corresponds to the onset of plagioclase crystallization. The plagioclase onset can be delayed by more than 1.5 wt.% MgO between dry and 1 wt.% H_2O LLD. (b) $Fe_{8.0}$ vs. MgO calculated for the LLD from (a). $Fe_{8.0}$ equation is from *Taylor and Martinez* [2003]. If not taken into account, the delay in plagioclase appearance can lead to errors of 1.5 wt.% on the calculated $Fe_{8.0}$.

slopes and $MgO_{plag.\ in}$ for each of the back-arc segments are reported in Table 2. For corrections where MgO > $MgO_{plag\ in}$, the olivine crystallization slopes were used. For MgO < $MgO_{plag\ in}$, the ol-plag-cpx slopes were used, since the three phase slopes are very similar to the slopes of ol-plag for the elements under consideration.

To illustrate the difference that hydrous fractionation corrections make on the calculation parameters, in Figure 12 we compare our values with those calculated using the method of *Kelley et al.* [in press] for $Fe_{8.0}$, $Ti_{8.0}$, and $Na_{8.0}$ for samples with >1 wt.% water and MgO contents between 7 and 7.5

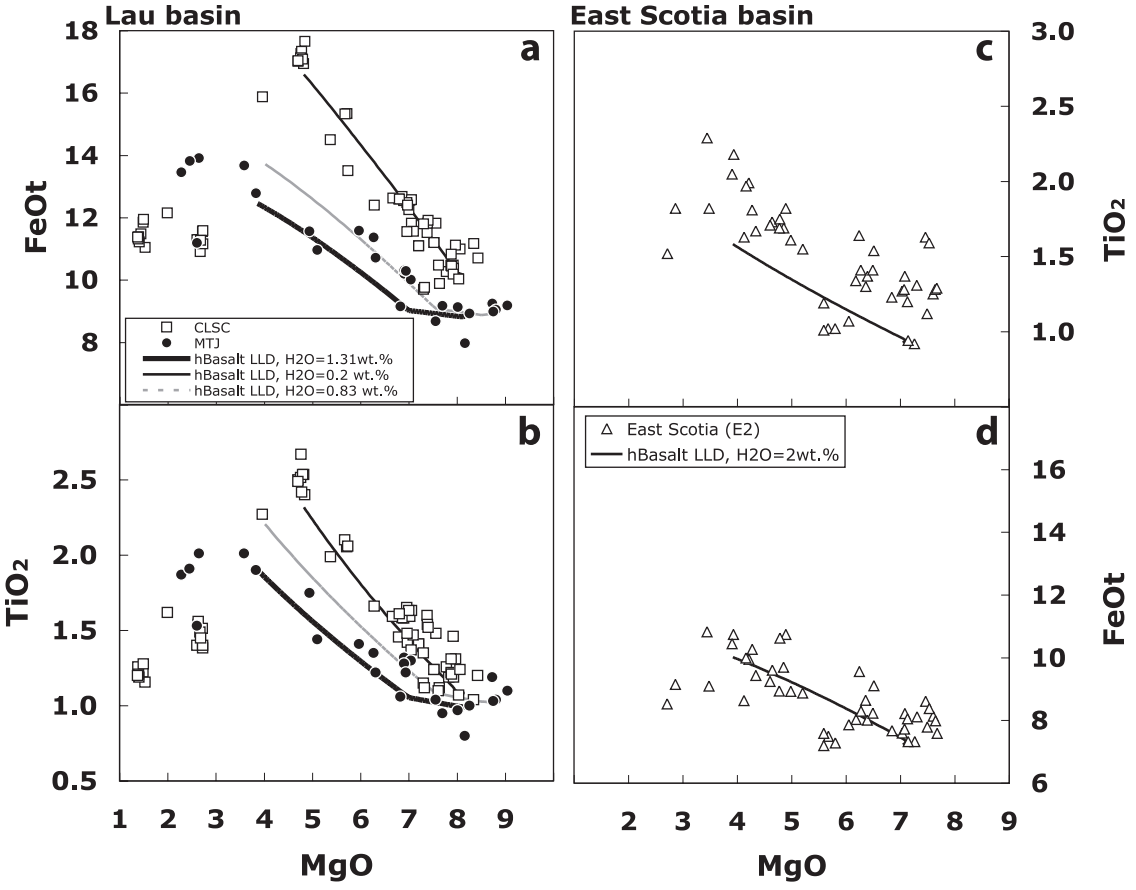

Figure 11. FeOt and TiO_2 vs. MgO for selected segments from the Lau and East Scotia basins, with calculated liquid lines of descent (LLD) from hBasalt. (a, b) Lau basin: square, Central Lau spreading center (CLSC); dots, Mangatolu triple junction (MTJ); thin curve, hBasalt LLD for sample SONO048-G042 from the CLSC with P = 800 bars and measured H_2O = 0.2 wt.%; bold curve, hBasalt LLD for sample MIR2218-008 from MTJ with P = 800 bars and measured H_2O = 1.31wt.% gray curve, hBasalt LLD for sample MIR2218-010 from MTJ with P = 800 bars and measured H_2O =0.83 wt%. (c, d) Triangle, segment E2 from the East Scotia basin; light curve, hBasalt LLD for sample wx7 from the segment E2 with P = 800 bars and measured H_2O = 2.0 wt.%. The fit of the LLD to the data validates the use of hBasalt slopes to correct for low-pressure fractionation.

wt.%. *Kelley et al.'s* corrections do not take into account water or variations in the slope of the LLD for different basins. This results in substantially lower values of $Fe_{8.0}$, $Ti_{8.0}$, and $Na_{8.0}$ for their method. Of course, for low-water samples or those near 8 wt.% MgO, the differences would be smaller.

What is most important from this discussion is that even with hydrous fractionation correction, which leads to substantially higher values of $Ti_{8.0}$ and $Fe_{8.0}$ than anhydrous correction, hydrous back-arc basins samples have lower Fe and Ti than open ocean ridges do. This is not a correction artifact; rather, it is a characteristic of the parental magmas. In fact, this conclusion is independent of fractionation correction because there are back-arc samples with 6–7 wt.% MgO that have only 7 wt.% FeO and 0.6 wt.% TiO_2, much lower than normal MORB (see Table 3). Since fractionation correction at such MgO contents causes the same or lower $Fe_{8.0}$and $Ti_{8.0}$ values compared to raw values, the conclusion of low Fe and Ti for hydrous parental magmas is robust.

4.4. Correction to 8 wt.% MgO or Fo_{90}?

An issue that has arisen in the literature is the common point at which fractionation-corrected compositions are compared. *Klein and Langmuir* [1987] adopted 8 wt.% MgO because it was close to primitive values and also intersected the data arrays for most ridge segments. Therefore all segment averages would be pegged to data near 8 wt.% MgO that required no correction. *Langmuir et al.* [1992] emphasized

that data trends were independent of correction by showing that samples with ~8 wt.% MgO, hence with no corrections, showed the same systematics as corrected data. *Stolper and Newman* [1994] added olivine back to equilibrium with Fo_{90}, a procedure also adopted by *Kelley et al.* [in press], and took these as primitive compositions. Such a procedure presumes that all samples were derived from the same extent of melting of a homogeneous source, since both extent of melting and source composition influence the forsterite content of residual olivine, which may vary from Fo_{89} to Fo_{92}.

While there has been much discussion of this topic, both in the literature and informally, in the end it is immaterial,

Table 2. Slopes from regression of liquid line of descent data calculated by using basalt, and corresponding to the data from multiple samples from each ridge segment.

Basin	Segment	Sample group	SiO_2	TiO_2*	FeO	Na_2O	incompatible*	MgO plag. in
Oliviine-plagioclase ± clinopyroxene multisaturated slopes								
MANUS BASIN								
	ER-SR-MSC-ETZ	TiO_2<0.8wt.%	-0.410	-0.087	-0.964	-0.216	-0.090	7.7
	ER-SR-MSC-ETZ	TiO_2>0.8wt.%	-0.410	-0.102	-1.800	-0.216	-0.107	8.5
EAST SCOTIA BASIN								
	E6 & E7	all samples	-0.410	-0.101	-1.628	-0.238	-0.110	8.0
	E1 & E2	all samples	-0.410	-0.072	-0.983	-0.199	-0.087	8.0
	E8 & E9	TiO_2<1.4wt.%	-0.410	-0.072	-0.983	-0.272	-0.087	8.0
	E8 & E9	TiO_2>1.4wt.%	-0.410	-0.103	-1.146	-0.272	-0.113	8.0
	E3-E4-E5	K_2O<0.4wt.%	-0.410	-0.103	-1.719	-0.436	-0.113	8.0
	E3-E4-E5	K_2O>0.4wt.%	-0.410	-0.077	-1.060	-0.436	-0.095	7.0
LAU BASIN								
	CLSC	all samples	-0.410	-0.100	-2.020	-0.244	-0.117	8.5
	ILSC	olivine saturated	-	-	-	-	-	7.5
	ELSC	K_2O<0.1wt.%	-0.410	-0.096	-1.709	-0.218	-0.108	8.5
	ELSC	K_2O>0.1wt.%	-0.410	-0.085	-1.288	-0.218	-0.096	8.0
	VFR	all samples	-0.410	-0.085	-1.107	-0.224	-0.096	7.0
	MTJ	all samples	-0.410	-0.087	-1.301	-0.238	-0.098	7.5
MARIANA TROUGH								
	1	all samples	-0.410	-0.078	-0.870	-0.246	-0.086	7.0
	2	all samples	-0.410	-0.078	-0.870	-0.246	-0.086	7.3
	3	all samples	-0.410	-0.088	-0.660	-0.167	-0.088	8.0
	4	all samples	-0.410	-0.085	-0.970	-0.172	-0.088	8.8
	5	all samples	-0.410	-0.055	-0.920	-0.338	-0.067	7.5
	6	K_2O/TiO_2>0.8	-0.410	-0.073	-0.740	-0.160	-0.076	7.5
	6	K_2O/TiO_2<0.8	-0.410	-0.078	-0.810	-0.297	-0.080	7.5
Pagan fracture zone		all samples	-0.410	-0.071	-0.630	-0.201	-0.072	7.5
	8	all samples	-0.410	-0.061	-0.990	-0.298	-0.071	7.5
	10	all samples	-0.410	-0.060	-0.840	-0.222	-0.069	7.3
	11	K_2O<0.4wt.%	-0.410	-0.061	-0.660	-0.211	-0.070	7.3
	11	K_2O>0.4wt.%	-0.410	-0.055	-0.660	-0.211	-0.061	7.3
	12	all samples	-0.410	-0.082	-1.000	-0.264	-0.092	7.7
	13	all samples	-0.410	-0.075	-0.860	-0.379	-0.076	7.5
	14	K_2O<0.2wt.%	-0.410	-0.105	-1.680	-0.379	-0.110	8.0
	14	K_2O>0.2wt.%	-0.410	-0.075	-0.860	-0.379	-0.076	7.5
	16	all samples	-0.410	-0.083	-1.300	-0.326	-0.087	8.0
	17	all samples	-0.410	-0.083	-1.300	-0.326	-0.087	8.0
	18	all samples	-0.410	-0.070	-0.820	-0.203	-0.082	7.5
Olivine saturation slope								
ALL BACK-ARC BASINS			-0.2	-0.0144	0.122	-0.0144	-0.0144	

Power law regressions were used for TiO_2 and other incompatible elements (i.e., H_2O, K_2O, and Nb and other trace elements), following the equation for Ce from *Langmuir et al.* [1992]. Linear regressions were used for SiO_2, FeOt, and Na_2O. $MgO_{plag.\ in}$ is the estimated MgO value for plagioclase saturation, below which multiple saturation slopes were used. Above this value, corrections were made for olivine addition or subtraction. Samples with MgO < 5.5 wt.% were not used. Samples with 5.5 < MgO > $MgO_{plag.\ in}$ were first corrected to the lesser of 8 wt.% MgO or $MgO_{plag.\ in}$. When $MgO_{plag.\ in}$ was less than 8 wt.%, samples were then corrected to 8 wt.% MgO by using the olivine saturation slope.

as long as the data are compared with quantitative calculations of melting that are themselves corrected to the same value. For example, if mantle melts have residual Fo_{92}, then these melts would need to be fractionated to 8 wt.% MgO (or to an equilibrium with Fo_{90}), to be compared with the data. This procedure was adopted by *Langmuir et al.* [1992] and is used in this paper. When we compare melting models to "8.0" values, we do not claim that the values at 8 wt.% MgO are parental magmas. Instead, we fractionate mantle melts, which are in equilibrium with various olivine compositions, to 8 wt.% MgO to compare with the data. As long as this is done rigorously, the point of comparison is a matter of preference and is immaterial to results and interpretations. One could even "correct" some samples to a constant Mg/Fe ratio, others to 7 wt.% MgO and others to 9 wt.% MgO. As long as the calculated mantle melts were fractionated to the appropriate point for each comparison, the results would be exactly the same. We prefer 8 wt.% MgO because it facilitates easy comparison with the existing MORB data, it is a value that overlaps with the observations, and it does not assume a constant mantle residue composition.

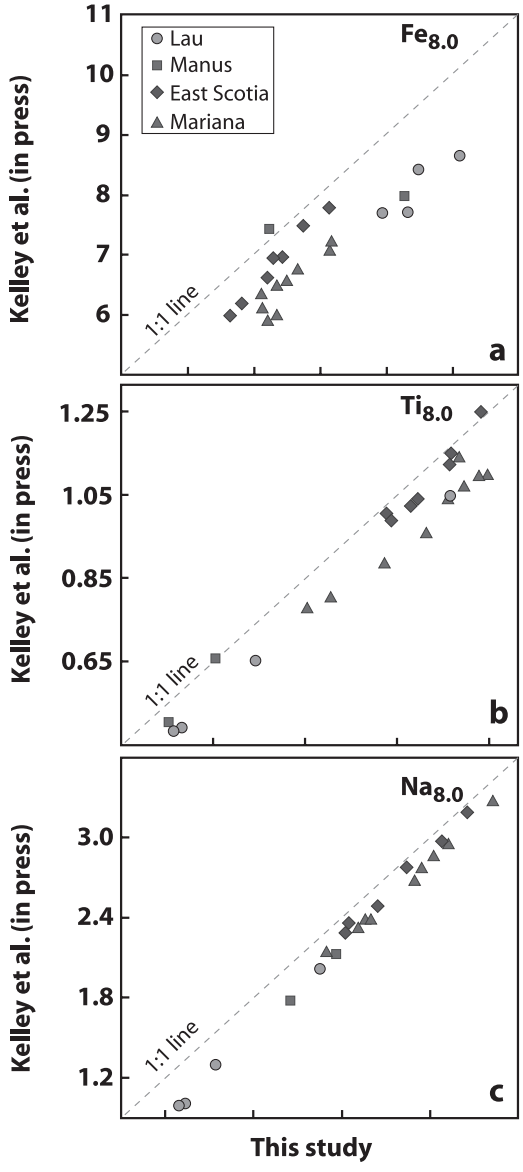

Figure 12. Comparison of $Fe_{8.0}$, $Ti_{8.0}$, and $Na_{8.0}$ calculated by using the methods of this paper and that of *Kelley et al.* [in press] for samples with >0.9% water and less than 7.5 wt.% MgO. Taking hydrous fractionation into account leads to significantly higher values for all parameters.

5. PRESENTATION OF DATA FROM THE FOUR MAJOR BACK-ARC BASINS

The filters and fractionation correction discussed above have the aim of accurate determination of parental magma compositions, because the problems we wish to address relate to mantle wedge composition and melting processes. Melting processes and mantle temperature can be addressed by using the major element parameters such as $Na_{8.0}$ and $Fe_{8.0.}$ Source variations in the mantle wedge that are relatively independent of subduction contributions can be addressed by using HFSE, Zr, Y, Nb, and Ti (e.g., *Woodhead et al.* [1993]; *Pearce et al.*, [1995]; *Woodhead et al.* [1998]).

Aspects of the interpretation will be based on comparison with basalt systematics from open ocean ridges. For these ridges, relationships between chemical composition and axial depth can be related quantitatively to variations in mantle temperature [*Klein and Langmuir*, 1987; *Langmuir et al.*, 1992]; moreover, there are also well determined average compositions [*Su*, 2002]. A significant reference is the average composition at 8 wt.% MgO of "normal" ridge segments that are far from hot spots and do not have enriched trace element and isotope signatures. These basalts have an average of 3 ppm Nb, 100 ppm Zr, 33.5 ppm Y, and 1.49 wt.% TiO_2, and their $Na_{8.0}$ and $Fe_{8.0}$ values (2.74 and 9.78, respectively) lie along "global correlations" that relate average segment compositions to one another and to the axial depth and crustal thickness, for which average values are 2600 m and 6 km,. repectively [*Su*, 2002]. Back-arc basins differ considerably from these relationships. Values for these parameters in back-arc basins are given in Table 3.

In this paper we evaluate data from the four major back-arc basins—Manus, Lau, Scotia, and Mariana. A description of the structure of the basins and the data sets available from each of them is presented in the Appendix. For presentation in the figures, the samples from each basin have been divided into separate

TABLE 3. Regional averages of ridge-arc distance, axial depth and parameters of lava chemistry for back-arc basins.

Segments	Arc distance (km)	Depth (m)	1σ	N	$Si_{8.0}$	1σ	$Ti_{8.0}$	1σ	$Fe_{8.0}$	1σ	$Na_{8.0}$	1σ	$K_{8.0}$	1σ
MANUS BASIN														
ER	69	1900	430	4	52.13	1.66	0.39	0.03	6.99	0.91	1.98	0.32	0.42	0.22
SR	155	2500	220	3	50.60	0.4	0.67	0.13	8.83	0.51	2.10	0.07	0.21	0.06
MSC	237	2330	330	13	50.18	0.34	0.95	0.14	10.37	1.30	2.27	0.10	0.06	0.02
ETZ	227	2262	315	7	50.14	0.46	0.95	0.09	10.40	0.67	2.23	0.11	0.05	0.02
EAST SCOTIA BASIN														
E2	164	3317	233	18	52.12	0.81	1.02	0.16	6.87	0.48	2.53	0.24	0.31	0.13
E3	215	3374	164	7	51.04	0.93	1.25	0.10	7.57	0.61	2.69	0.30	0.17	0.09
E4	227	3551	318	3	51.55	1.27	1.17	0.18	6.35	1.07	2.56	0.35	0.46	0.28
E5	221	3900	103	6	50.69	0.74	1.26	0.18	7.71	0.79	3.03	0.36	0.12	0.01
E6	199	3600	209	6	50.44	0.65	1.45	0.17	8.40	0.65	2.94	0.12	0.17	0.14
E7	210	3638	93	4	50.75	0.35	1.51	0.19	8.65	0.53	3.01	0.21	0.17	0.05
E8	145	3221	231	5	51.21	1.67	0.90	0.43	7.52	1.12	2.34	0.81	0.12	0.01
E9	133	3900	291	8	50.88	0.43	1.13	0.22	7.46	0.64	3.06	0.37	0.26	0.07
LAU BASIN														
CLSC	188	2293	66	24	49.93	0.37	1.22	0.11	10.30	0.73	2.51	0.19	0.06	0.04
ELSC	82	2618	213	6	52.52	1.60	0.91	0.19	8.91	1.17	2.10	0.28	0.08	0.02
VFR	41	1866	196	2	51.25		0.79		8.91		1.95		0.18	
MTJ	130	2281	130	17	50.44	0.81	1.04	0.1	9.13	0.48	2.53	0.26	0.24	0.09
MARIANA TROUGH														
1	116	4152		2	51.13		1.02		7.42		2.57		0.23	
2	120	4268		4	50.33	0.76	1.08	0.19	7.37	0.53	2.90	0.31	0.39	0.19
3-4	100	4556		8	50.90	0.91	1.21	0.22	7.98	0.87	3.07	0.32	0.29	0.09
5-6	96	4230		40	50.69	0.71	1.15	0.20	7.81	0.79	2.84	0.27	0.28	0.12
8-10	132	4079		7	49.66	0.83	1.16	0.19	8.15	0.70	2.88	0.37	0.28	0.04
11-12	130	3916		8	50.40	0.33	1.02	0.13	7.56	0.33	2.66	0.23	0.33	0.10
13	142	4369		2	50.03		1.28		8.16		3.10		0.29	
14	131	4131		2	50.36		1.34		8.68		3.20		0.21	
16-17	130	3887		4	50.28	0.09	1.21	0.12	8.37	0.28	2.83	0.12	0.12	0.02
18	95	3290		7	48.81	0.43	0.94	0.21	8.05	1.00	2.36	0.30	0.16	0.06
MORB (normal segments average)*				151	50.48	0.54	1.49	0.27	9.98	0.95	2.77	0.35	0.12	0.07

groups—either on the basis of tectonic location or on the basis of the relative enrichment in incompatible elements that are not strongly influenced by the subduction component. For the Manus Basin, samples are divided between the northern and southern Manus spreading center and the samples that come from rifts and the extensional transform zone where spreading has not been shown to occur. For the Lau Basin, we put the Eastern Lau spreading center and Valu Fa ridges, which are relatively continuous with no transform offset, into a single group. The Intermediate Lau spreading center and Central Lau spreading center are separated as individual

TABLE 3. Regional averages of ridge-arc distance, axial depth and parameters of lava chemistry for back-arc basins (continued).

$H_{8.0}$	1σ (N)	$Nb_{8.0}$	1σ (N)	$Ta_{8.0}$	1σ (N)	$Zr_{8.0}$	1σ (N)	$Hf_{8.0}$	1σ (N)	$Y_{8.0}$	1σ (N)	$Yb_{8.0}$	1σ (N)
MANUS BASIN													
1.00	0.22(4)	0.59	(2)			25	(2)			8.6	(2)		
1.23	(2)	0.58	0.04(3)			34	7(3)			14.6	1.9(3)		
0.52	0.25(11)	0.99	0.18(14)	0.07	0.01(3)	53	8(15)	1.58	0.27(3)	23.0	3.6(15)	2.81	0.41(3)
0.40	0.27(5)	0.98	0.20(6)			50	4(6)			21.2	2.4(6)		
EAST SCOTIA BASIN													
1.05	0.37(15)	5.06	3.02(18)	0.31	0.19(17)	71	12(17)	1.79	0.29(17)	20.7	3.2(17)	1.97	0.31(17)
0.46	0.39(6)	2.73	0.62(7)	0.17	0.04(7)	76	11(7)	2.27	0.27(7)	24.6	3.6(7)	2.60	0.25(7)
1.14	(2)	3.50	0.75(3)	0.23	0.05(3)	76	18(3)	2.27	0.37(3)	20.7	4.8(3)	2.35	0.50(3)
0.29	0.13(4)	2.15	0.35(6)	0.15	0.03(6)	89	18(6)	2.39	0.36(6)	23.5	3.9(6)	2.56	0.40(4)
0.24	0.06(4)	2.33	0.46(5)	0.15	0.03(5)	91	9(5)	2.77	0.23(5)	28.2	2.0(5)	3.15	0.26(5)
0.02	0.04(3)	2.58	0.36(4)	0.17	0.02(4)	94	26(4)	2.77	0.52(4)	27.6	6.0(4)	3.09	0.55(4)
0.77	0.98(3)	1.02	0.72(4)	0.08	0.05(4)	59	32(4)	1.55	0.79(4)	17.6	7.7(4)	1.90	0.78(4)
0.43	0.27(6)	3.65	1.53(7)	0.23	0.09(7)	75	27(7)	2.00	0.63(7)	18.1	4.8(7)	1.93	0.50(7)
LAU BASIN													
0.24	0.05(16)	1.53	1.27(9)	0.07	0.01(3)	63	9(10)	1.69	0.12(3)	29.4	3.7(10)	2.72	0.34(8)
0.63	0.31(5)	0.62	(2)	0.04	(2)	30	(2)	0.79	(2)	14.1	(2)	1.49	(2)
		0.36											
0.93	0.31(13)	2.44	0.88(14)			69	14(14)	1.66	0.29(8)	27.0	5.9(14)	2.37	0.25(7)
MARIANA TROUGH													
1.58	(2)	2.41	(2)	0.17	(2)	72	(2)	1.90	(2)	26.2	(2)	2.42	(2)
1.00	0.47(6)	4.61	1.97(7)	0.30	0.12(7)	96	22(7)	2.34	0.48(7)	29.0	4.2(7)	2.77	0.40(7)
1.13	0.34(11)	2.87	2.46(29)	0.17	0.03(12)	87	14(31)	2.20	0.11(2)	27.6	4.9(31)	2.34	0.67(7)
1.09	0.53(3)	3.97	(2)	0.26	(2)	87	(2)	1.91	(2)	25.2	(2)	2.45	(2)
1.72	0.38(6)	3.34	1.36(7)	0.20	0.06(6)	66	12(7)	1.71	0.32(6)	23.3	2.3(7)	2.18	0.23(6)
0.33	(2)	3.27	(2)	0.21	(2)	100	v	2.50	(2)	31.4	(2)	2.91	(2)
		1.95	0.88(4)	0.14	0.06(4)	90	16(4)	2.25	0.37(4)	26.7	2.1(4)	2.56	0.20(4)
		1.12	(2)	0.08	(2)	63	(2)	1.63	(2)	21.9	(2)	2.14	(2)
MORB		3.05	2.0(112)	-	-	101	28.3(121)	2.63	0.65(107)	33.5	6.8(128)	3.36	0.68(145)

These averages are based on all samples that pass the screens used in the text and therefore include both hydrous and less hydrous samples where both exist within a segment. Accordingly, no segment average actually represents the dry and wet end members that reflect the end- member compositions of individual samples. *N*: number of samples averaged within a segment. 1σ: one standard deviation of the individual samples within each segment.

groups. The substantial amount of data from off-axis seamounts are also distinguished, since these are not from a spreading center. The Mangatolu triple junction samples, which are a completely separate spreading center system some 450 km to the northeast, are presented as their own group. For the Scotia and Marianas basins, all of the samples are from spreading centers, and therefore a tectonic distinction is not necessary. For these basins

we separate sample groups on the basis of their Nb/Zr or Ta/Yb ratios. Samples with Nb/Zr > 0.06 are classified as "highly enriched", those with 0.045–0.06 are "enriched", 0.03–0.045 is "normal", and <0.03 is "depleted." These values compare with the value for normal MORB given above of 0.03.

5.1. Evaluation of Source Heterogeneity in the Mantle Wedge

Early work on back-arc basins viewed the chemical variations as resulting from sources created by mixing of two components: a background mantle component similar to normal MORB, and a slab component that added water and other incompatible elements (e.g., *Hawkins and Melchior* [1985]; *Stolper and Newman* [1994]). While this was a reasonable first-order approach, the abundance of new data shows that multiple components are necessary to account for back-arc data (e.g., *Danyushevsky et al.* [1993]; *Sinton et al.* [2003]; *Pearce et al.* [2005]. *Pearce and Stern* (this volume) summarize much trace element data from back-arc basins and ascribe the variations to shallow and deep subduction components, and to a variable background mantle wedge composition ranging from depleted to enriched.

The diversity of source components is evident from any figure of an incompatible element vs. H_2O. Figure 13 plots $K_{8.0}$ vs. $H_{8.0}$ for the various back-arc basins, and as pointed out originally by *Danyushevsky et al.* [1993], there are very different apparent K/H ratios among the mixing components. Indeed, most of the back-arc basin data are quite scattered on these diagrams, showing that a two-component model is insufficient.

The importance of source heterogeneity that is not related to a subduction component can be investigated with the HFSE, which show very large variations in back-arc basins. The Lau and Manus Basins mostly have very low abundances of the HFSE. The strong relative depletion of the Manus Basin lavas (see Table 3) is evident from their mean $Nb_{8.0}$, $Zr_{8.0}$, $Ti_{8.0}$, and $Y_{8.0}$ contents of 0.9 ppm, 46 ppm, 0.87 wt.%, and 20 ppm, respectively. These values are as much as 70%-depleted relative to the average basalt from ocean ridges far from hot spots.

The Scotia and Mariana basins have a much larger range that extends to high values. Both Scotia and Mariana sample compositions range from enriched samples with 10 ppm Nb and Nb/Zr = 0.1 to highly depleted samples with less than 1 ppm Nb and Nb/Zr = 0.01–0.02. These are very large source variations in terms of highly incompatible elements, encompassing much of the range of MORB, including data from ridges influenced by hot spots.

Mangatolu triple junction samples are intermediate in terms of the HFSE. Nb_8 ranges from 1 to 4 ppm and for all but one sample the Nb/Zr ratio is less than 0.05.

Figures 14 and 15 plot Nb/Zr vs. $Nb_{8.0}$ and $Nb_{8.0}$ vs. $Ti_{8.0}$ for the various back-arc basins, along with a melting curve for melting of the depleted MORB source of *Salters and Stracke* [2004]. No suites of back-arc basin data plot along melting curves from a homogeneous source, even for these elements that are little influenced by subduction components. Melting leads to large variations in Nb abundance, small changes in the Nb/Zr ratio, and well-correlated variations in $Ti_{8.0}$ and $Nb_{8.0}$, which is not in accord with the observations. These simple calculations demonstrate that the data require substantial heterogeneity in the background mantle composition, even within individual basins.

The importance of this heterogeneity is also evident when comparing H_2O and Nb abundances. As pointed out above in section 2, for simple melting models making use of a homogeneous source, all HFSE elements should show linear variations with water and have similar intercepts of the water axis. Figure 16 shows that this is not the case for Nb data. None of the back-arc basins have good correlations between $Nb_{8.0}$ and $H_{8.0}$, and for the Scotia samples, the poor correlation is positive and not negative. Therefore, the data are clearly inconsistent with any assumption of a homogeneous source, and slab components calculated on that basis would not be valid.

This heterogeneity is also important for other elements that are often attributed to a hydrous subduction component in the back-arc environment. Figure 17 plots Ba/Nb vs. La/Sm for the back-arc basins, along with a suite of open ocean enriched MORB. The slab component observed in back-arcs does not mobilize Nb, and hence has a very high Ba/Nb ratio and only slightly elevated La/Sm. Enriched basalts far from convergent margins, on the other hand, have a small range of Ba/Nb and large increases in La/Sm. The diagram thus leads to a clean separation of the two types of enrichment.

From the diagram it is evident that most of the southern Lau and Manus samples have a relatively pure "arc component", while the Mangatolu triple junction, Mariana, and Scotia samples all have an important source influence akin to what is observed for enriched basalts from open ocean ridges and from ocean islands. The large scatter on this diagram also shows that mixing of two sources is not an adequate model for most of these data sets.

The data thus demonstrate a large range of source compositions in elements that are not normally attributed to subduction components. These variations range from compositions more depleted than normal ocean ridge mantle to compositions that are similar to what is observed for enriched mantle observed in enriched basalts on ocean ridges and on ocean islands. These enrichments and depletions would influence other incompatible elements as well as the HFSE. Therefore, particularly for the Marianas and Scotia back-arc basins, both "OIB" and "arc" enrichments

need to be taken into account. This will also be important for any evaluation of melting models.

5.1.1. Causes of wedge heterogeneity in back-arc basins. In the open ocean ridge environment, there are two principal sources of source variation: depletion caused by prior melting events, and enrichment, which has a characteristic major and trace element signature that is diagnostic of addition of low-degree melts [*Donnelly et al.*, 2004], although it is often ascribed to recycled ocean crust (e.g., *Hofmann and White*

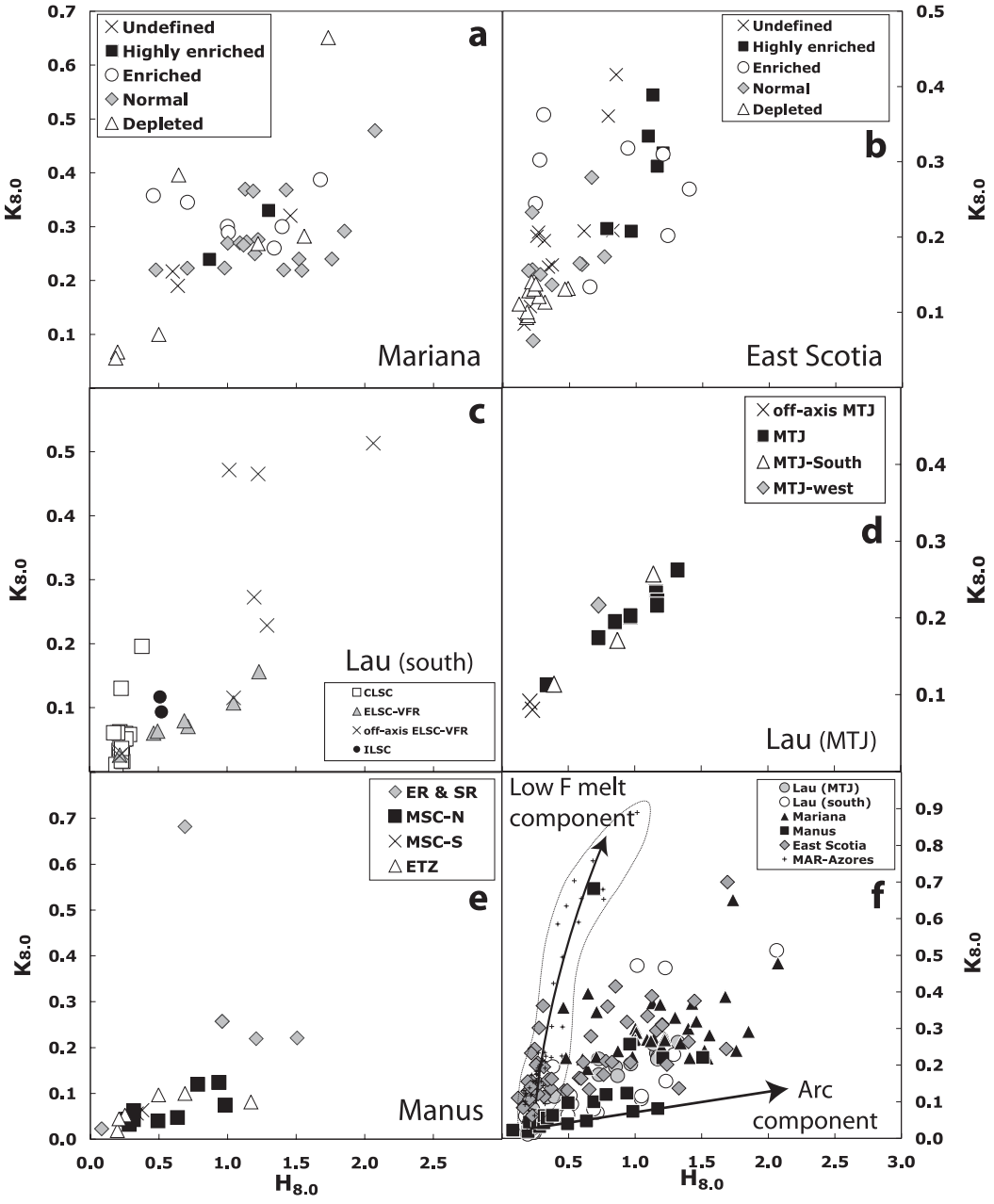

Figure 13. (a–e) $K_{8.0}$ vs. $H_{8.0}$ for individual samples from the different back-arc basins. (f) All data combined, emphasizing the very large range in K/H ratios both within and between back-arc basins. The ratios range from a component characteristic of ocean islands (the "low-F melt component") to a water-rich component characteristic of convergent margins (for comparison, notice the very low relative K/H of the back-arc basin component in Figure 5. MAR data from the Azores region are from PetDB.

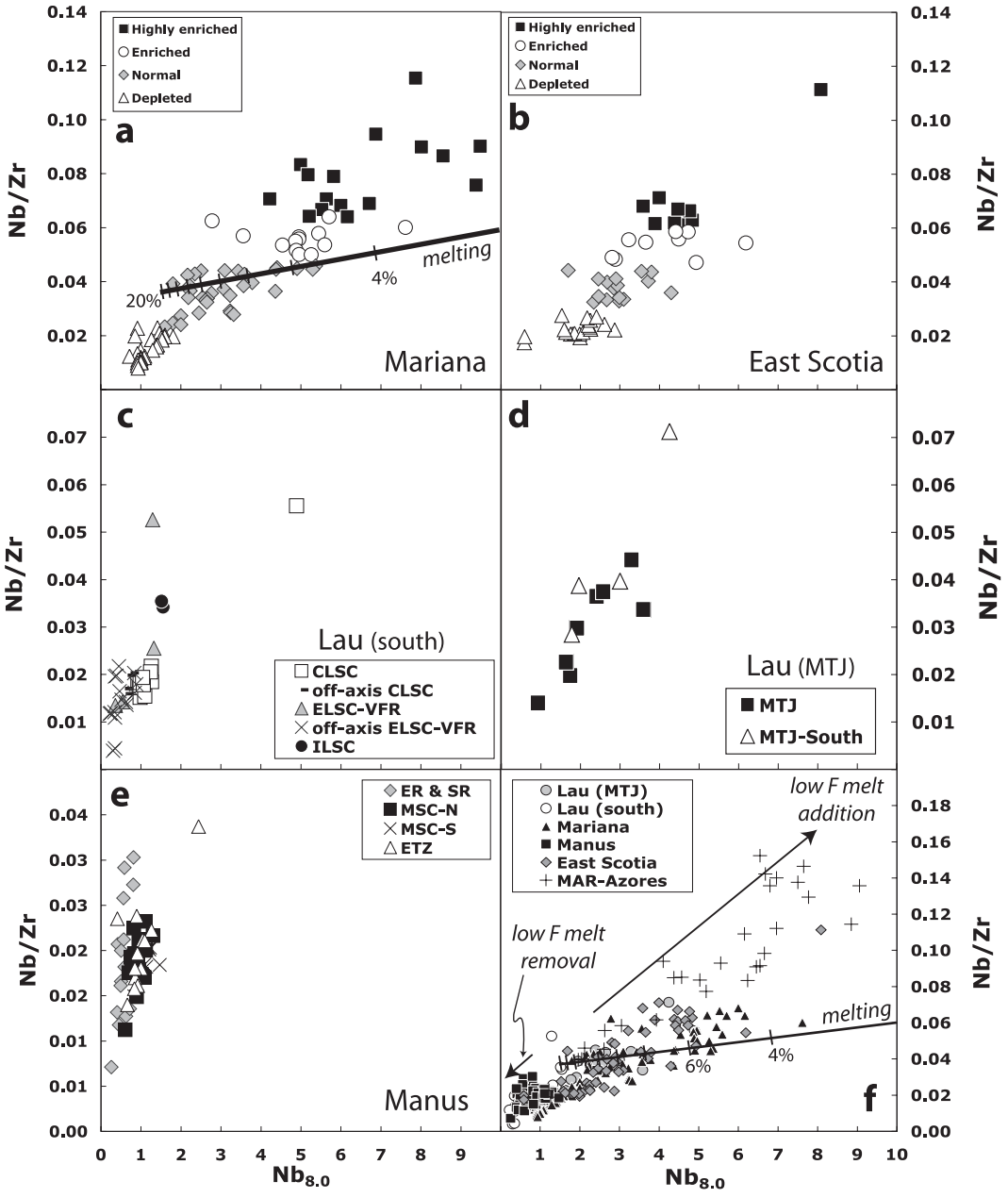

Figure 14. Nb/Zr vs. $Nb_{8.0}$ for individual samples from the different back-arc basins. All data points are corrected for wet differentiation. For each basin, samples have been divided into separate groups on the basis of either tectonic location or the relative enrichment in incompatible elements that are not strongly influenced by the subduction component (see discussion in text and Appendix). Melting curves shown in (a) and (f) are calculated from the DMM composition of *Salters and Stracke* [2004], using nonmodal batch melting with D's of 0.006 for Nb and 0.03 for Zr. All the back-arc basins are compared together and with MORB in (f). The arrows illustrate the effects of removal or addition to the source of low-F melts. These sources are then melted to various extents to generate the back-arc data, suggesting that this is the mechanism for generation of the substantial source heterogeneity observed.

[1982]; *Niu and Batiza* [1997]). Whatever the ultimate cause of the enrichment is determined to be, the vector in compositional space is well defined, as Nb, K_2O, and H_2O, for example, behave coherently and are enriched and depleted together. This signature is also apparent in the back-arc data. In addition to this type of mantle enrichment and depletion, the arc environment has other complexities. Multiple slab components are recognized, some attributed to hydrous fluids from altered basalts

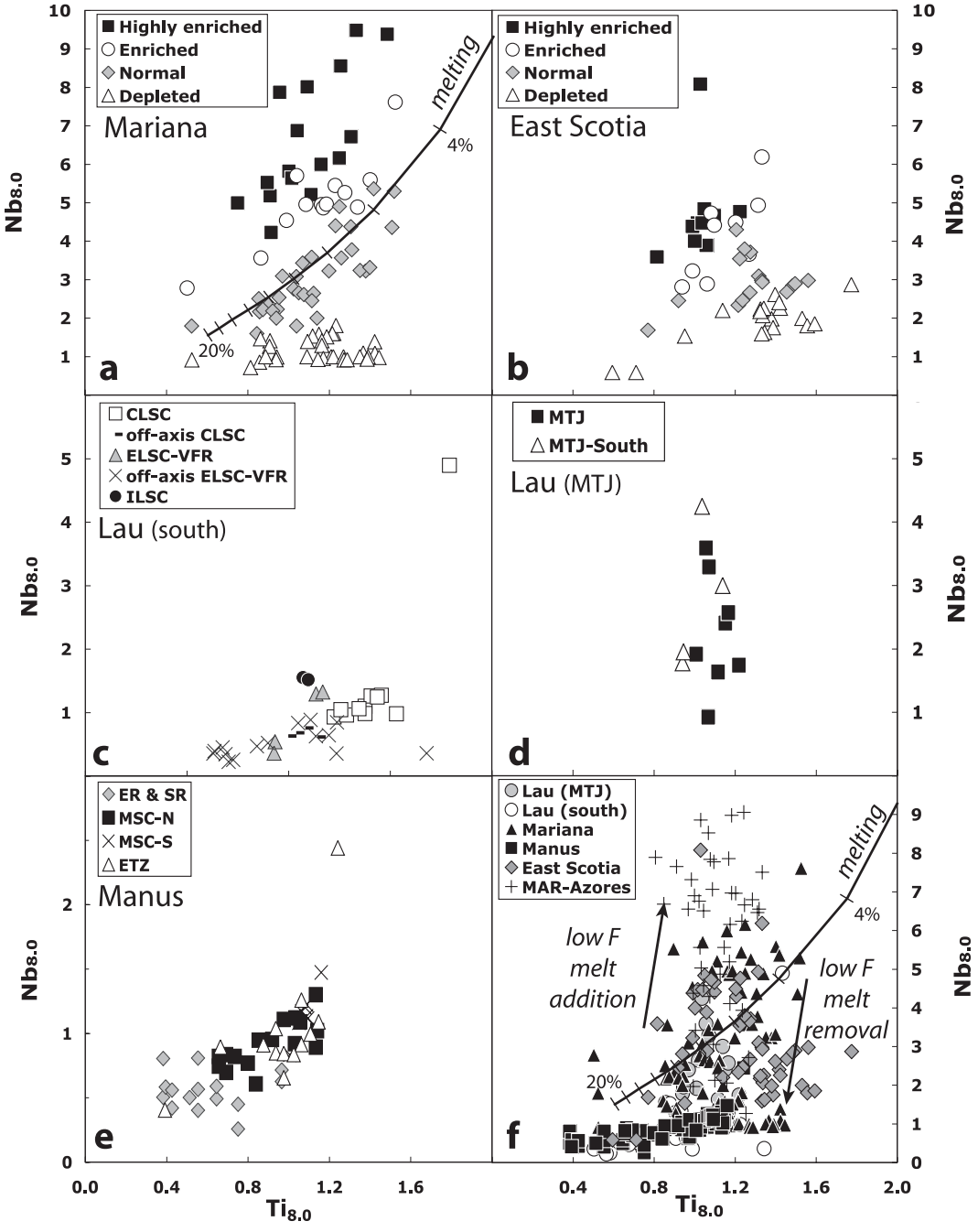

Figure 15. $Nb_{8.0}$ vs. $Ti_{8.0}$ for individual samples from the different back-arc basins. All data points are corrected for wet differentiation. Melting curve is calculated from the DMM composition of *Salters and Stracke* [2004] using modal batch melting with a D of 0.006 for Nb and 0.04 for TiO_2.

(e.g., *Gill* [1981]; *Miller et al.* [1994]), and others to sediments [*Kay*, 1978], to sediment melts [*Plank*, 1993; *Elliott et al.*, 1997] or to fluids from sediment [*Class*, 2000].

The heterogeneity problem is particularly difficult because in the back-arc environment many different mantle sources and histories can be encountered over very short distances. This is true for all the back-arc basins. The spreading centers are at various distances from the arc, and they propagate into arc lithosphere that may have had complex removals and additions of source components. The spreading centers

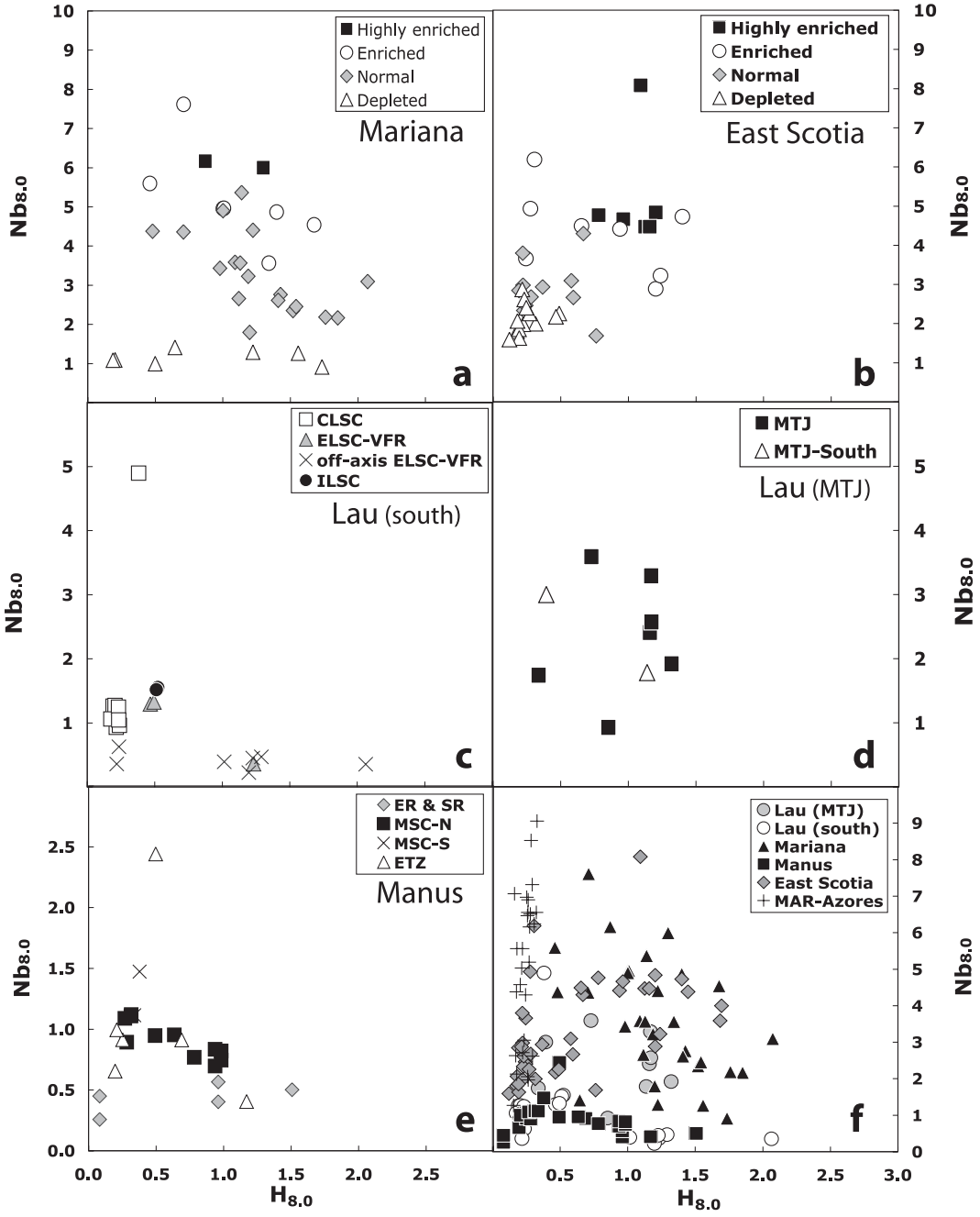

Figure 16. $Nb_{8.0}$ vs. $H_{8.0}$ for individual samples from the different back-arc basins. All data points are corrected for wet differentiation. Note the generally poor correlations on these diagrams, emphasizing the importance of source heterogeneity both within and between back-arc basins.

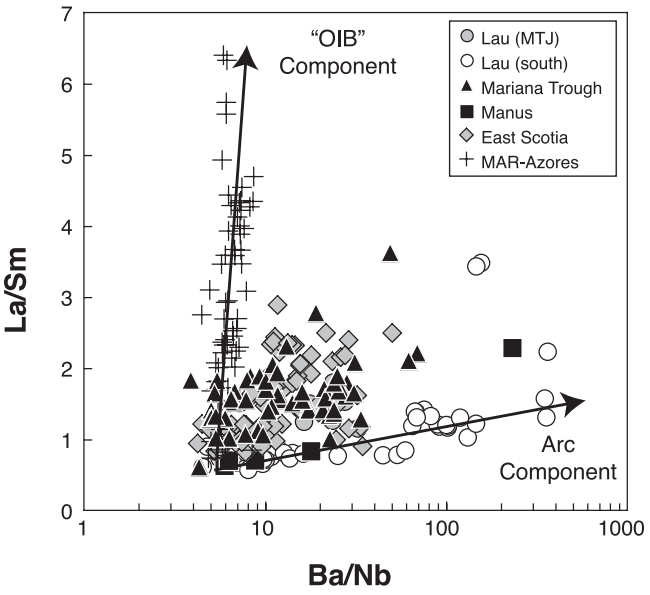

Figure 17. La/Sm vs. Ba/Nb systematics for BABB and MORB from the Azores vicinity. showing the strong enrichment of fluid mobile elements (e.g., Ba) in the BABB source relative to conservative elements (Nb, Zr, Y). This is the arc signature. The enriched component sampled at open ocean ridges (e.g., MAR-Azores) leads to a vector orthogonal to the arc trend. Note that back-arc basin data span the range from arc to "OIB" components, showing the importance of both influences in this setting, despite the absence of hot spots.

are tectonically complex, with different sorts of ridge offsets than are observed in open ocean ridges, flips in the polarity of subduction, complex subduction histories, and volcanism that is not clearly associated with organized spreading systems. Assumptions of constant source for back-arcs are sure to be wrong, and possible variations in source composition need to be carefully considered in the context of the detailed tectonic environment [*Hochstaedter et al.*, 2000].

While these are daunting complexities, what we find striking in the HFSE data is the relatively coherent trajectory of the data from all the back-arc basins (Figure 14f). While there are large variations in Nb/Zr among the back-arc basins, the data as a whole show a coherent trend extending from $Nb_{8.0}$ less than 1 with Nb/Zr of 0.01 to $Nb_{8.0}$ of 8 and Nb/Zr of 0.1. What are the likely causes of these variations?

One cause, well documented by previous work, is a previous melting event causing mantle depletion [*Woodhead et al.*, 1993; *Ewart et al.*, 1998; *Hochstaedter et al.*, 2000], or "pre-conditioning" as it is called by *Pearce* [2005]. Melting removes incompatible elements and easily fusible components from the residue, leaving it "depleted." While this problem is conceptually simple and easily modeled, the details of the melting process lead to rather different results for estimates of the amount of melt extracted, and also for relationships between highly and moderately incompatible elements. We adopt a simple approach of nonmodal, batch melting, and compare sources depleted by 1% melt extraction with the normal MORB mantle composition of *Salters and Stracke* [2004].

In the open ocean environment, the characteristic of the enrichment process is that highly incompatible elements are efficiently fractionated from one another. Such fractionation occurs only at very small extents of melting. For example, the Nb/Zr ratio varies by only 40%, from 4% to 20% melting—and by 300% from 0.1% to 4% melting. The large changes in this ratio, observed in back-arcs and elsewhere, suggest that such enrichment processes are associated with low-F melts. Such enrichments change the concentrations of the incompatible HFSE, Nb and Ta, to a similar degree as those of the "fluid mobile" elements such as water, K, Ba, Cs, and so on. We find that mixing of sources enriched by a low-F melt with sources having undergone 1% melt depletion leads to the HFSE data arrays of the various back-arc basins, as illustrated in the figures.

The back-arc data shown above for the Mariana and Scotia data sets clearly require enriched components that can fractionate the Nb/Zr ratio. Is this simply a generic "enriched component" that resides in the upper mantle and is observed at ocean islands and elsewhere? Or is it somehow specific to the back-arc environment? Consideration of the detailed spatial distribution of the data, and their relationship to radiogenic isotopes, provides a possible answer to this question.

Figures 18a and b present the Mariana data in a spatial context. For this back-arc basin there is no spatial organization to the data. The entire range of source compositions reflected in the Nb/Zr ratio is present over very short spatial distances. A second critical observation is the lack of correlation between HFSE incompatible element enrichment and isotopic composition, as illustrated in the Nb/Zr vs. $^{87}Sr/^{86}Sr$ diagram (Figure 18c), at the same time as the very good correlation between $H_{8.0}$ and $^{87}Sr/^{86}Sr$ (Figure 19a). This suggests that an isotopically uniform source with variable trace element enrichment has been modified by addition of a high-H_2O, high-$^{87}Sr/^{86}Sr$ subduction component. A plot of Nb/U vs. $^{87}Sr/^{86}Sr$ shows distinct trends for the enriched and depleted samples. The trends are from a uniform, low-Nb/U, high-H_2O, high-$^{87}Sr/^{86}Sr$ component to a high-Nb/U component with distinct curvature depending on the enrichment of the high-Nb/U end member (Figure 19b). If these trends are produced by mixing, then the more depleted the source, the stronger the mixing curvature. This is consistent with the lower U/Sr ratios that would exist in the more depleted source.

These results show that

(a) The enriched component has high concentrations of the most highly incompatible elements such as Nb,

but small concentrations of moderately incompatible elements such as TiO_2, since TiO_2 does not correlate with Nb (Figure 15a).

(b) The process that created the Nb enrichment is geologically very recent, because it has created no variation in the Sr isotopes. Low-$^{87}Sr/^{86}Sr$ samples exhibit the entire range of Nb/Zr.

(c) There is no or little spatial pattern to the enrichment, as it is distributed widely along the entire length of the basin (Figure 18).

The first observation suggests that the enriched component is a low-F melt, because otherwise TiO_2 would be significantly enriched as well as Nb. The second observation requires that this melt be generated in the recent past, because it has not generated any isotopic variation and therefore is not associated with a long-term enriched reservoir. Instead, it appears to be created as a part of the subduction process, and would be consistent with deep low-F melting of the subducted slab as a low-F melt-enriching mechanism [*Langmuir*, 2003; *Donnelly et al.*, 2004]. This would also contribute to the random distribution of the enriched samples.

In contrast to the Mariana basin, the Scotia samples show a correlation between Nb/Zr and $^{87}Sr/^{86}Sr$ (Figure 20c). In addition, the enrichment is spatially well defined and restricted to the end segments (Figures 20a and b). The variations in Nb/U ratio are well correlated with water contents, and a large range of $^{87}Sr/^{86}Sr$ exists for high Nb/U

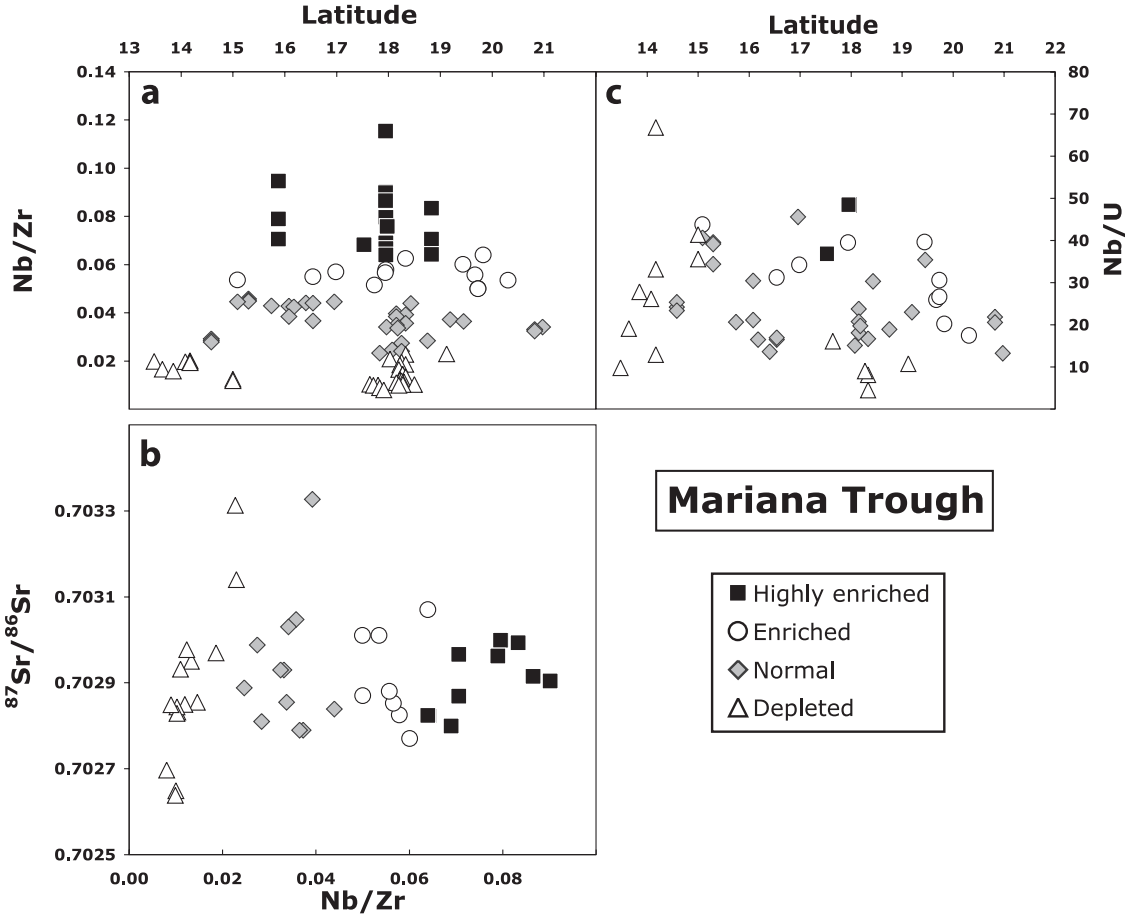

Figure 18. Spatial distribution of variations in source parameters for Mariana samples. Enriched and depleted sources are distributed without apparent organization in this basin. (a, b) Nb/Zr and Nb/U vs. latitude. The Nb/U ratios are low compared with typical MORB average (47 ± 10), showing the importance of an arc component. (c) $^{87}Sr/^{86}Sr$ vs. Nb/Zr for individual Mariana trough samples. Enriched and depleted lavas types are recovered in the middle of the basin while the northern and southern ends of the ridge tend to have only depleted-type samples. The enriched and depleted end members do not show any correlation between strontium isotopes and Nb/Zr, unlike samples from open ocean ridges, where those with elevated strontium isotopes have low Nb/Zr. This suggests recent enrichment for the Mariana sources.

ratio. These observations suggest that the enrichments are relatively long-lived heterogeneities created before the subduction process. Therefore, addition of enriched source material around tears in the slab ends, as suggested by *Fretzdorff et al.* [2002], seems a reasonable explanation. While an ancient Bouvet influence inherited by the mantle that leaks into the Scotia Basin might be an explanation

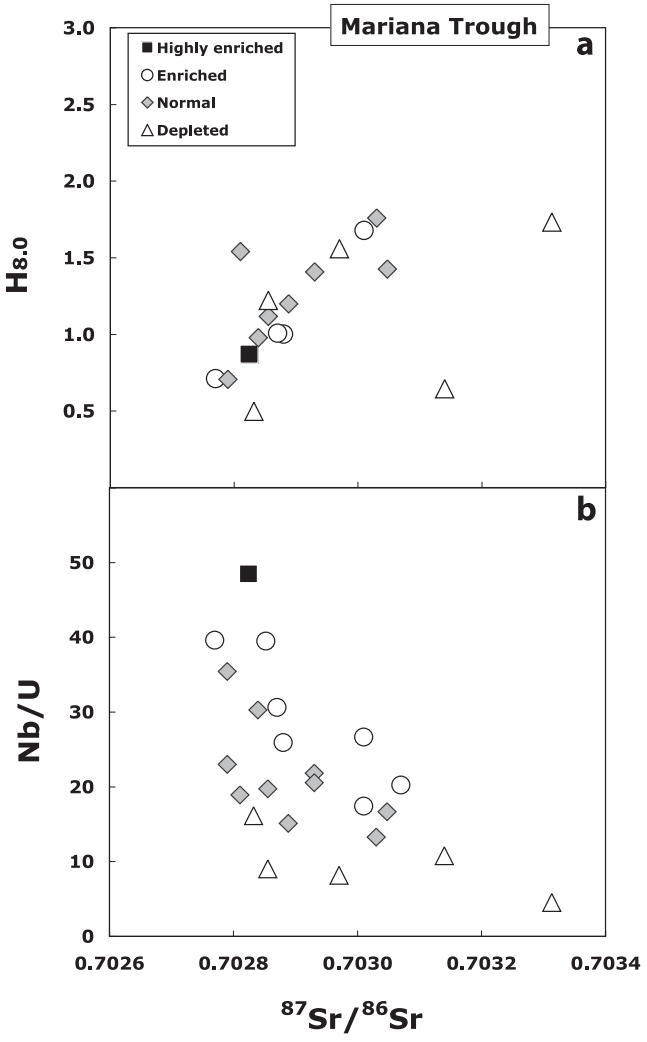

Figure 19. Source variations in the Mariana Basin. (a) Correlation of high $^{87}Sr/^{86}Sr$ with high $H_{8.0}$, showing that Sr isotope variations are associated with the subduction component. (b) Samples with different amounts of enrichment defined by Nb/Zr fit onto distinct trajectories for Nb/U vs. $^{87}Sr/^{86}Sr$. If these arrays are caused by mixing, the data are consistent with an arc component mixing and a diversity of wedge sources, ranging from low U/Sr-depleted sources to high-U/Sr enriched sources. Both enriched and depleted wedge sources have low $^{87}Sr/^{86}Sr$, showing that the variations in the trace element enrichment of the wedge source was created too recently to generated isotope variations.

[*Pearce et al.*, 2001], an alternative is that these heterogeneities need not be related to the Bouvet plume. Instead these could be ambient heterogeneities in the upper mantle created by low-F melts. They have many of the same characteristics as the E-MORB described by *Donnelly et al.* [2004] from the North Atlantic and elsewhere.

In agreement with the Mariana data, there is only a small effect of the enrichment on the TiO_2 concentrations of the source, since TiO_2 vs. H_2O shows a simple correlation independent of source enrichment, as indicated by Nb/Zr (see Figure 22b), and much of the range in TiO_2 can occur for all degrees of enrichment. Therefore, for both Mariana and Scotia basins the moderately incompatible element abundances seem little affected by the enrichment processes that are so dominant for the highly incompatible HFSE. This supports the low-F melt hypothesis for the origin of these enrichments—recent for the Mariana basin, ancient for the Scotia basin.

While the amount of enrichment by low-F melts is most evident for the Scotia and Mariana samples, there is also evidence for this component in the data from the other back-arc basins. All back-arc shows large variations in Nb/Zr ratio with Nb content, and these steep trends are not consistent with melting models. The steep trends can be quantitatively accounted for by a spectrum of sources created by low-F melts mixing with sources that have been slightly depleted by previous melt extraction. Figure 21 demonstrates the efficacy of this model for the overall source variations.

It is noteworthy that all back-arc basins show the evidence of source heterogeneity created by low-F melt addition; for the Marianas in particular, this addition must be a very recent phenomenon, not an ancient heterogeneity. The ubiquitous presence of an "OIB-like" enriched component in back-arcs, and evidence for its recent generation, supports deep low-F melting of slabs as an important agent of mantle heterogeneity [*Donnelly et al.*, 2004].

What is critical for a discussion of major element variations in this context is that the observed source heterogeneity is created by movements of very small quantities of melt. This leads to large changes in abundances of incompatible elements, but insignificant changes in SiO_2, MgO, and FeO and modal mineralogy and only small changes in TiO_2. Therefore despite the robust evidence for source effects, it still appears possible to evaluate melting models by using small and quantifiable source variations for the less incompatible elements.

5.2. Coupled Variations of Major Elements and Water

The classic diagram that has been used for understanding back-arc basins is TiO_2 vs. H_2O [*Stolper and Newman*,

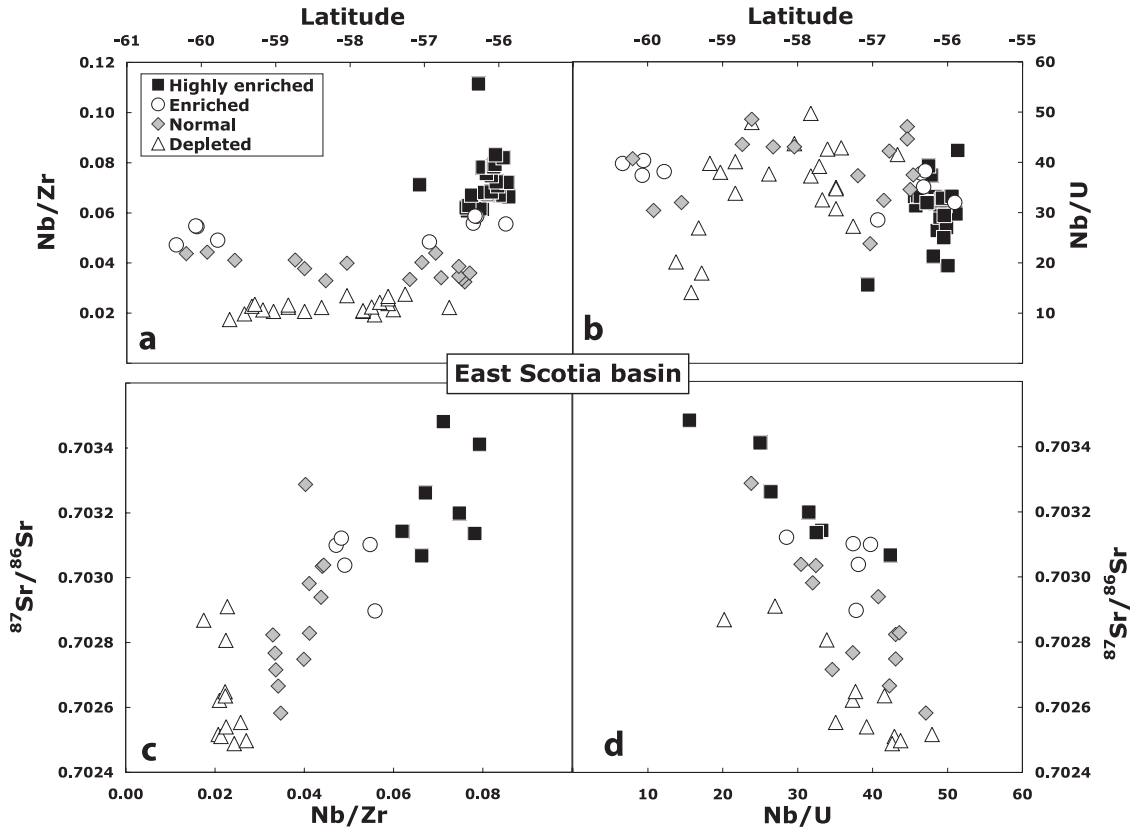

Figure 20. Spatial distribution of heterogeneity in the Scotia Basin, In contrast to the Mariana Basin, enrichment and depletion are organized spatially with enrichments occurring at the northern and southern ends of the basin (a, b). Furthermore, isotopes and conservative trace elements correlate for Scotia samples, in contrast to the Marianas (c). (a) Nb/Zr ratio and (b) Nb/U ratio vs. latitude; (c) $^{87}Sr/^{86}Sr$ vs. Nb/Zr ratio and (d) $^{87}Sr/^{86}Sr$ vs. Nb/U ratio. Enriched compositions are found in the northern and southern end of the ridge (high Nb/Zr), while the center of the basin is characterized by depleted compositions. See discussion in text.

1994]. This diagram for the five back-arc regions we investigate using our fractionation-corrected values is presented in Figure 22. All of the back-arcs show negative correlations, and the correlations are improved if consideration of slight source variations are taken into account. Depleted samples from the Mariana trough have slightly lower $Ti_{8.0}$ than other samples. The samples from rifts and seamounts in the Manus Basin create scatter for the data as a whole, while the Manus Spreading Center samples produce a clear linear trend. Despite important differences in detail, these results generally correspond with similar diagrams presented by *Kelley et al.* [in press]. The exceptions are for the Lau Basin samples. The very good correlation they present for the southern Lau spreading center is owing to unpublished melt inclusion data from off-axis seamounts. It is an open question whether mixing of seamount and ridge data leads to reliable systematics for back-arc melting models—it would not, for example, for open ocean ridges. We present seamount data with separate symbols. They also combine the Intermediate Lau and Central Lau Spreading centers with the Mangatolu triple junction samples, and we keep these ridges in separate groups. There is complete agreement, however, among all publications, and independently of sample selection, sample grouping, data quantity, and fractionation correction—TiO_2 vs. H_2O form linear trends that are negatively correlated.

Other major elements show as clear or clearer systematics. Figure 23 presents the well-defined linear trends of $Fe_{8.0}$ and $Ti_{8.0}$ that are present for all spreading center samples from back-arcs, a result noted by *Taylor and Martinez* [2003]. Noisier positive correlations are present for $Na_{8.0}$ vs. $Fe_{8.0.}$ (Figure 24). $Fe_{8.0}$ correlates well and negatively with $H_{8.0}$ (Figure 25). $Na_{8.0}$ correlates less well with $H_{8.0}$ (Figure 26).

The various back-arc basins thus have shared systematic relationships among elements. There are significant offsets in

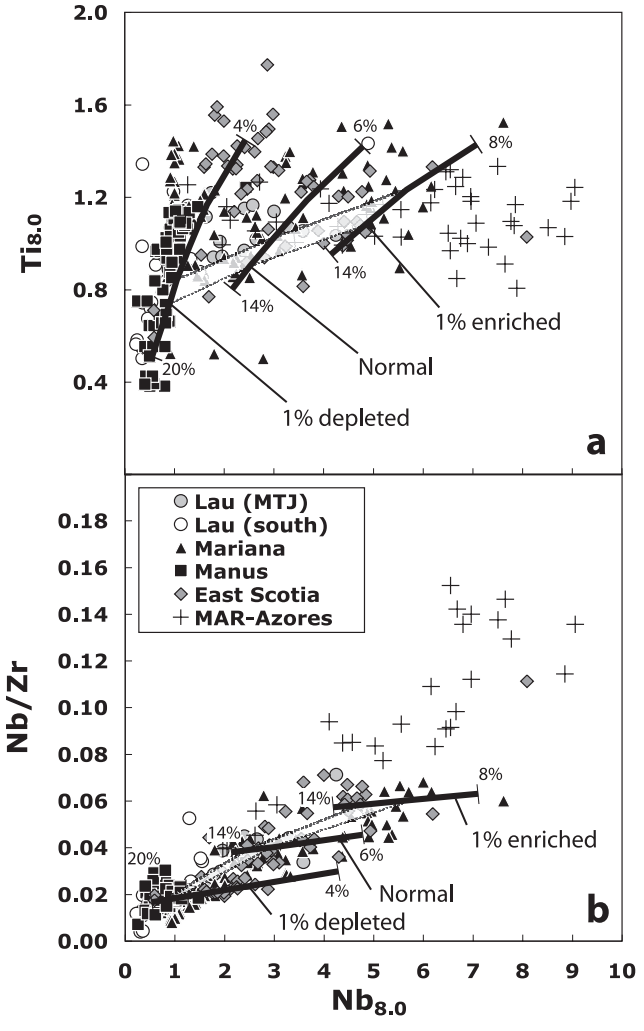

Figure 21. (a) $Ti_{8.0}$ vs. $Nb_{8.0}$ and (b) Nb/Zr vs. $Nb_{8.0}$ for individual samples from all the back-arcs. All data points are corrected for wet differentiation. Melting models for three different sources are shown. The normal source is that of *Salters and Stracke* [2004]. Depleted source is the residue from 1% melting of the *Salters and Stracke* [2004] source, using Ds for Nb, Zr, and Ti of 0.006, 0.03, and 0.04, respectively. Enriched source is created by addition of a 1% low-F melt to the *Salters and Stracke* [2004] source. Solid black curves are for varying extents of melting of the respective sources. The light band shows how the overall trend of the back-arc data is consistent with lower degree melts of a diversity of sources appropriate for Scotia and Mariana and higher degree melts of more depleted sources for Manus and Lau.

the absolute values, however. Lau and Manus samples have very low $Ti_{8.0}$, $Zr_{8.0}$,and $Na_{8.0}$, which goes along with their very low values of Nb. As originally pointed out by *Klein and Langmuir* [1987], Marianas and Scotia basins generally have low $Fe_{8.0}$ and high $Na_{8.0}$, while Lau has low $Na_{8.0}$ and high $Fe_{8.0}$.

5.3. Evidence for Enrichment of Na_2O in the BABB Source

The TiO_2 vs. Na_2O relations place constraints on the relative behavior of the two oxides. There is an overall positive correlation between $Na_{8.0}$ and $Ti_{8.0}$ for back-arc segments (Figure 27), and all of the segment averages are offset relative to the reference for open ocean ridges. The offset is to lower TiO_2 or higher Na_2O. During melting of the mantle at the shallow pressures indicated for back-arcs by the major elements and Dy/Yb ratios, the partition coefficient for Na_2O is lower than that for TiO_2. In this case, depletion caused by melting would lead to a larger depletion in Na than Ti and to a data array that is similar to MORB, or slightly offset to lower Na values for a given Ti, as shown in Figure 27. The observations show the opposite effect. Another aspect of the data systematics is that the back-arc array for $Na_{8.0}$ vs. $Ti_{8.0}$ intersects the $Na_{8.0}$ axis. Ordinarily this result would require a higher partition coefficient for Na than Ti, a result that is not in accord with the experimental data. These observations can be explained by Na addition through the fluid component. The more depleted the source, the greater the relative Na enrichment by the fluid, leading to high relative Na/Ti ratios in the source. A correspondence between TiO_2 source depletion and high Na/Ti ratios would lead to the observations, where the data array as a whole intersects the $Na_{8.0}$ axis.

The source enrichment of Na_2O also explains the less good correlations between $Na_{8.0}$ and water (Figure 26), and between $Na_{8.0}$ and $Fe_{8.0}$, than between $Ti_{8.0}$ and $Fe_{8.0}$ (see Figures 23 and 24). $Na_{8.0}$ will decrease in the melt with increasing extents of melting as water is added but will also rise as the Na is added by the hydrous fluid. This also leads to a higher intercept on the water axis or on the $Na_{8.0}$ vs. $H_{8.0}$ diagrams compared with the $Ti_{8.0}$ vs. $H_{8.0}$ diagrams (Table 4).

Na may also be slightly enriched by the OIB-like enriching component. Close inspection of the Marianas and Scotia $Na_{8.0}$ vs. $Fe_{8.0}$ diagrams shows that the enriched source samples are slightly offset to higher Na relative to samples from the depleted source for the same $Fe_{8.0}$.

Since there are good constraints on the TiO_2 contents of the back-arc basin sources from the modeling of HFSE, one can then constrain the source contents of Na_2O quantitatively from the TiO_2 vs. Na_2O correlations, as discussed in a later section.

6. DATA SYNTHESIS

Each of the back-arc basins has distinct characteristics in terms of tectonic history and source variations, and therefore each one has a unique story to account for the data and its distribution in physical and compositional space. Important observations and interpretations have been explored in the specific papers devoted to each basin (see references in

Appendix). There are also general characteristics particularly pertinent to the understanding that is the aim of this paper.

We have gone to substantial effort to make fractionation corrections that take into account the effects of water on plagioclase suppression and the evolution of the liquid line of descent, and thereby to remove these effects from the values normalized to 8 wt.% MgO, so that these values are directly comparable with the data from the open ocean

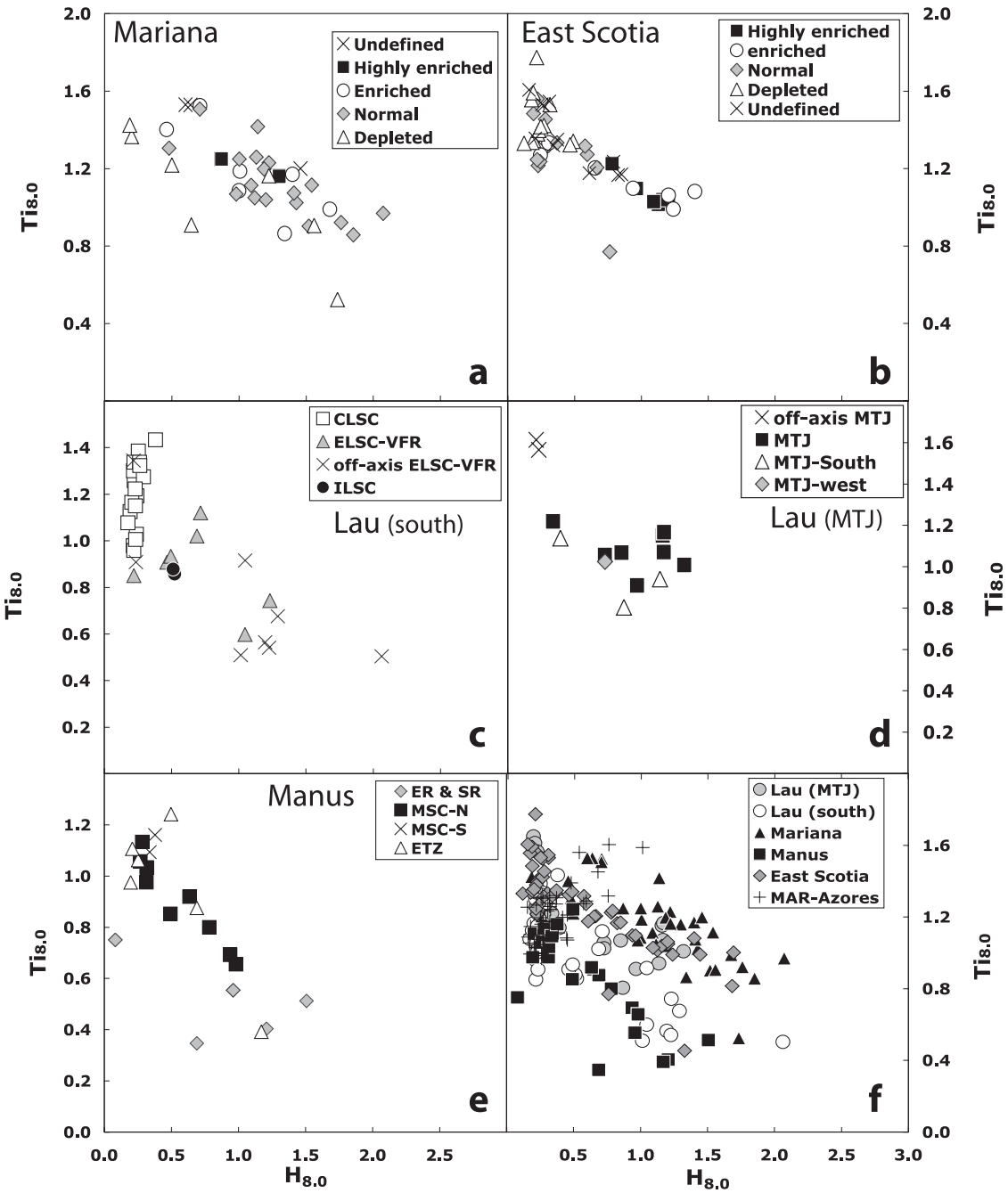

Figure 22. (a–e) $Ti_{8.0}$ vs. $H_{8.0}$ for the various back-arc basins, showing the common characteristics of roughly linear, negative correlations for the data. Note the slightly lower trend for depleted samples from the Mariana Basin and the less systematic data for Manus samples that are not associated with a spreading center (ETZ, ER, and SR samples). (f) Broad range of the back-arc basin data as a whole, with rather different water intercepts for the various back-arc basins.

ridges. This has not been done by other treatments of back-arc data [*Stolper and Newman,* 1994; *Taylor and Martinez*, 2003; *Kelley et al.*, in press] except that by *Sinton et al.* [2003]. The detailed attention to the corrections makes important differences in terms of absolute values, but the overall conclusions of these other papers are not strongly

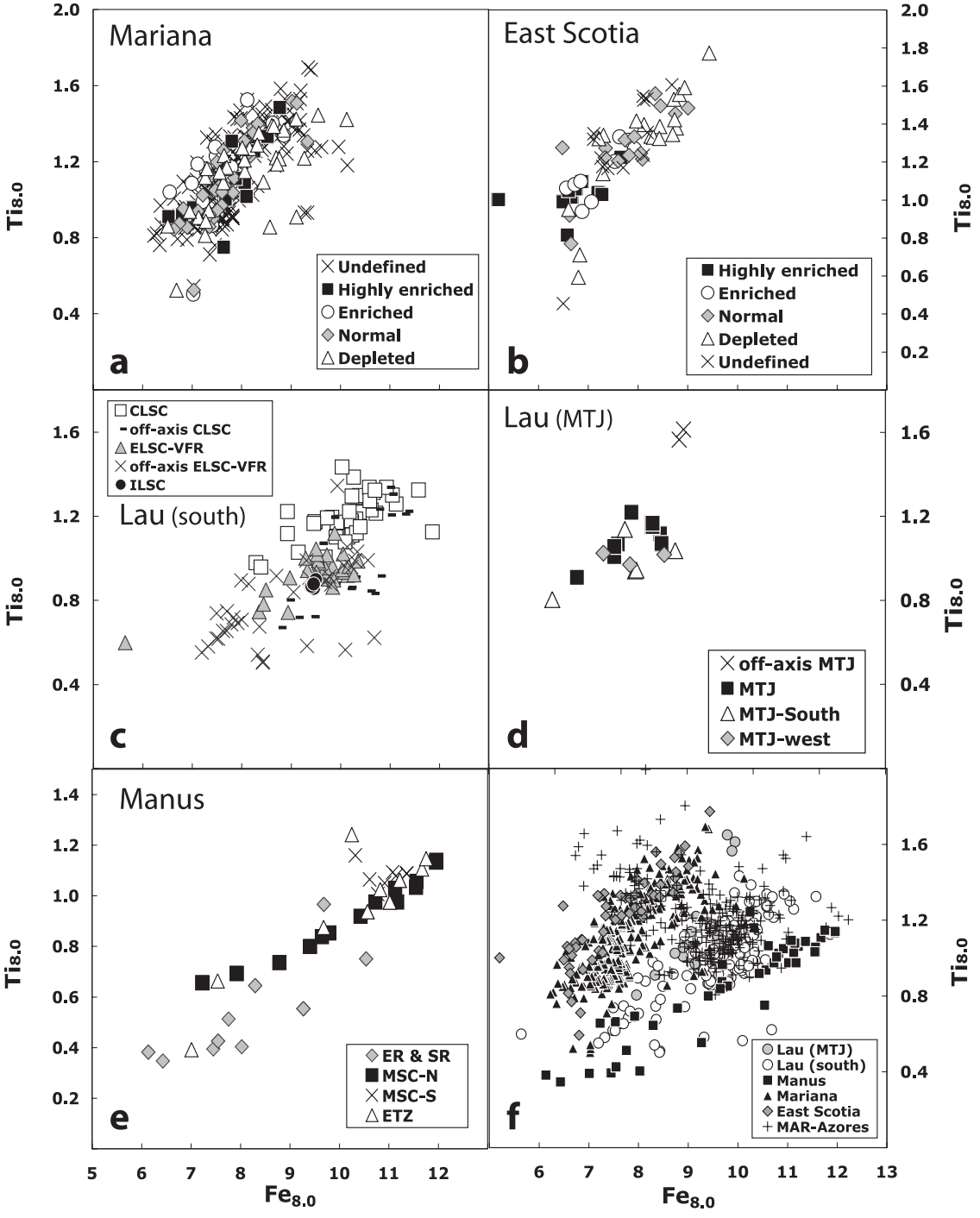

Figure 23. $Ti_{8.0}$ vs. $Fe_{8.0}$ for the various back-arc basins. Note the well-defined negative correlations for all spreading center samples. Off-axis samples from Manus and Lau are more scattered. Depleted samples from the Marianas have slightly lower $Ti_{8.0}$ on average. The very large variations in $Fe_{8.0}$ for each basin place significant constraints on the origin of these trends.

affected by the different methods of fractionation correction. For example, we find the same positive correlations of $Fe_{8.0}$ and $Ti_{8.0}$ in our treatment that were presented by *Taylor and Martinez* [2003], who did not take into account explicitly the effects of water on the liquid line of descent, and confirm *Kelley et al.'s* demonstration of the generality

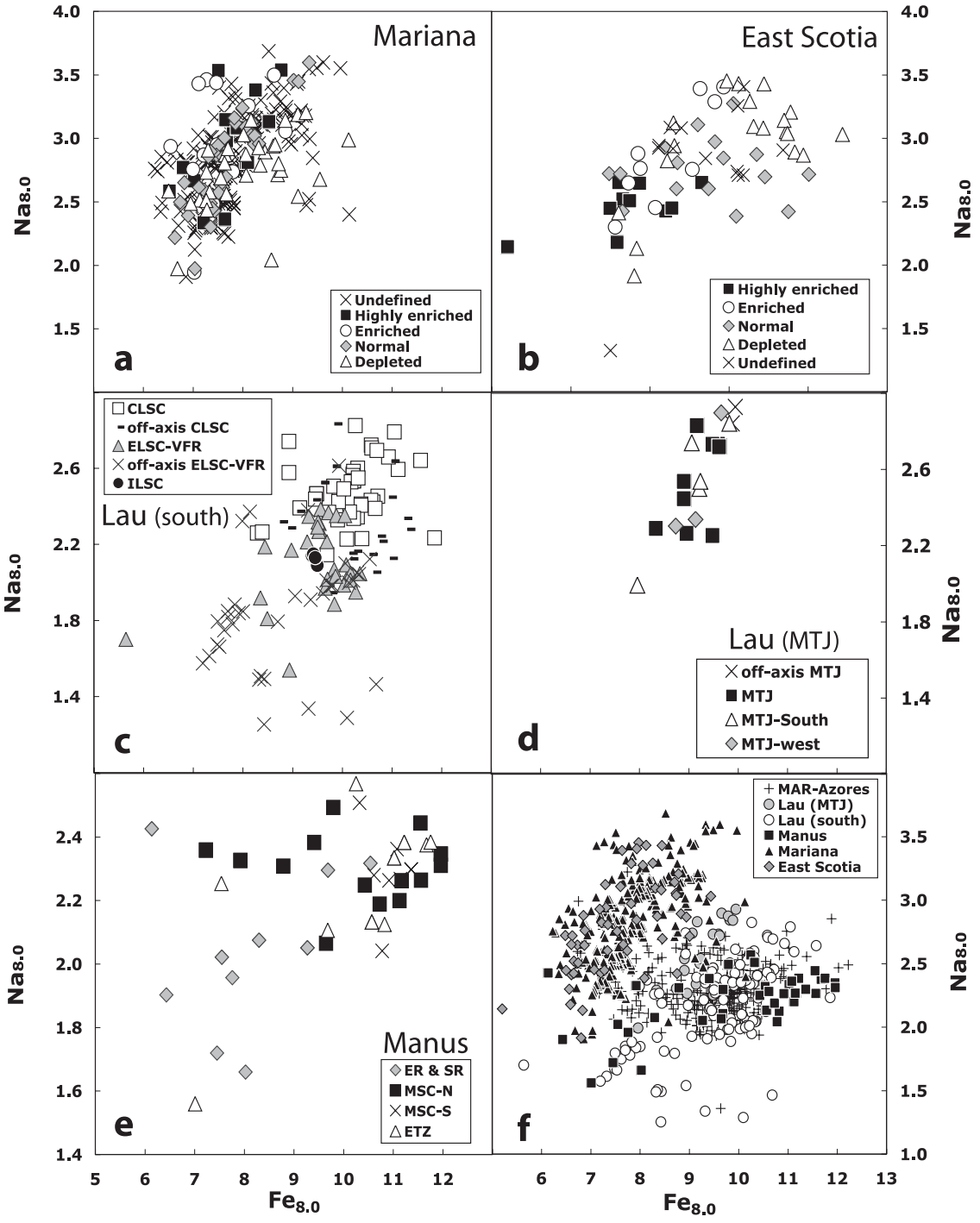

Figure 24. $Na_{8.0}$ vs. $Fe_{8.0}$ for the various back-arc basins. Correlations are negative but less well defined than $Fe_{8.0}$ vs. $Ti_{8.0}$ (see Figure 23). See discussion in text.

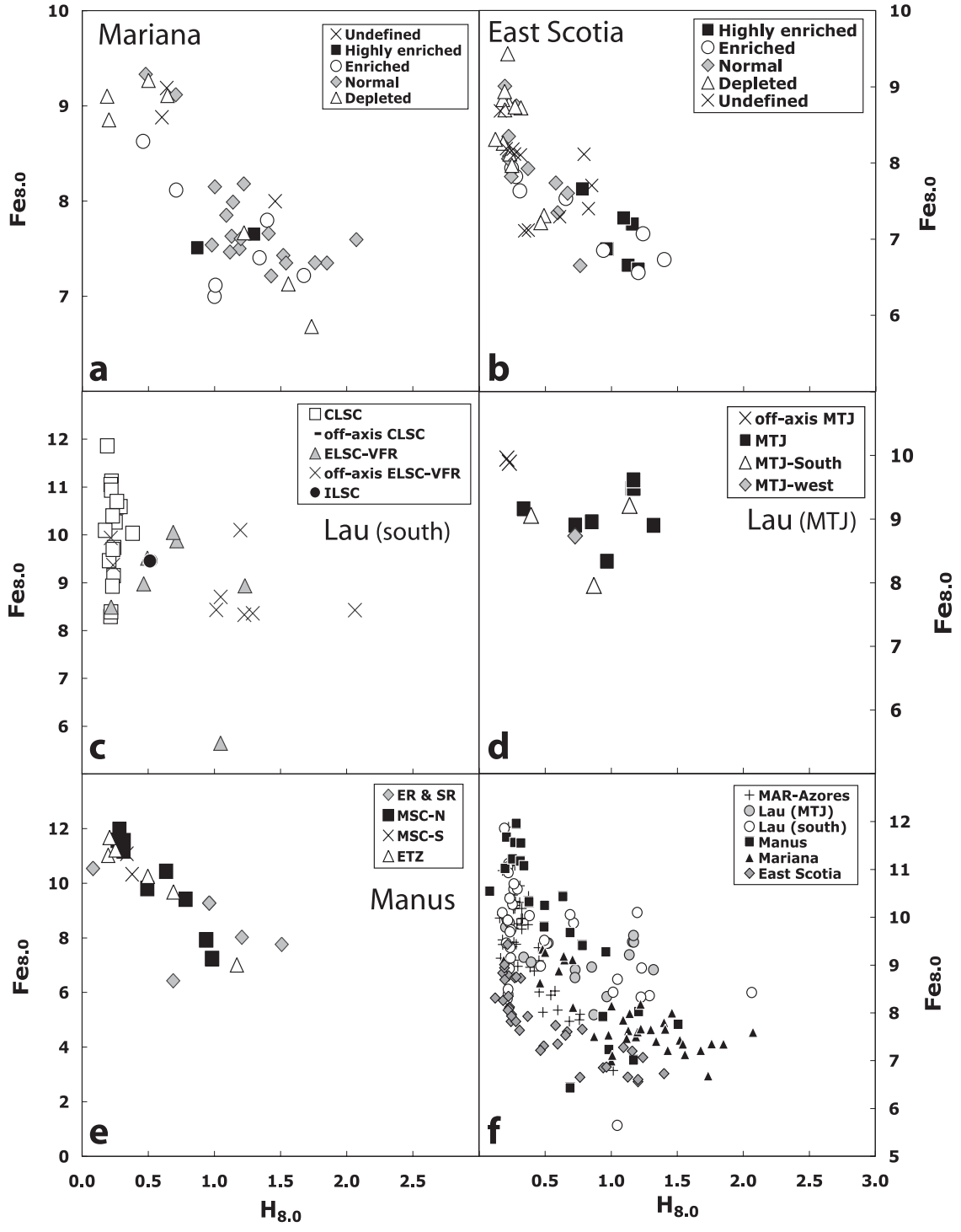

Figure 25. $Fe_{8.0}$ vs. $H_{8.0}$ for the various back-arc basins. Good correlations exist for the Mariana, Scotia, and Manus Basins. For the Lau Basin, a disproportionate number of samples are from off-axis locations, and there are large variations at low water content for the Central Lau spreading center. Note that the Mariana data show a negative correlation for $Fe_{8.0}$ vs. $H_{8.0}$ independently of enrichment of the mantle wedge in terms of Nb/Zr, showing that Fe and H_2O variations are reflecting the addition of a hydrous component that is independent of wedge composition, as also evident from Figure 19.

of the negative TiO_2 vs. H_2O correlations. This shows the overall robustness of the differences between BABB and basalts from other ridges.

Several aspects of the data are of particular import and must be accounted for by a comprehensive model.

First, the systematics of back-arc basin basalts contrast with the results from the Azores and Galapagos, two regions on normal ridges where water enrichment is observed. Water in the back-arc and open ridge environment has the opposite effects on extent of melting. Away from back-arc basins,

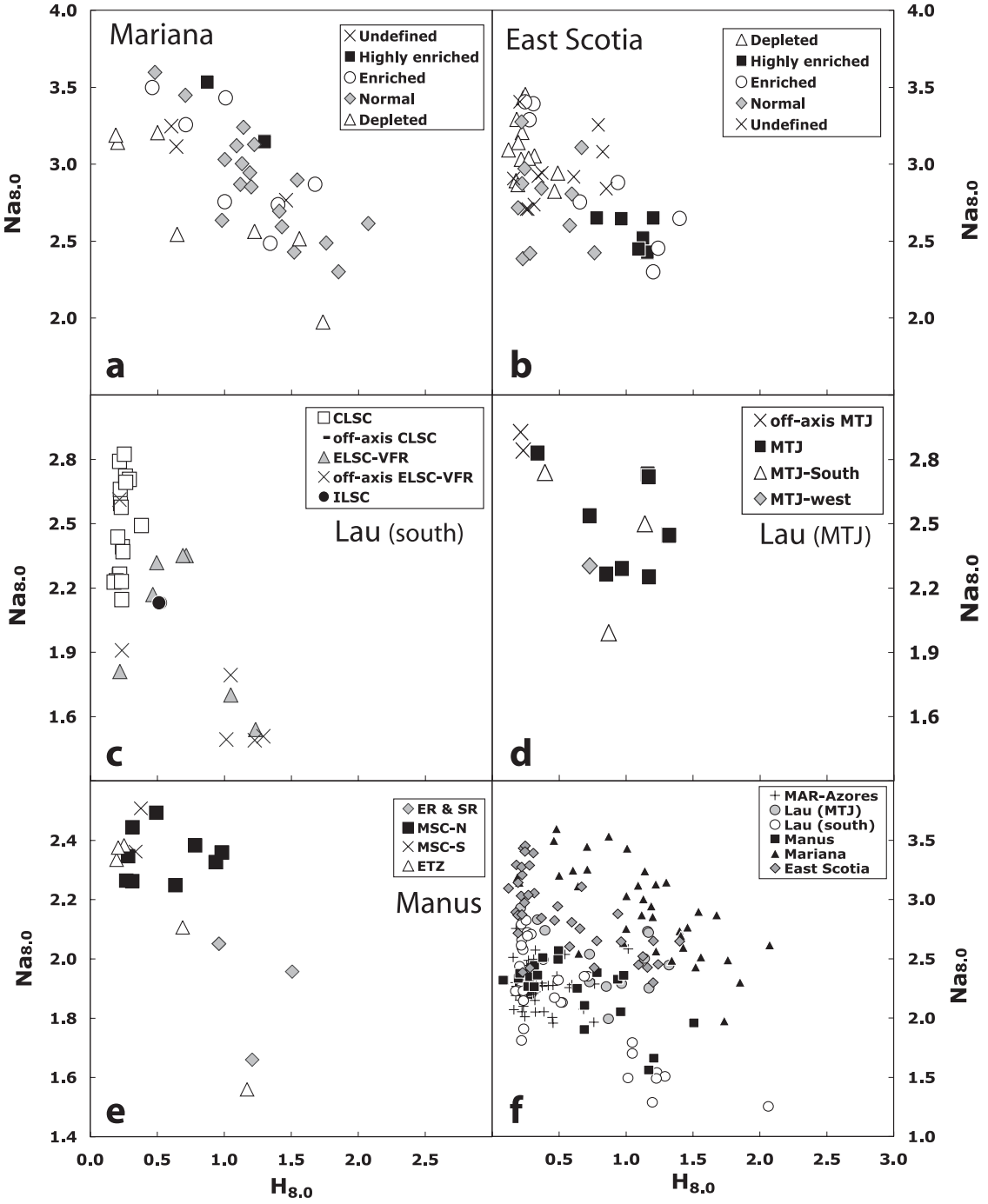

Figure 26. $Na_{8.0}$ vs. $H_{8.0}$ for the various back-arc basins. See discussion in text.

increased water leads to a deepening of the melting regime, a decreased mean extent of melting, and an increased garnet influence on the erupted basalts. This is reflected in positive correlations between $Ti_{8.0}$ and $H_{8.0}$, and a positive correlation between the Dy/Yb ratio, which is sensitive to the presence of garnet, and $H_{8.0}$. In all of the back-arc basins, however, there is an inverse relationship between Ti and water.

Figure 28 shows that back-arc basin basalts have constant Dy/Yb ratios with increased water content. For those back-arc basins where the extent of melting is smaller, the ratio is slightly higher, as is also observed for other spreading centers. Since the incremental addition of water produces no change in Dy/Yb, increased water in back-arc basins does not lead to melt production and removal at depths where garnet is a stable phase, greater than roughly 60 km. Such an absence of garnet influence is also reflected in the U-series data [*Peate et al.*, 2001]. Back-arcs generally have very little of the ^{230}Th excess that is characteristic of melting at open ocean ridges. This is a fundamental constraint on models. In back-arc basins, water leads to increased extent of melting, and both major and trace elements show no evidence for a deep "tail" of melting in the garnet regime. In principle it is possible that the mantle composition is sufficiently depleted that garnet is no longer present, or that melting is not fractional so that melt remains with its residue and is extracted only at shallow levels. Or possibly, melt channeling focuses melting such that garnet is absent. These special circumstances would render the garnet invisible. While deep melt generation may not be definitively excluded, there is no evidence for it.

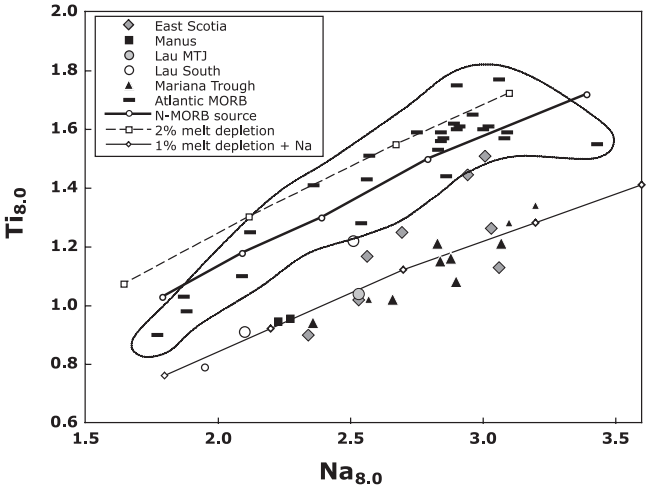

Figure 27. $Ti_{8.0}$ vs. $Na_{8.0}$ for segment averages using wet fractionation corrections. Horizontal dashes, Atlantic MORBs [Langmuir *et al.*, 1992]; triangles, Mariana Trough segments; squares, Manus basin segments (SR and ER rifts excluded); circles, southern Lau (without off-axis samples); filled circles, Mangatolu triple junction average; diamonds, East Scotia segment averages. Small symbols are for averages for only two samples. BABB segments are offset to low $Ti_{8.0}$ for a given $Na_{8.0}$ compared to MORB. The bold line is for different extents of melting of a normal MORB source with 0.27 wt.% Na_2O and 0.15 wt.% TiO_2. The dashed line is for a source with 2% melt depletion, using equilibrium nonmodal melting, with a D of 0.04 for TiO_2 and 0.025 for Na_2O. Note that source depletion alone does not move the calculations towards the back-arc basin data. The light solid line is for 1% melt depletion plus Na enrichment. Note also that extrapolation of the back-arc basin data would intersect the Na axis, suggesting a higher partition coefficient for Na than Ti—which is not in accord with experimental data. These data suggest that back-arc basins have undergone both melt depletion and Na enrichment. Addition of 0.07 wt.% Na_2O to a depleted source produces the back-arc basin trend for hydrous segments (thin line). Note that individual segments also contain a range of sources, since segments usually contain both high- and low-H_2O samples.

A second important general result concerns the mean compositions of back-arc basin segments. Figures 27 and 29 show that the back-arc basin segments have distinct relationships among the major elements, and Figure 30 shows the distinct relationships between major elements and depth compared to other ridges. $Fe_{8.0}$, and $Ti_{8.0}$ are low relative to the depth of the ridge segments. $Na_{8.0}$ is also significantly enriched relative to $Ti_{8.0}$, and the $Fe_{8.0}$ vs. $Na_{8.0}$ data are offset to significantly lower values.

Third, as shown above, individual samples and segment averages both define positive slopes on plots of $Na_{8.0}$ vs. $Fe_{8.0}$ and $Fe_{8.0}$ vs. $Ti_{8.0}$ for every basin. This contrasts with normal ridges, where individual samples from slow spreading ridges may define such "local vectors", but segment averages do not [*Klein and Langmuir*, 1989; *Langmuir et al.*, 1992; *Niu and Batiza*, 1997]. For BABB, the higher the water content of individual samples, the lower the $Na_{8.0}$, $Fe_{8.0}$, and $Ti_{8.0}$. In addition to having high water contents, low-$Ti_{8.0}$ samples often have high $Si_{8.0}$. Significantly, *all of these relationships are linear*, and models that account for them must have linear systematics. The simplest such model is mixing, which produces straight lines on these diagrams.

Fourth, although hot spots are not in the immediate vicinity of back-arc basins, Scotia, Manus, and Mariana all are influenced by enriched components that are not ordinarily attributed to a subduction setting. Most back-arcs are influenced by both" arc-like" and "OIB-like" enrichment components (e.g., see Figure 17). The prevalence of enriched components far exceeds that observed on most ocean ridges far from hot spots. Addition to wedge sources of low-F melts accounts well for the incompatible trace element systematics. For the Mariana back-arc basin, this addition was very recent, suggesting it accompanies the subduction process and is not inherited from the mantle wedge or ancient lithosphere. While this effect is important for the highly incompatible elements, and would influence any calculations of a "sub-

duction component", it has only small effects on TiO_2 and no significant effect on FeO; therefore, melting models can still be evaluated with these elements.

Finally, Na_2O and TiO_2 have a different relationship in back-arcs than in Atlantic and Pacific ridges. Some of this difference can be accounted for by slight TiO_2 depletions in some back-arc sources, but not all back-arcs show this effect. All the back-arc basins we have investigated show evidence for Na_2O enrichment in the mantle source, presumably carried by the hydrous fluid. Such enrichments need to be taken into account when comparing back-arc to open ocean ridges.

These observations constrain the origin of back-arc basin ridges, and indicate significant contrasts with ridges in the open ocean. Our task is then to develop a coherent model that explains the major and trace element variations, their relationships to water content, and the different relationships between tectonic variables such as axial depth and crustal thickness as compared with open ocean ridges.

7. QUANTITATIVE MODELING OF THE EFFECTS OF WATER ON MANTLE MELTING

Interpretation of the back-arc data hinges on modeling of hydrous melting of the mantle. A difficulty is that calculations of hydrous mantle melting do not show good agreement by different methods. While all agree that water enhances melting, *Hirschman et al.* [1999] and *Gaetani and Grove* [1998] calculate that water has a greater effect on melting at higher temperatures. *Katz et al.* [2003] do not find this effect. Quantitative interpretation of the back-arc data requires a resolution of these discrepancies.

The significance of water to mantle melting is its pronounced influence on the melting temperature (Figure 31). This strong effect of water is one of the great contributions of classical igneous petrology (e.g., *Yoder and Tilley* [1962]; *Burnham and Davis* [1971]; *Mysen and Boetcher* [1975]). There have been several attempts to model quantitatively the effects of water on mantle melting [*Gaetani and Grove*, 1998, 2003; *Hirschmann et al*., 1999; *Asimow and Langmuir*, 2003; *Katz et al*., 2003; *Asimow et al*., 2004; *Smith and Asimow*, 2006]. While some of these approaches are quite complex, for example the MELTS program, the essentials of the water effect are straightforward. For liquid compositions similar to mantle melts there is a monotonic relationship between the amount of water added and the drop in liquidus temperature (Figure 32). An important aspect of this relationship is the large apparent changes in liquidus temperature with small amounts of water, and a more moderate effect with larger amounts of water, results that may have to do with water speciation (e.g., *Stolper* [1982]). *Asimow and Langmuir* [2003] modeled this relationship with a step change at 0.75% water. *Katz et al.* [2003] adopted a single function for the relationship:

$$\Delta T(X_{H2O}) = K * X_{H2O}^{\gamma},\ 0<\gamma<1 \qquad (11)$$

Figure 32 shows that the coefficients of the Katz equation capture the overall trajectory of the data but do not provide a good fit for the lower water contents appropriate to studies of back-arc basins. Therefore we have adopted an equation that fits the lower water content data:

$$\Delta T(C_L^{H2O}) = 60 * (C_L^{H2O})^{0.54} \qquad (12)$$

As discussed at length by *Katz et al.* [2003], calculation of the effects of water is then quite straightforward. The amount of water in the liquid is controlled by the source abundance and the extent of melting through the batch or fractional melting equations (see equation (1)). The D for melting of water is well constrained by its analogous behavior to Ce in oceanic ridge basalts [*Michael*, 1988] and

Table 4. Slopes and intercepts for $Na_{8.0}$ vs. $H_{8.0}$ and $Ti_{8.0}$ vs. $H_{8.0}$ correlations obtained using the reduced major axis linear regression method.

Diagram:	$Na_{8.0}$-$H_{8.0}$		$Ti_{8.0}$-$H_{8.0}$	
Back-arc basin	Slope	Intercept	Slope	Intercept
Lau ELSC-VFR	-1.01	2.70	-2.00	2.40
Lau MTJ	-1.22	3.92	-2.61	3.64
Manus	-1.60	4.19	-1.50	1.84
East Scotia	-1.18	3.90	-1.87	2.95
Mariana	-1.22	4.66	-2.06	3.50

Fitted datasets are from Figures 26 and 22, respectively. Note that all the water intercepts for $Na_{8.0}$ are higher than for $Ti_{8.0}$, which suggests that Na is added with the hydrous fluid to back-arc basin sources. See discussion in text.

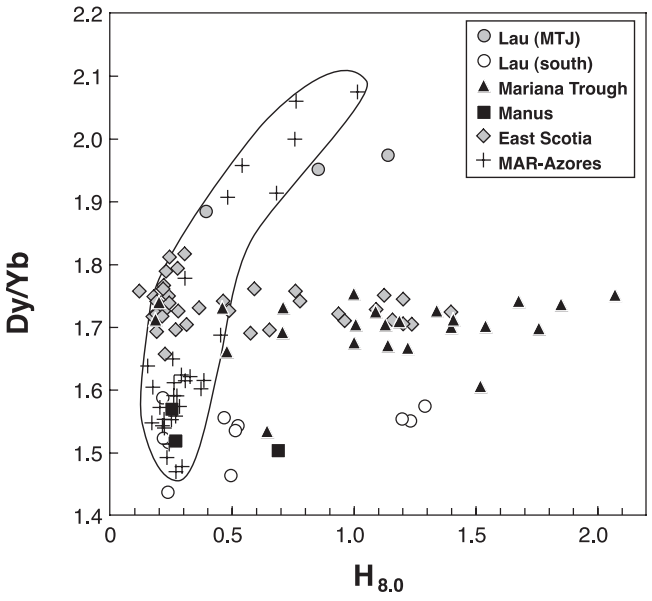

Figure 28. Dy/Yb vs. $H_{8.0}$, showing the lack of fractionation between middle and heavy rare earth elements in water-rich BABB samples. The lack of Dy/Yb variation with increasing water content indicates there is no significant melt extraction in the presence of garnet, which is stable at high pressures. This places depth and source constraints on hydrous melting for back-arc basin melting regimes. See discussion in text.

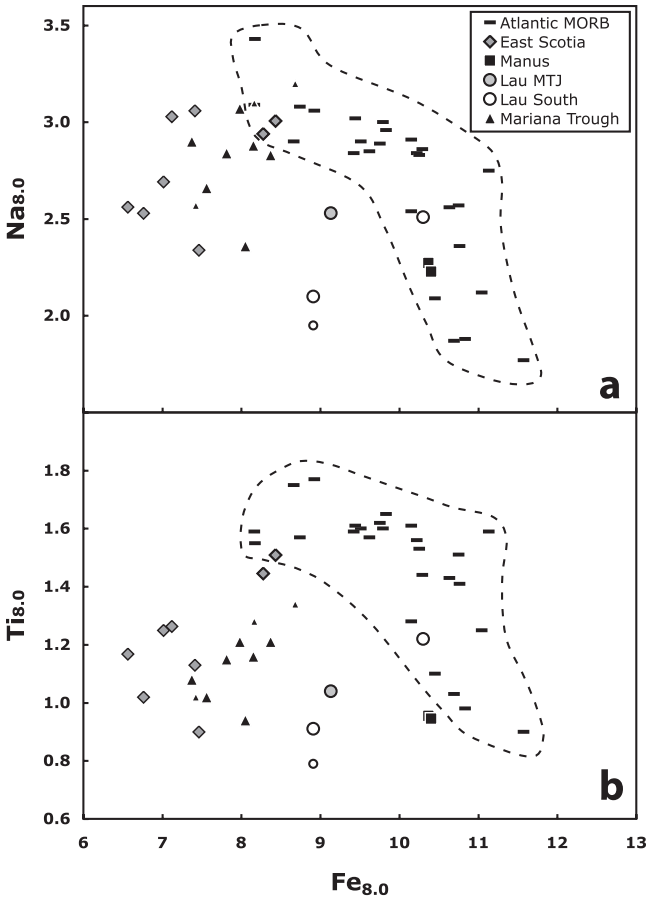

Figure 29. (a) $Na_{8.0}$ vs. $Fe_{8.0}$ and (b) $Ti_{8.0}$ vs. $Fe_{8.0}$ for back-arc basin ridge segment averages using hydrous fractionation corrections. See Table 3 for segment definitions and segment averages. Segments in the open ocean MORB field generally have low water contents. For each basin, the segment averages are broadly orthogonal to the global trend. Low $Fe_{8.0}$ is associated in BABB with low $Ti_{8.0}$ and $Na_{8.0}$. The Manus Basin segments do not show such a trend because the eastern and southern rifts are not included on these diagrams (they are not developed spreading centers). Small symbols are averages for two samples.

recent experimental data [*Aubaud et al.*, 2004] to be about 0.01 (see Figure 1).

A remarkable aspect of the effect of water on melting is that water appears to lower the temperature of melting without causing changes in the relative compositions of the other elements apart from the dilution caused by addition of water. This has been established for the compositions of mantle melts [*Hirose and Kawamoto*, 1995] and also for the partitioning of Fe and Mg between olivine and liquid [*Gaetani and Grove*, 1998]. *Gaetani and Grove* [2003] suggest that the normative olivine content of natural liquids decreases with increasing water content, and they also show that the change lies on an olivine control line. In this case, the effect would not be apparent in lower MgO liquids. Thanks to this aspect of the influence of water, the calculation of the effects of water on mantle melting is straightforward. For any given dry temperature and pressure of melting, the effect of water is to lower the liquidus temperature of the melt, which can be determined from equation (12). The magnitude of the temperature drop depends on the water content of the liquid, which can be calculated from equation (1), and hence depends on the water content of the source, C_0^{H2O}, and the extent of melting, F. This means that in a partially molten system, the effect of adding water at a constant temperature is to raise the temperature of the fluid above its liquidus (by lowering the liquidus), analogous to raising the temperature at constant water content. Thus isothermal addition of water leads to increased melting.

To determine the amount of increased melting, it is necessary to know the relationship between extent of melting (F) and T and P. There is substantial data to evaluate this relationship, of which perhaps the best are the extensive experimental studies carried out on bulk-composition MM3 (see caption to Figure 33). The data relating T and F at a pressure of 10 kb are shown in Figure 33, along with a simple parameterization that fits these data well.

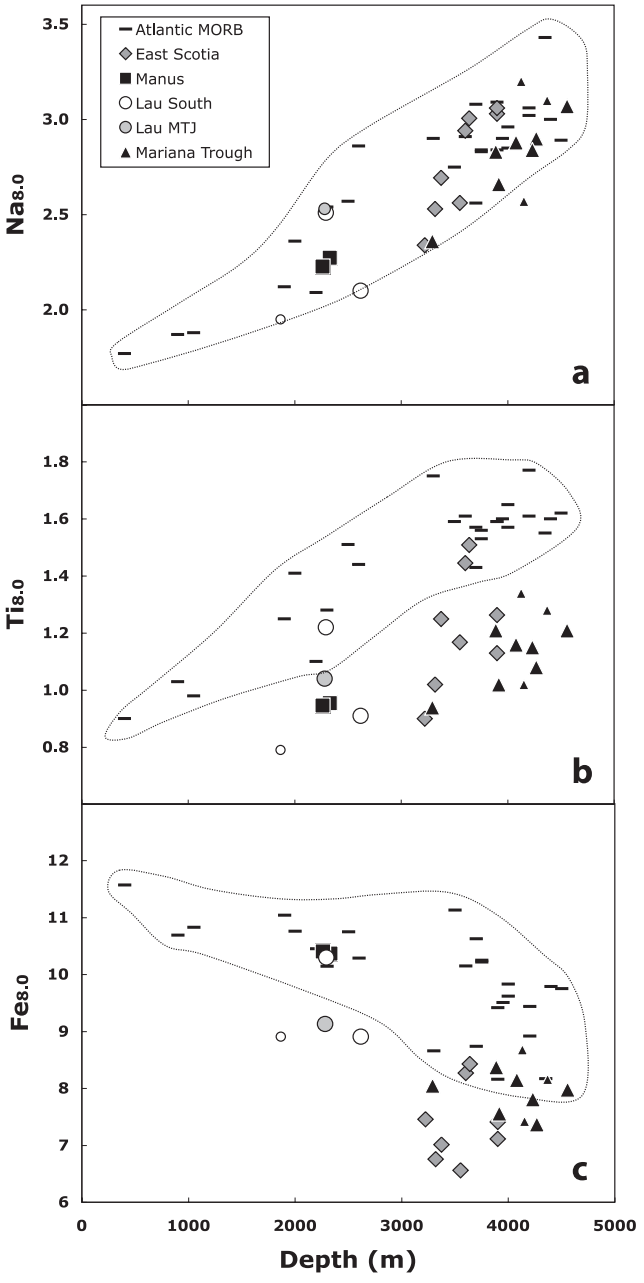

Figure 30. $Na_{8.0}$, $Fe_{8.0}$, and $Ti_{8.0}$ vs. ridge axial depth for back-arc basin segment averages (corrected for hydrous fractionation). See Table 3 for segment definitions and segment averages. Larger symbols are segment averages with more than two samples. Smaller symbols are for one or two samples. Depths are average depths for the segment. The BABB systematic in $Na_{8.0}$ vs. depth does not show any differences compared to MORB, while $Ti_{8.0}$ and $Fe_{8.0}$ are in the MORB field for the segments least affected by water and are shifted toward low $Fe_{8.0}$ and $Ti_{8.0}$ for a given depth for segments that contain hydrous samples.

$$T(F) = 1235 + 539F \quad (13)$$

To determine the extent of melting for given source of water content, pressure, and temperature is then a matter of balancing the temperature change needed to melt the amount F with the temperature made available by the drop in liquidus temperature, caused by the amount of water in the liquid. That is, for a given T and P in a dry system,

$$T(F) - T = \Delta T(C_L^{H2O}) \quad (14)$$

Rearranging equation (14), and substituting equations (1) and (12) for $\Delta T(C_L^{H2O})$, we can write for P = 10 kb,

$$T = 1235 + 539 * F - 60 * \left(\frac{C_0^{H2O}}{\left(D*(1-F)+F\right)}\right)^{0.54} \quad (15)$$

From equation (15) we can obtain F as a function of C_0^{H2O} for any T.

Equation (15) is a reformulation of equation (19) of *Katz et al.* [2003], relaxing the constraint of having an equation for T(F) that applies from solidus to liquidus (this is not necessary because we are dealing always with small extents of melting where there are good experimental calibrations) as well as the constraint of having a single equation that applies to both low and very high water contents. This permits us to calculate with greater accuracy the conditions specific to back-arcs.

In the following figures we present the results in terms of $T - T_o$, where T_o is the dry solidus temperature at the given pressure. This is convenient because there can be absolute temperature differences that result from differences in the parameterization of the solidus, T_0, as a function of pressure. For example, *Hirschman et al.* [1999] note that the MELTS calculations generally lead to temperatures that are 100°C too high (e.g., see Figure 33a), and the *Katz et al.* [2003] equation for the solidus gives temperatures that are some 50°C too low relative to the solidus equation of *Hirschman et al.* [1999], because of the inclusion of compositions more fertile than the primitive mantle in the calibration data base. Thus, in comparing various models, it is often informative to use $T - T_0$ as the parameter with which to compare, rather than T itself.

Calculated curves for F vs. C_0^{H2O} are shown in Figure 34 for temperatures ranging from 50ºC below the solidus to 75ºC above the solidus. Note that variations in the water ΔT parameterization that encompass the entire range of experimental data shown in Figure 32 lead to very small changes in these curves, and hence the substantial noise in the T vs. C_l^{H2O} raw data is of little importance to the overall results. As apparent from the figure, there is a major contrast with the MELTS calculations (compare also Figure 4).

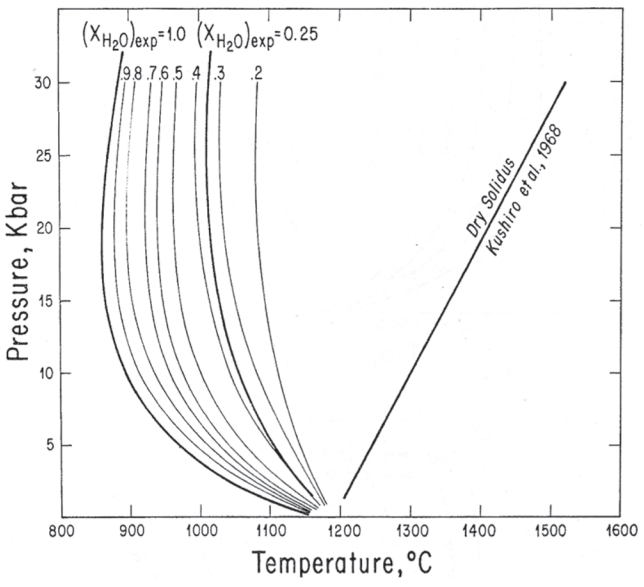

Figure 31. P vs. T diagram showing the major effect of water on the peridotite solidus (from *Mysen and Boetcher* [1975]; #239). The characteristic curvature of the water-saturated solidus results because of the increasing solubility of water with increasing pressure. As more water dissolves in the melt, the solidus temperature is progressively lowered. Note the comparatively large effects of small amounts of water, an effect similar to that observed in Figure 32.

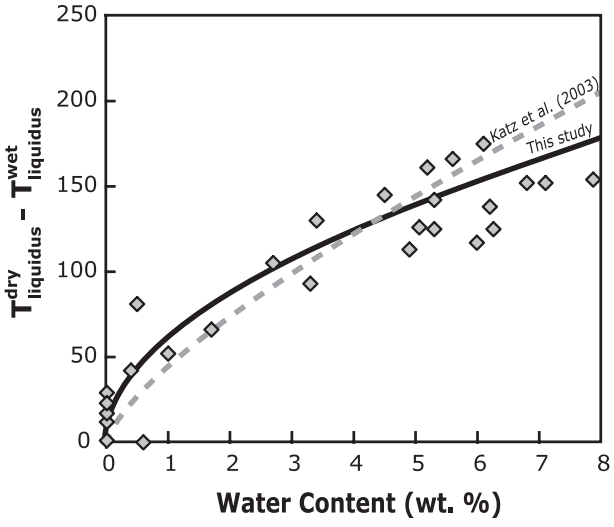

Figure 32. Calibration of the effect of water on liquidus temperature based on experiments summarized in *Katz et al.* [2003]. Dashed gray line, calibration from *Katz et al.* [2003]; solid line, calibration from this study tuned to the low water contents found in back-arc basins. Note the comparatively larger effect of water at small water contents.

What is important for the results is the T–F relationship. While Figure 33 shows a simple linear dependence for the experimental data, there is substantial controversy on this subject, since it can be argued on thermodynamic grounds that the F vs. T the relationship should not be linear [*Hirschmann et al.*, 1999]. For this reason, various authors (e.g., *Pickering-Witter and Johnston* [2000]; *Katz et al.* [2003]) have modeled data that are adequately fit by a line with a function that has decreasing dT/dF with increasing F. For bulk compositions that are not appropriate for the mantle, some of the data do show the predicted curvilinear relationship between F and T, although the curvature is slight [*Schwab and Johnston*, 2001]. Although the approximately linear relationship between T and F (Figure 33) for the anhydrous system is a characteristic of all the experimental data that have been obtained on peridotite of a composition similar to the upper mantle, to deal with the theoretical concerns we also need to consider the effects of curvilinear functions on hydrous melting.

It is important also to note that the linear T–F relationship is for anhydrous experiments. The addition of water creates a very nonlinear T–F relationship for hydrous systems, hence the "deep low-F tail" to the melting regime discussed by *Asimow and Langmuir* [2003] and *Gaetani and Grove* [2003]. A strongly curved T–F relationship is intrinsic to hydrous melting. The controversy applies to the anhydrous baseline experiments.

The low-F tail produced by the addition of water could also be produced by addition of other low-melting compounds, such as Na_2O and K_2O, as discussed by *Gaetani and Grove* [1998, 2003]. For fertile mantle composition such as MM3, this appears to be restricted to less than 2% melting. To determine whether this is important, we modified our calculations so that equation (13) applies down to 2% melting, and at less than 2% melting, T(F) = 1195 + 2500F. This makes differences in the curves of Figure 34 only below 2% melting and is immaterial to the conclusions presented here.

7.1. Comparison to Previous Calculations of F vs. H_2O_0

There are substantial differences between the calculated results presented here and calculations previously presented by *Gaetani and Grove* [1998, 2003] and *Hirschman et al.* [1999], as is apparent in Figure 34. Because these results have substantial implications for how we understand melting in back-arc basins and more generally, in convergent margins, it is important to understand the causes of the differences, as well as which results are more likely to reflect what is actually occurring on Earth. There are three major differences between the calculated results. Our results show a substantial change in intercept with $T - T_0$, little variation in dF / dC_0^{H2O} for C_0^{H2O} greater than 0.05, and significant upward curvature. In con-

trast, the MELTS results (see Figure 4) show little change in intercept, have strongly varying slopes, and are approximately linear with C_0^{H2O}. Similar results are presented by *Gaetani and Grove* [2003], where they are compared favorably with the experimental data of Hirose and coworkers [*Hirose and Kushiro*, 1993; *Hirose and Kawamoto*, 1995]. These differences are neither minor nor small.

As emphasized by *Katz et al.* [2003], equation (15) is a general solution to the hydrous melting problem. Hence differences in the calculated results depend on the two specific parameterizations, for T(F) and $\Delta T(C_0^{H2O})$. *Hirschman et al.* [1999] and *Asimow et al.* [2001] have pointed out that MELTS predicts a strongly curved function for T(F) even for the anhydrous system. MELTS calculates high dT/dF at low extents of melting, and lower dT/dF at higher extents of melting, as apparent from Figure 6 of their paper and shown in Figure 33a. These authors emphasize that this behavior is predictable from consideration of simple systems, and thereby justify the behavior predicted by the MELTS program.

For example, a simple two-component system where water is added to the system has a freezing point depression curve with downward curvature, as illustrated in Figure 35. As *Hirschman et al.* [1999] correctly point out, in such a system the water content of the liquid specifies a temperature, which remains constant independently of the amount of water in the bulk composition (i.e., C_0^{H2O}). Since H_2O is an incompatible element, $C_l^{H2O} / C_0^{H2O} = 1/F$. Then, since C_l^{H2O} is constant for a given temperature in a binary system, C_0^{H2O}/F is constant (see Figure 35). And, since C_l^{H2O} decreases with temperature, C_0^{H2O}/F also must decrease. Therefore this simple system has behavior similar to the MELTS calculations: C_0^{H2O} vs. F is linear for constant temperature, and dF / dC_0^{H2O} increases with increasing temperature. Examples of these curves are illustrated in Figure 35. A significant aspect of this analysis of the binary system is that the dF / dC_0^{H2O} curves, independent of temperature, have a zero intercept.

Since hydrous melting depends on the form of equations (12) and (13), it is instructive to consider the form of these equations for a binary eutectic system. *Hirschman et al.* [1999] note that a binary eutectic can be readily calculated from

$$C_l^{H2O} = K*(T_l - T) \qquad (16)$$

where T_l is the liquidus temperature of the solid phase and $K = \dfrac{\Delta H_{fus}}{RT_{fus}^2}$. Equation (16) is the equivalent of equation (12), and shows a linear dependence between ΔT and water content of the liquid. The binary diagram calculated from equation (16) also leads to a strongly curved relationship between extent of melting and temperature, as illustrated in Figure 33b. The exact position of the binary T vs. F curve varies with source concentration. In Figure 33b, the source composition has 5% of the minor component. As a rule of thumb, when the extent of melting is two to three times the percentage of the minor component in the source, the melting curve shows a relatively low and flat dT/dF, similar to the MM3 results. From this perspective, the MM3 data

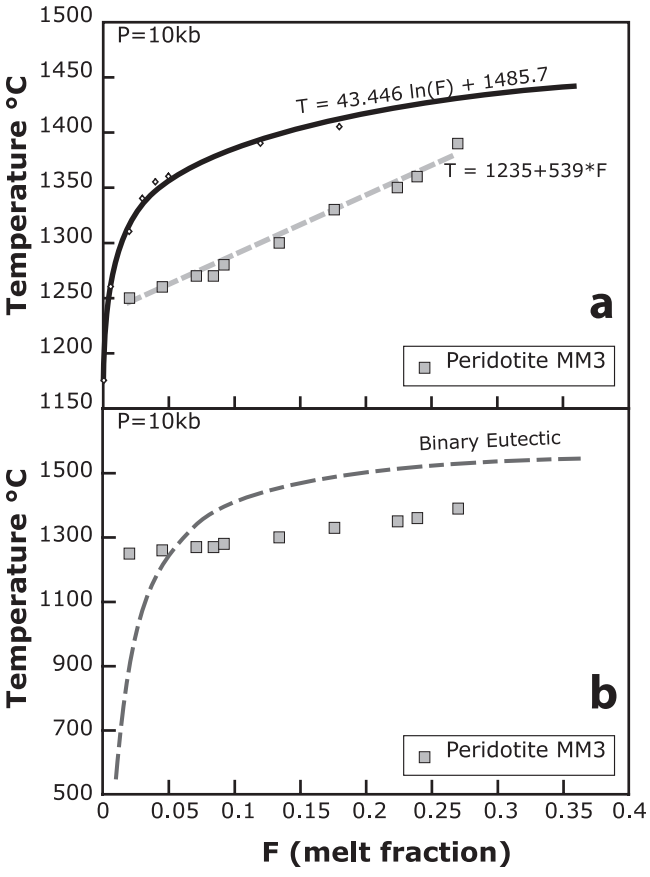

Figure 33. Temperature vs. experimentally determined melt fraction (F) for peridotite composition MM3 [*Baker and Stolper*, 1994; *Baker et al.*, 1995; *Hirschmann et al.*, 1998] compared to the T vs. F parameterizations of the MELTS program (a) and the binary eutectic example (b) given by *Hirschmann et al.* [1999]. The MELTS calculation was that performed by *Hirschmann et al.* [1999] for the same MM3 composition. The binary eutectic calculation is for an incompatible element source fraction of 0.05. Both the binary eutectic and MELTS give logarithmic dependence of melt fraction on temperature, in contrast to the experimentally determined dependence, which is almost linear. These differences have large consequences for calculations of hydrous melting, as discussed in the text. Equations on the curves are those used for hydrous melt modeling to compare MM3 and MELTS results.

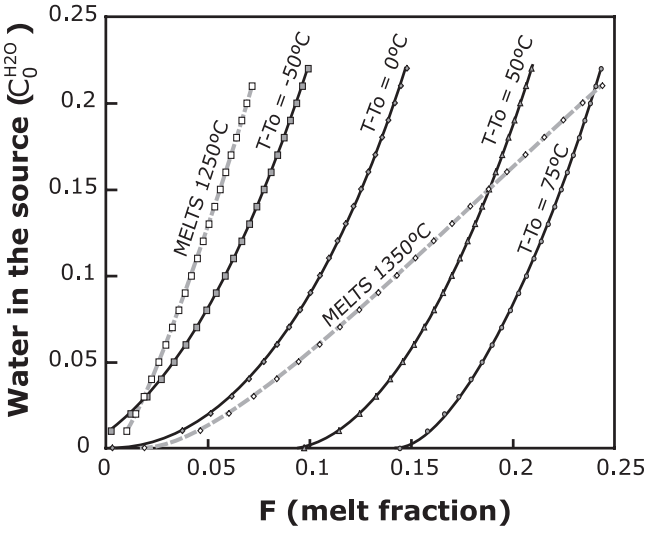

Figure 34. Calculations of water in the source vs. melt fraction determined with the methods described in this paper, compared with the same method using the MELTS T vs. F relationship shown in Figure 33. The curves labeled "MELTS" are calculated using our method of hydrous melting calculation and the T vs. F equation based on calculations reported by *Hirschmann et al.* [1999] shown in Figure 33. Note the calculations using the MELTS T vs. F relationship show a more linear dependence of F on source water content, a marked decrease in slope with increasing temperature, and low intercepts of the melt fraction axis. These characteristics are shared with the MELTS results shown in Figure 4 and show that the primary difference between the MELTS results and our parameterization results from the differences in the T-F dependence shown in Figure 33.

could be interpreted as reflecting very small amounts of low-melting-temperature minor components, less than 1% in the source. This is not far off for mantle compositions, where the sum of Na_2O and K_2O is less than 1%. Thus for extents of melting less than 1%, it is possible that mantle melting has a high dT/dF tail, as we discussed above. And of course, the addition of water to the system creates a strongly curved T vs. F relationship for hydrous melting, a general result on which all models agree. Only for the dry systems is there a discrepancy.

In the general case, the functional characteristics of the binary system differ significantly from those observed in the natural system. In the natural system, anhydrous F increases with increasing temperature, whereas the binary system has zero intercepts on F vs. C_0^{H2O} independent of temperature. The natural system has an approximately linear relationship between $T - T_0$ and F, at least down to 2% melt fraction, while in the general case the binary system has an exponential relationship. The natural system has logarithmic relationship between ΔT and water content, while the binary system has a linear relationship. These differences justify caution about conclusions for the mantle inferred from the binary.

While the MELTS program is multicomponent and far more complicated than a simple binary, the T vs. F relationship has similar characteristics to the simple binary. Figure 33a shows T vs. F for MELTS for the same dry MM3 composition [*Hirschmann et al.*, 1999] for which experimental data exist. The MELTS relationship shows the same strong curvature as the general case for the binary system, which does not correspond with the dry observations.

Figure 34 takes the F vs. ΔT relationship from Figure 6 of *Hirschman et al.* [1999] (see equation in Figure 33a) and our water parameterization (equation 12) to show the importance of the functional relationship to the C_0^{H2O} vs. T systematics. Adopting the logarithmic relationship from MELTS and applying it to our method of calculation of hydrous melting leads to a linear relationship between F and C_0^{H2O} and a significant change of slope with temperature (see Figure 34). Therefore the fundamental difference between our results and those of MELTS is not the complex thermodynamic engine of the MELTS program, but simply the difference in the ΔT vs. F relationship. Our calibration is based on experimental data from the natural systems and corresponds with that. The MELTS calculation produces a ΔT vs. F relationship that is not in accord with the data.

The robustness of the general characteristics of our calculations can also be understood from a consideration of mantle melting and the behavior of water as an incompatible element. As the temperature increases above the solidus, the extent of melting increases. Therefore at some T greater than T_o, F will be 20% rather than 0%. Now consider the addition of 0.05% water to the source at the two different temperatures. Near the solidus where dry F ~ 0, liquids will start with 5% water($C_0/D = 0.05/0.01$). For the hotter mantle, with dry F ~ 20%, all this water is diluted by the existing melt, and the liquid contains only 0.25% water, 20 times less. For the dF / dC_0^{H2O} slope to be greater at the higher temperature, 0.25% water would have to cause a greater melting increment than 5% water. This is nonsensical. Instead, dF / dC_0^{H2O} must be greater at the lower temperature than at the higher temperature. For higher C_0^{H2O}, the extent of melting is greater for all temperatures, and therefore the difference between temperatures becomes progressively less. Therefore, for low source water contents, and small extents of melting, there must be high dF / dC_0^{H2O} for lower temperatures, and lower dF / dC_0^{H2O} for higher temperatures, as observed in our calculations. As F increases, either due to increased temperature or increased water contents, the slopes become similar. The change in dF / dC_0^{H2O} slope with temperature observed in simple systems results largely from the common zero intercept for all dF / dC_0^{H2O} slopes. As long as F goes

to 0 as C_0^{H2O} goes to 0, slope variations are possible. That is the not the case for mantle peridotite, where the F-intercept depends on the temperature.

These considerations suggest that comparison with a simple system where F increases with T in the absence of water (not the case for the binary system discussed above) might be more analogous to the melting behavior of the mantle. This is possible with the simple ternary diagram used by *Hirschman et al.* [1999] (their Figures 3 and 5). The advantage of this diagram is that it combines an incompatible element with a phase with solid solution, and therefore T increases with all extents of melting in the dry system. A plot of C_0^{H2O} vs. F at various temperatures is shown in Figure 36. These curves show the same characteristics as our calculations and the reasoning discussed in the previous paragraph. There is no change in dF / dC_0^{H2O} with temperature.

These conclusions appear to disagree with the experimental data of *Hirose and Kawamoto* [1995] as presented in *Grove and Gaetani* [2003] and reproduced here as Figure 37. These data appear to show that addition of water at high temperatures causes a significantly greater increase in the extent of melting than water added at lower temperatures.

Figure 37 does not indicate the errors in the estimation of the extent of melting from the experiments. Hirose and coworkers [*Hirose and Kushiro*, 1993; *Hirose and Kawamoto*, 1995] used the Na_2O contents of the glasses to estimate F, assuming that Na_2O is perfectly incompatible. Their reported errors for Na_2O, however, are very large. The high degree of melting of the water-rich 1350°C experiment, for example, is calculated from a Na_2O content of 0.79, which has a reported 2σ uncertainty of $\pm$0.4. Including these errors gives an extent of melting for this experiment between 25% and 75%. Aluminum is measured much more accurately than Na_2O, and using aluminum with a D = 0 gives a maximum extent of melting of 33%. Thus the high extent of melting reported for this experiment is not correct.

As an indication of the uncertainties in determination of F for these experiments, we have recalculated F, using TiO_2 and Al_2O_3 to estimate the extents of melting for both hydrous [*Hirose and Kawamoto*, 1995] and anhydrous [*Hirose and Kushiro*, 1993] experiments on the KLB-1 composition. TiO_2 is measured more precisely than Na_2O. Results are shown in Figure 38 along with our calculated model curves. The data appear to be curved, and are broadly consistent with our calculations. We conclude that extents of melting determined from the imprecise Na_2O contents have very high uncertainties. The apparent change in slope with temperature is based largely on a single highest melt fraction point at 1350°C (see Figure 37), which violates mass balance for other elements. Therefore while the uncertainties are large, there is no inconsistency between extents of melting from these experiments and our results.

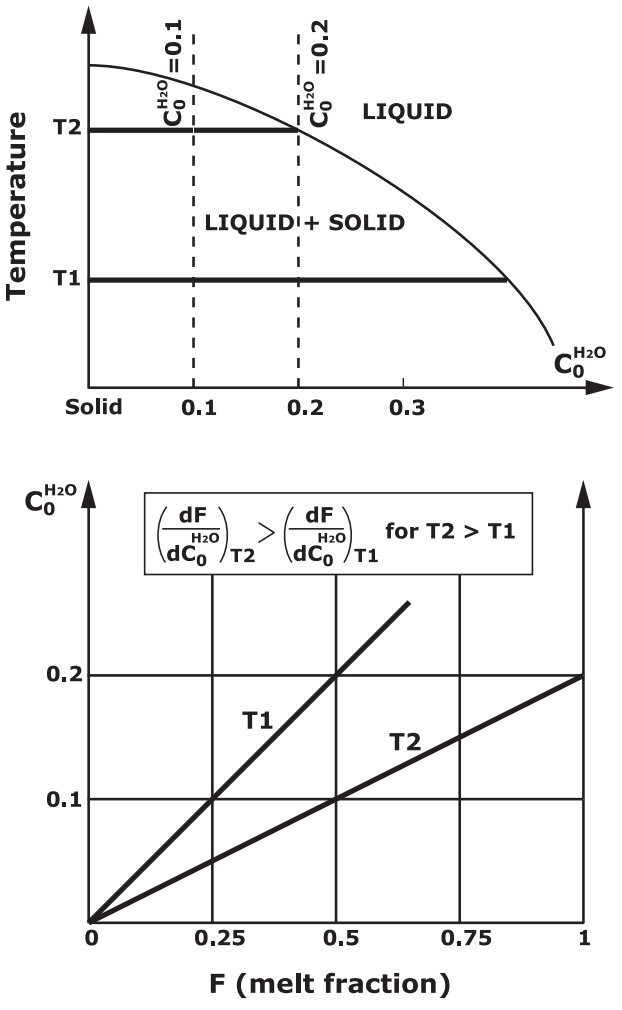

Figure 35. Illustration of calculation of extent of melting (F) vs. source water content from a binary eutectic diagram, as discussed in the text, based on parameters used by *Hirschmann et al.* [1999]. In contrast to mantle melting, this simple system has 0% melting for two very different temperatures, such as T1 and T2 for dry systems. This leads to slopes on the bottom panel that intersect the origin. The change in slope from T1 to T2 results because there is 0% melting for the anhydrous system independent of temperature. In contrast, mantle melting at temperatures above the mantle solidus shows significant variation of melt fraction with temperature, which leads to very different systematics, as discussed in the text. Compare Figure 36.

We conclude that dF / dC_0^{H2O} does not, and cannot, show a strong dependence for mantle compositions on temperatures that are above the solidus, which is the case for all back-arc basins.

With these arguments we do not intend to imply that MELTS is not useful for certain types of calculations, or could not be modified or "tuned" to be more consistent with

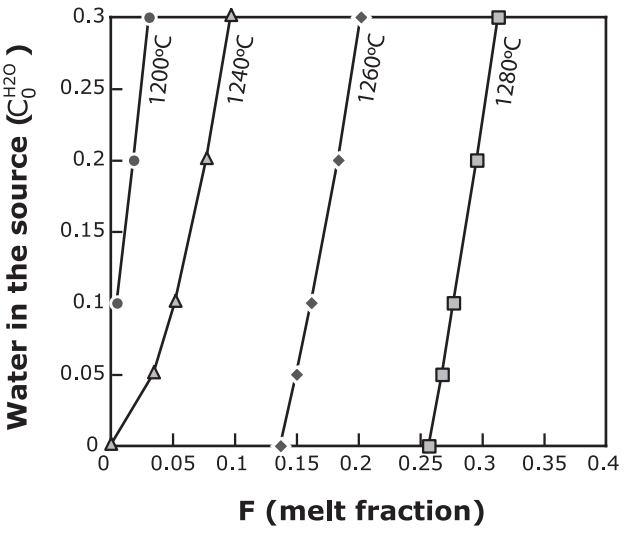

Figure 36. A second simple system illustration using the idealized ternary system presented by *Hirschmann et al.* [1999]. In this case the anhydrous system is a solid solution which has variations in melt fraction with temperature even at 0% water content. Note that for this system there is no significant change of dF / dC_0^{H2O} with increasing temperature. These simple system curves share the characteristics of the hydrous calculations reported in this paper, and contrast with the MELTS results shown in Figures 4 and 34.

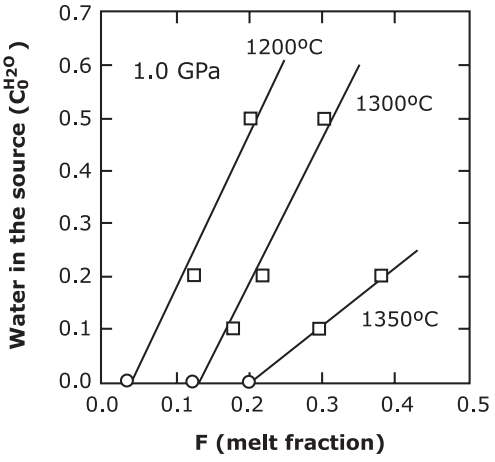

Figure 37. A reproduction of the figure from *Gaetani and Grove* [2003], showing data reported by *Hirose and Kawamoto* [1995], that purports to show the increased productivity of water-induced melting at high temperatures. Melt fractions reported by *Hirose and Kawamoto* [1995] were estimated on the basis of Na contents in the experimental liquids. Compare to Figure 38.

the experimental results. Examination of Figure 33 shows that for extents of melting higher than about 5%, the T vs. F relations for MELTS have a similar slope to the experiments, offset by about 100°C. If the low temperature portions of the T vs. F curve are ignored, and a further adjustment is made for temperature discrepancies with the natural system, then results akin to those we present can be tuned from the later MELTS parameterizations [*Smith and Asimow*, 2006; Asimow, personal communication], without the strong temperature dependence of dF / dC_0^{H2O}. The earlier conclusions of a strong temperature dependence of dF / dC_0^{H2O}, however, do not appear to be consistent with modeling that is more closely tied to the experimental constraints.

8. WATER AND MELTING IN BACK-ARC SPREADING SYSTEMS

We now can compare the data with the calculations to test hypotheses for the origin of the distinctive back-arc basin systematics. The data that need to be accounted for are the first-order differences in major elements among the various back-arc basins, the overall increase of extent of melting with water contents, the low-Fe and -Ti contents of the water-rich melts, the linear correlations among the various parameters, and the large range of Fe observed.

8.1. Mantle Temperature Variations in Back-Arc Basins

The low-water (high-Fe) data from the various back-arc basins lie close to the array of data from open ocean ridges, which are quantitatively accounted for by fractional melting of a range of mantle temperatures [*Langmuir et al.*, 1992]. Dry fractional melting is necessary to account for the generally high $Fe_{8.0}$ that is observed. Complicating this picture for the back-arcs is the evidence for mantle depletion in the Lau and Manus Basins, as seen in TiO_2 and Nb, and Na addition by the water-rich component. The net result is that the Lau and Manus Basins have less Na in their sources than do the Mariana and Scotia basins. This lessens the temperature difference required to account for the dry end members, as compared with a constant source model. In detail, a constant Na content of the source would require a 150°C difference in mantle temperature to account for the large $Na_{8.0}$ differences among the basins. But taking into account the depleted Na_2O in the Lau source, the range of $Na_{8.0}$ can be accommodated by a 100°C difference, ranging from a mantle potential temperature of 1350°C for the Marianas data to 1450°C for Lau. Parameters for the melting calculations are presented in Table 5. Thus, despite the important source variations, we confirm the earlier conclusions [*Klein and Langmuir*, 1987] that there are first-order temperature differences among back-arc basins. *Kelley et al.* [in press] concur with this conclusion, and *Wiens et al.* [2006] show correspondence between these temperature variations and the seismic structure of the Lau, Scotia, and Mariana basins.

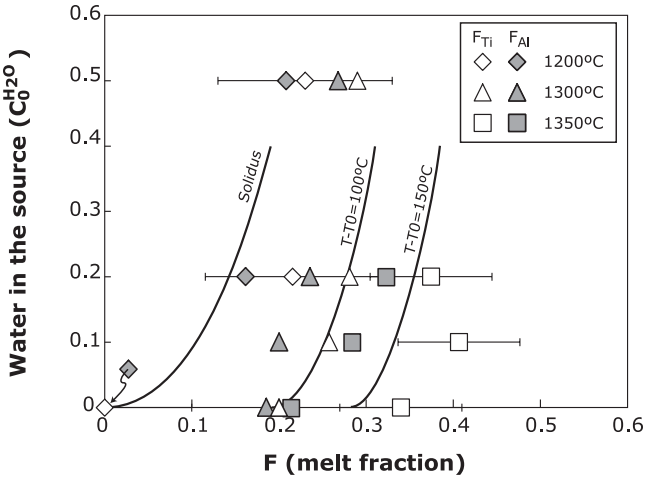

Figure 38. The same data as Figure 37, with F calculated from Ti and Al contents rather than Na contents, using equation (2) in the text and a D for TiO_2 of 0.06 and 0.04 for Al. A higher D for Al would lead to slightly lower values of F. Error bars on F for Ti are those that result from the 2σ errors reported by *Hirose and Kawamoto* [1995]. Anhydrous data for extent of melting [*Hirose and Kushiro*, 1993] were also recalculated using Ti and Al by the same method as the hydrous data. In principle, Ti, Na, and Al all should lead to consistent results for F. Na data (see Figure 37) at the low levels of the experiments are subject to the largest errors. Clearly, large errors are associated with the experimental results, and no definitive increase of hydrous productivity with temperature is evident. The data are approximately consistent with the hydrous calculations reported here, indicated by the solid curves in the figure.

8.2. Evaluation of isothermal, isobaric addition of water

We are now in a position to test whether the supposition of melting control on the $Ti_{8.0}$ vs. $H_{8.0}$ systematics is correct. Figure 39 presents the Scotia and Mariana back-arc data for three HFSE along with melting curves calculated by using our hydrous melting parameterization. The "normal" source is the N-MORB source of *Salters and Stracke* [2004]. The depleted source has undergone removal of a 1% batch melt, and to the enriched source has been added a low-F melt as discussed above. Addition of water to a mantle at a single temperature leads to curves on plots of the HFSE vs. $H_{8.0}$, not straight lines. No single melting curve corresponds to the back-arc data arrays. The Nb data show that the entire range of sources is necessary to account for the more incompatible elements.

Figure 40 presents model curves and data for the Manus Basin. Again, isothermal melting with various water contents produces curves, not the linear data arrays. In general, only depleted sources at higher temperatures come close the Manus data, while less depleted sources at lower temperatures are in the vicinity of the Mariana and Scotia data (compare Figure 39). This is consistent with the overall inferences of mantle temperature discussed above. However, these calculations produce curves, not straight lines, and none of the curves reproduces the data on the $Ti_{8.0}$ vs. $H_{8.0}$ diagrams.

An even more definitive test comes from the $Fe_{8.0}$ data. $Fe_{8.0}$ varies by very small amounts upon isothermal water-induced melting at constant pressure. This is apparent in our calculations of hydrous melting, and also in the raw experimental data of *Hirose and Kawamoto* [1995]. Figure 41 shows that isothermal melting models with water addition are orthogonal to the negative correlation between $Fe_{8.0}$ and $H_{8.0}$ that is characteristic of data from each of the back-arc basins. For the Mariana data, for example, $Fe_{8.0}$ decreases from 9% to 7% as water increases, while calculations and experiments vary by about 0.5%. The large changes in the data are not consistent with the isobaric isothermal model.

These comparisons suggest that the model of differential melting owing to water addition fails to account for the central observations of the back-arc data. Such a model produces curves, not lines, on $Ti_{8.0}$ vs. $H_{8.0}$ diagrams and fails to account for the systematics of $Fe_{8.0}$ vs. $H_{8.0}$ variations.

This then turns the question to what combination of source contents, extents of melting, and melting processes can give rise to the observations? A successful model for BABB needs to account not only for the negative H_2O vs. HFSE correlations but also for the robust and well-established major element constraints.

A promising means of creating linear trends of diverse slope on $Ti_{8.0}$ vs. $H_{8.0}$ and analogous plots is mixing between two compositions, one water-poor and Fe-rich, and the other water-rich and Fe-poor.

8.3. Major Element Constraints on Hydrous Melting Models for Back-Arc Basins

The critical features of all the back-arc data are the positive correlation between $Ti_{8.0}$ and $Fe_{8.0}$ and negative correlations between these parameters and $H_{8.0}$. The data require that the water-rich component have very low FeO contents. As pointed out originally by *Hanson and Langmuir* [1978], FeO contents of mantle melts are sensitive to the pressure of melting. *Langmuir et al.* [1992] showed that equilibrium melting also leads to substantially lower FeO contents below spreading centers than does fractional melting. Low FeO and TiO_2, therefore, suggest high degrees of equilibrium melting at low pressures.

A simple hypothesis to account for the characteristics of the back-arc data is mixing of melts produced by two processes. The high-Fe, high-Ti end member is produced by fractional melting similar to what occurs on open ocean ridges. The second mixing end member is a low-pressure,

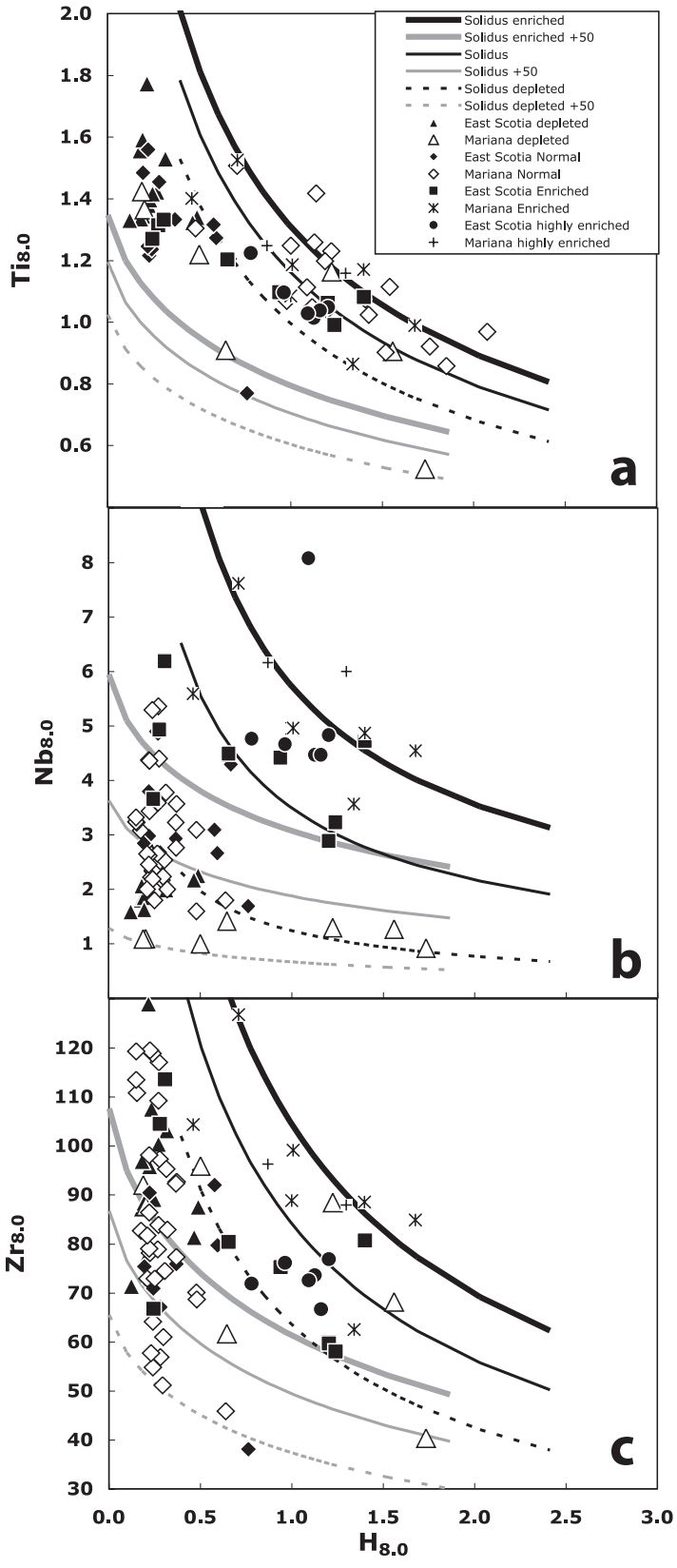

Figure 39. Comparison of the Mariana Trough and East Scotia Basin data with calculations of melting produced by changes of source water content under isobaric, isothermal conditions for the "cooler" back-arc basins. Note that melting under these conditions produces curves, not straight lines, and none of the curves matches the linear data arrays well. All three panels are for elements not carried in the hydrous fluid but influenced by source enrichment and depletion. Thick lines are for enriched sources (at two different mantle temperatures), thin solid lines are for intermediate sources, and dashed lines are for depleted sources. Darker lines are for anhydrous temperatures at the mantle dry solidus. Lighter lines are for a mantle temperature 50°C above that of the dry solidus. While the data are generally encompassed by a range of sources at the cooler mantle temperature, no single curve matches the data. Note that these are isothermal, isobaric calculations, and thus do not correspond to the preferred model presented in this paper.

equilibrium melt that combines low-Ti and -Fe contents with high water.

Accounting for the low $Fe_{8.0}$ quantitatively is problematic. The only way we have been able to produce such low $Fe_{8.0}$ (and low $Ti_{8.0}$, low $Na_{8.0}$) values is through equilibrium melting at pressures less than 12 kb, with concomitant addition of Na and K in the hydrous component. The low pressure of equilibration, the process of equilibrium melting, and the addition of alkalis all cause a lowering of Fe content. In addition, the dry liquids crystallize plagioclase upon differentiation above 8 wt.% MgO, while the wettest liquids do not. This augments the difference in $Fe_{8.0}$. All of these effects are necessary to generate the range of $Fe_{8.0}$ values observed. Mixing between such a melt and the normal melt from a ridge melting regime would then create the back-arc array.

The success of such a model is demonstrated in Figures 42–44. The high-Fe, dry end member is produced by pooled fractional melts as at normal ocean ridges, discussed above. The low-Fe, wet end member is a low-pressure, equilibrium melt of a source that has enhanced Na due to the hydrous addition of that element and a cooler temperature environment due to proximity to the arc. Detailed parameters for these models are presented in Table 5.

Note also that in the $Fe_{8.0}$–$Na_{8.0}$ diagram (Figure 42), the BABB data tend to converge at lower Fe. This results because all trajectories tend towards a low-pressure equilibrium melt composition, with similar Fe contents. The Na contents vary owing to mantle temperature and Na source effects. Mariana and Scotia data arrays tend towards a lower degree, low-pressure equilibrium melt, and Manus and Lau arrays to a higher degree, low-pressure equilibrium melt. All of the data require a low-Fe mixing end member, which we are able to generate only by low-pressure equilibrium melting.

Mixing between these two distinct melts accounts well for the essentially linear characteristics aspects of the BABB data arrays such as, for example, in the $Ti_{8.0}$ vs. $Fe_{8.0}$ diagram (Figure 43b). In addition to the success with the $Na_{8.0}$ vs. $Fe_{8.0}$ and $Ti_{8.0}$ vs. $Fe_{8.0}$ diagrams, the same calculations that account for the end members of the major element data produce appropriate end members on $Ti_{8.0}$ vs. $H_{8.0}$ diagrams to reproduce the negative slopes that are so characteristic of the BABB data and have been so extensively modeled (Figure 44). Note the far better fit to the data from the mixing model in Figure 44 compared with the isothermal water addition model (Figures 39a–40a).

The challenge then becomes how to accommodate this successful chemical model with a physical understanding of back-arc spreading centers, and why back-arc and open ocean spreading centers have such contrasting characteristics.

8.4. Geometric Constraints on the Back-Arc Basin Melting Regime

Melting regimes beneath ocean ridges are considered to be roughly triangular in shape (e.g., *McKenzie and Bickle* [1988]; *Langmuir et al.* [1992]), as a consequence of passive mantle flow driven by spreading. The water effect on open ocean ridges occurs in the deep parts of the melting regime, and the melts that cause the effect must get to the ridge from the deep "wings" of the melting regime (Figure 45), between the hydrous and dry solidi (e.g., see *Plank and Langmuir* [1992]). The entire melting regime occurs in the context of an isobaric mantle solidus owing to the adiabatic gradient

Table 5. Parameters used for the successful melting models discussed in the text.

		Na_2O 0	H_2O 0	TiO_2 0	K_2O 0	$Fe_{8.0}$	$Na_{8.0}$	$Ti_{8.0}$	$H_{8.0}$	F
1350ºC	Polybaric fractional melting	0.28	0.02	0.14	0.02	8.8	3.1	1.41	0.3	0.065
1300ºC	Wet equilibrium melting, 10 kb	0.32	0.2	0.14	0.06	6.8	2.31	0.85	1.83	0.12
1450ºC	Polybaric fractional melting	0.24	0.01	0.11	0.015	10.8	2.16	1.07	0.1	0.105
1400ºC	Wet equilibrium melting, 10 kb	0.27	0.2	0.11	0.07	7.5	1.65	0.56	1.08	0.187

Hot (southern Lau, Manus) back-arc basins are modeled with mantle potential temperature of 1450ºC and pooled fractional melting for the dry back side of the melting regime, and with potential temperature of 1400ºC for equilibrium melting at 10 kb for the hydrous arc side. Cool back-arc basins (Marianas, Scotia) are calculated for mantle potential temperature of 1350°C pooled fractional melting for the back side, and 1300ºC equilibrium melting at 10 kb for the hydrous arc side. A 20°C-higher solidus is used for the high-temperature back-arc basins because of their lower Na_2O, TiO_2, and K_2O contents. Equilibrium melting potential temperatures lead to actual final temperatures of melting as 1241°C and 1300°C at 10 kb for the 1300°C and 1400°C potential temperatures, respectively. Melt compositions are calculated by the method of *Langmuir et al.* [1992], using Kd equations for Fe and Mg calibrated for water content and the source compositions given in this table.

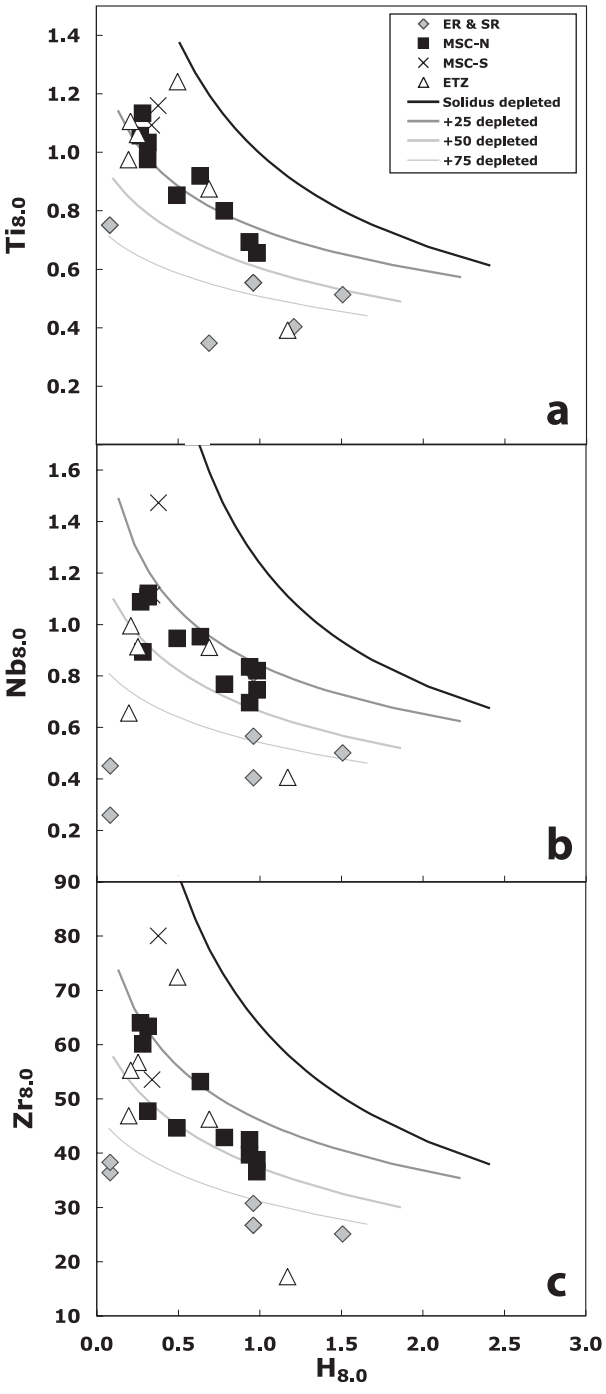

Figure 40. Analogous figure to Figure 39, for the Manus Basin data (published Lau data are not sufficiently complete). Only depleted source calculations are shown, for a range of mantle temperatures. The cooler temperature curve (solidus-depleted) does not intersect the data. A depleted source with temperatures some 50°C above the solidus intersects the data but does not reproduce it in detail. The spreading center data for $Zr_{8.0}$ and $Ti_{8.0}$, which have little source variations, are linear, not curved.

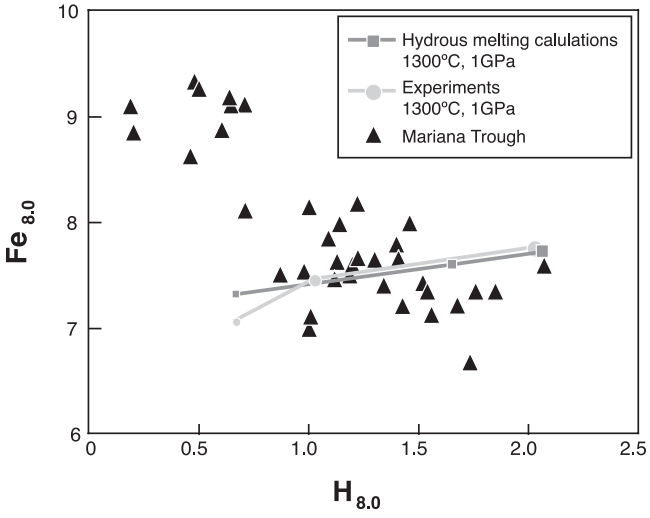

Figure 41. $Fe_{8.0}$ vs. $H_{8.0}$ diagram for the Mariana Trough data. The isobaric, isothermal model and the experiments do not correspond with the data array. Note that our isobaric, isothermal melting calculations produce a result similar to the experimental data. Increased melting at constant temperature and pressure does not lead to significant changes in Fe content, and hence is not in accord with the observations from any of the back-arc basins (see Figure 25). Experimental data from *Hirose and Kawamoto* [1995] at 1 GPa and 1300°C with water contents from different sources are shown (dot size increases with water content).

of the underlying mantle and the passive mantle flow driven by the spreading plates.

Placement of this geometry of melting onto the back-arc setting shows that a very different pattern of mantle flow and melting regime shape must apply in the back-arc environment. Figure 46 presents such melting regimes for the four back-arc basins we are considering. From geometry alone in many cases there is no room for a hydrous melting regime similar to ocean ridges. In addition, the mantle flow and thermal structure contrast markedly between the open ocean and back-arc setting. In back-arc basins, the thermal environment is not adiabatic owing to the inverted thermal structure imposed by the subducting slab. A symmetric open-ocean melting regime also has vertical flow of mantle beneath the spreading center. Subduction imposes strong lateral shallow mantle flow towards the slab and downward flow adjacent to the slab.

Because the "wings" of the melting regime are the deep and distal portions, clearly these regions are generally not available as sources of low-F melts for back-arc spreading centers. The wing on the subduction side is influenced by the slab and the inverted thermal gradient above the slab, and occurs in a region of downward mantle flow. The wing far from the subduction zone is in a water-poor environment.

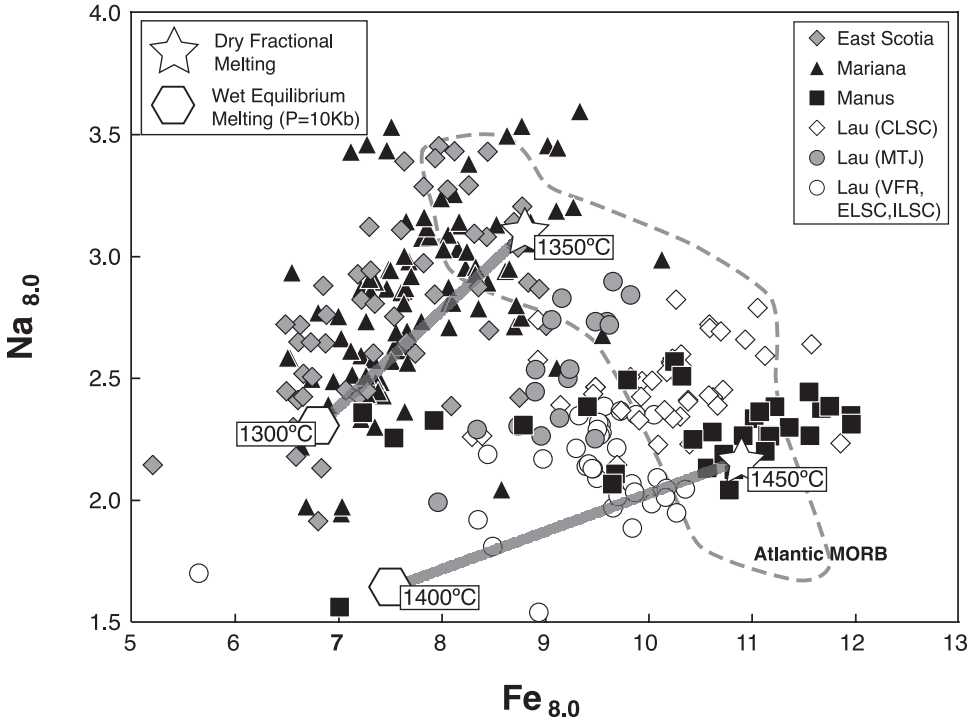

Figure 42. $Na_{8.0}$ vs. $Fe_{8.0}$ diagram, showing the individual data from the various back-arc basins, the MORB field for open ocean ridges [*Langmuir et al.*, 1992], and model calculations that are able to successfully reproduce the Ti, Fe, Na, K, and H data for back-arc basins. Parameters for the models are presented in Table 5. The pooled, average melt compositions for a fractional melting regime at two different mantle potential temperatures are shown by the large open stars. These compositions plot within the open ocean MORB field. The hexagons are hydrous equilibrium melts calculated at the temperature at 1 GPa but at 50ºC cooler potential temperatures. The 1450°C and 1400ºC calculations were carried out for more depleted sources, with source Na_2O and TiO_2 contents of 0.24 and 0.11 wt.%, respectively, for the anhydrous melts, and 0.27 and 0.11 wt.%, respectively, for the hydrous melts. The 1350°C and 1300ºC calculations used more fertile sources with respective Na_2O and TiO_2 contents of 0.28 and 0.14 wt.% for anhydrous melts and 0.32 and 0.14 wt. % for hydrous melts. For the hydrous calculations, 0.2 wt.% water was in the source. Calculations were carried out using the method of *Langmuir et al.* [1992] as modified for hydrous melting by *Asimow and Langmuir* [2003].

Therefore neither wing is likely to contribute to the melts sampled at the spreading center. This provides a simple qualitative rationale for the difference in the effects of water on extent of melting in back-arc basins as compared with that in open ocean ridges. At ocean ridges, low-F melts from the wings of the melting regime add water and a low-F melt component to sampled melts. At back-arcs, geometric and mantle flow constraints preclude such effects. In essence, there are no hydrous wings. *Kelley et al.* [in press] have a parallel but somewhat contrasting discussion of this issue, incorporating their conception of very deep, water-saturated melting beneath back-arcs.

8.5. Possible Models

The major element modeling poses an interesting challenge for understanding the origin of the chemical systematics of back-arc basins. It is easy to imagine a deep source for the water and the subduction component that it carries, but the trace element data show no evidence that this component is deep, and the data for major elements require low-pressure equilibrium melting. Delivering the water from the slab to shallow levels such that equilibrium melting can take place is problematic. These are the constraints that need to be met by successful models, however, whether they are of the genre discussed below or some other more clever idea that we have not considered.

8.5.1. Addition of variable amounts of water to the bottom of the melting regime. Generating a high-degree, low-pressure equilibrium melt is sufficiently problematic that it is worthwhile to consider carefully other models with deep water addition. An appealing scenario, for example, is to envisage a melting regime where water is added from below

to a melting regime with no wings, as drawn in Figure 16 of *Kelley et al.* [in press], and portrayed somewhat differently in Figure 47a. In this case there would no low-F, water-rich melts to be delivered. All the water-rich melts would melt to high extents, the total extent of melting being determined by the particular water content. Water derived from the slab

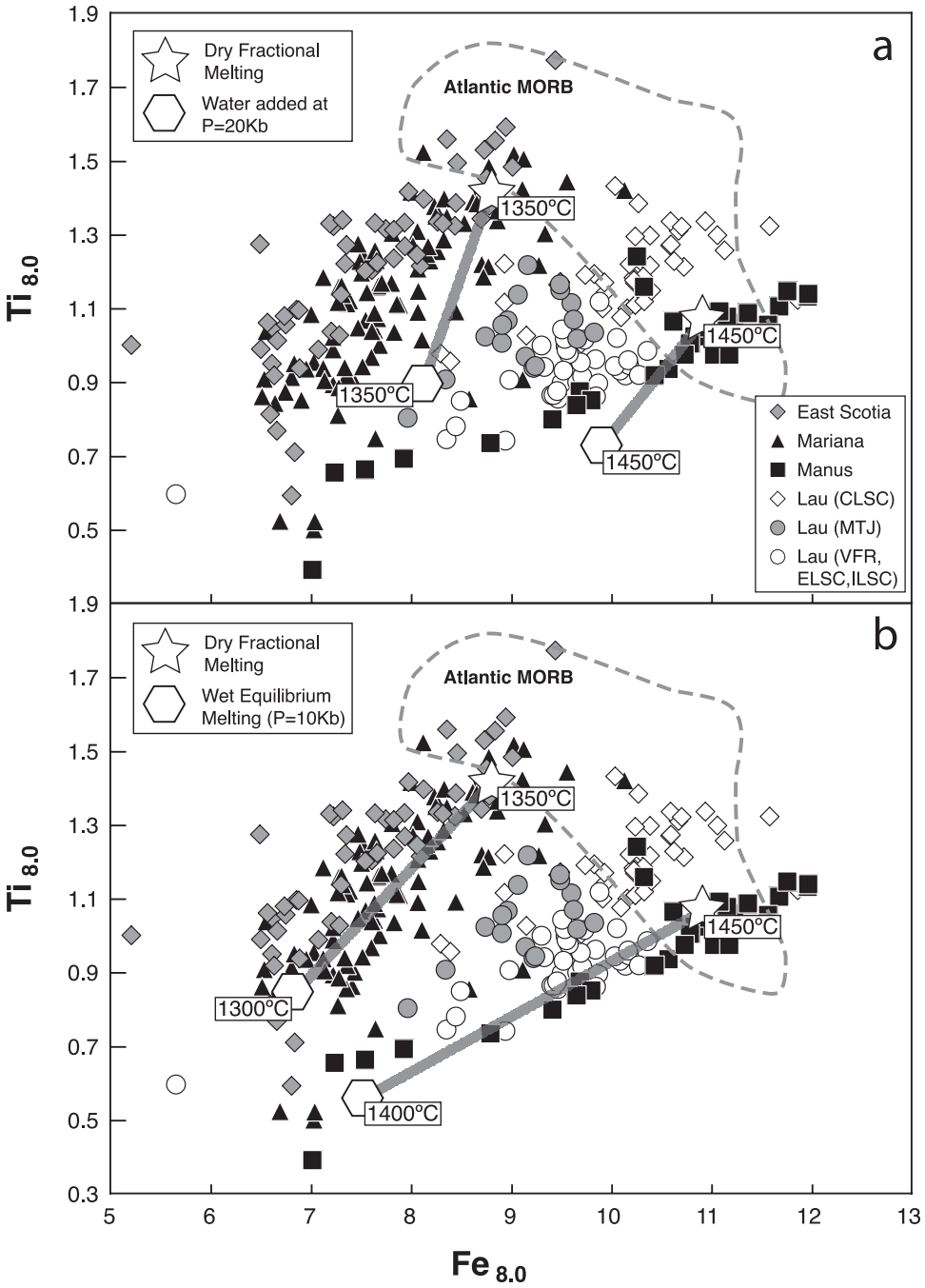

Figure 43. $Ti_{8.0}$ vs. $Fe_{8.0}$ diagram for the same data and models as Figure 42. (a) Diagram for the same model for the fractional melts as Figure 42, but hydrous melts are calculated for 0.2 wt.% water added to the base of the anhydrous melting regime and subsequently decompressed to the surface. This model does not reproduce the observed range in Fe contents, nor does it lead to low enough $Ti_{8.0}$. (b) presents the successful model of mixing of low pressure equilibrium melts with polybaric fractional melts. See discussion in text.

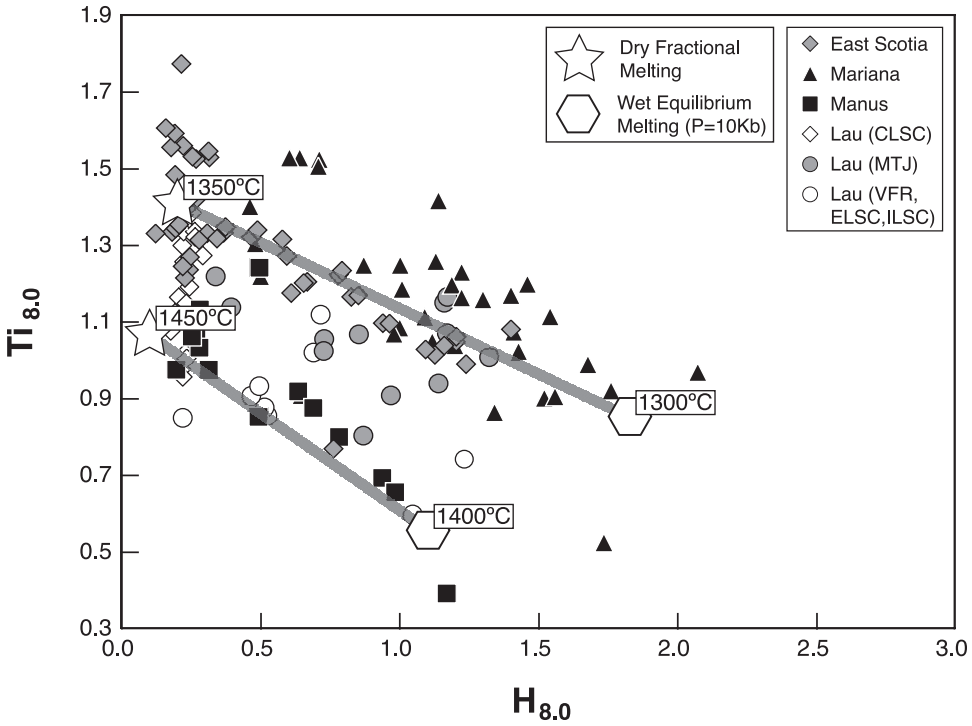

Figure 44. $Ti_{8.0}$ vs. $H_{8.0}$ diagram for the same model as Figures 42 and 43b. This model, which involves mixing between polybaric fractional melts and hydrous melts equilibrated at low pressures, also accounts for the classic negative $Ti_{8.0}$ vs. $H_{8.0}$ trends seen in back-arc basins.

would intersect the melting regime at its base, causing a pulse of melting at depth. We would argue that because of the lack of any garnet signature in BABB, the water cannot migrate from pressures greater than 20 kb to the base of the melting regime, Instead, source and water must move together, unless the extent of melting is immediately large enough to remove any garnet from the residue.

If a water-rich melt with no garnet signature can arrive at the base of the melting regime, then sources with different water contents would undergo polybaric melting on the way to the surface, and end up melting different amounts depending on the initial water contents. This leads to distinct paths of melt composition depending on the amount of water added. For a given water content, each portion of the mantle has the lowest degree of melting and highest water content at the base of the melting regime. Water and TiO_2 decrease progressively upwards as further melting takes place. At the same time, melting paths with higher water contents end up melting more than paths with less water, and hence the integrated melts show an inverse correlation between water and extent of melting, analogous to the BABB observations.

This model, however, does not pass the quantitative tests. At the base of the melting regime, the water vs. TiO_2 systematics of isobaric addition of water would prevail. Then every source will melt further during ascent. Hence if 0.05% water leads to 5% melting and 0.2% water leads to 10% melting, the maximum extent of melting after 20 kb of pressure release at a melting rate of 1%/kb would be 25% and 30% for the respective scenarios. This leads to a small contrast in extent of melting and TiO_2 content. The advantage of the isothermal model is that it can lead to large relative differences in extent of melting with increased water contents. Water addition followed by adiabatic decompression adds a substantial melting increment to both hydrous and anhydrous sources, reducing the relative difference in extent of melting.

This model also does not reproduce the necessary range in Fe contents, as shown in Figure 43a. The $Fe_{8.0}$ content of the hydrous end member is 1–2% too high, because the model does not incorporate the effects of either equilibrium melting or low pressure that are necessary to produce the low $Fe_{8.0}$ that is observed. Figure 43b in comparison shows the successful model of melt mixing proposed above. Thus, given the data and current experimental constraints, this model (Figure 47a) is difficult to reconcile with the observations. That said, this model has considerable common-sense appeal, and much further experimental data on hydrous melting are required. Conceivably, further hydrous melting experiments will modify the Fe constraints.

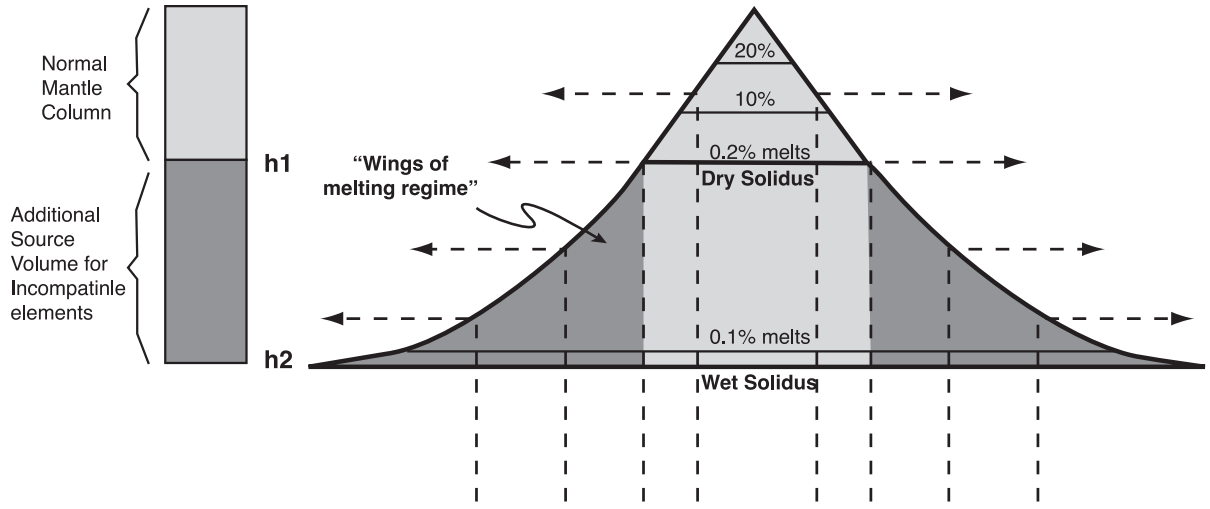

Figure 45. A wet melting regime, as illustrated by *Plank and Langmuir* [1992]. The additional source volume that leads to the effects discussed by *Asimow and Langmuir* [2003] is entirely within the distal "wings" of the melting regime, at greatest depth. As shown in Figure 46, there is no room for distal wings for back-arc spreading centers close to the volcanic front. Deep hydrous melting in the absence of melt contribution from the "wings" prevents in back-arc basins the effects seen in open ocean ridges.

8.5.2. Addition of water to the shallow portions of the melting regime. The second possibility is some mechanism of water transport and delivery in which water is added at shallow levels, less than 50 km, to portions of the melting regime. Addition of water at these levels would lead to enhanced melting over a narrow range of pressure and hence would generate the high-degree, low-pressure melt required by the data. Present-day addition of water is physically problematic, since the mechanism by which water could be added preferentially to shallow parts of the melting regime is not clear. Incorporation of older hydrous lithosphere, however, is an intriguing possibility.

One possible mechanism for introducing water at shallow depths recently might be active upwelling beneath the volcanoes of the volcanic front. While such upwelling does not appear in the normal two-dimensional flow models, pipe-like instabilities might occur in three dimensions, permitting shallow transport of water, and there is evidence for pressure release melting at the volcanic front [*Sisson and Bronto*, 1998]. In addition, work on convergent margin volcanics has also come to the conclusion of shallow (10 kb) equilibration of hydrous melts [*Sisson and Grove*, 1993]. Therefore an extension into the back-arc of a contribution of such low-pressure hydrous magmas is not as far-fetched as it may appear on two-dimensional flow diagrams.

A less problematic possible source of shallow water is the preexisting lithosphere. Lithosphere behind the arc could become progressively modified by arc components, leading to a shallow source that is water-bearing and has a subduction signature. In this case, the water addition would be ancient, not necessarily reflecting current subduction. The change in abundance of this component with distance from the arc could reflect the maturing of the back-arc basin such that lithospheric components become less and less abundant with time and distance. They could show up from time to time as eroded lithosphere became incorporated in the melting regime. The advantage of this conceptual scenario is that water does not need to be delivered from the slab. The water was there prior to back-arc spreading. Back-arc spreading then provides the thermal environment that would lead to shallow melting of this hydrous source, and the nature of the process could lead to erratic spatial distribution of the materials with the subduction signature.

An appeal of this process is the strong subduction component that is observed in the back-arc setting that is not a tectonic spreading center. Off-axis seamounts in the Lau Basin, and the rifts and extensional transform in the Manus Basin, have the strongest arc signature and yet are not underlain by the vertical transport of a ridge melting regime. These lavas are also very wet and low in Fe, suggesting a shallow source. Thus if they represent the lithospheric sources being rifted by the back-arc, then these sources would be wet, shallow, and an available source of hydrous, low-pressure melts that would mix with melts produced in the ridge melting regime.

8.5.3. Shallow level equilibration of hydrous melts. A third possibility is that there is a mechanism of melt transport that permits hydrous melts, or hydrous diapirs, to ascend to shal-

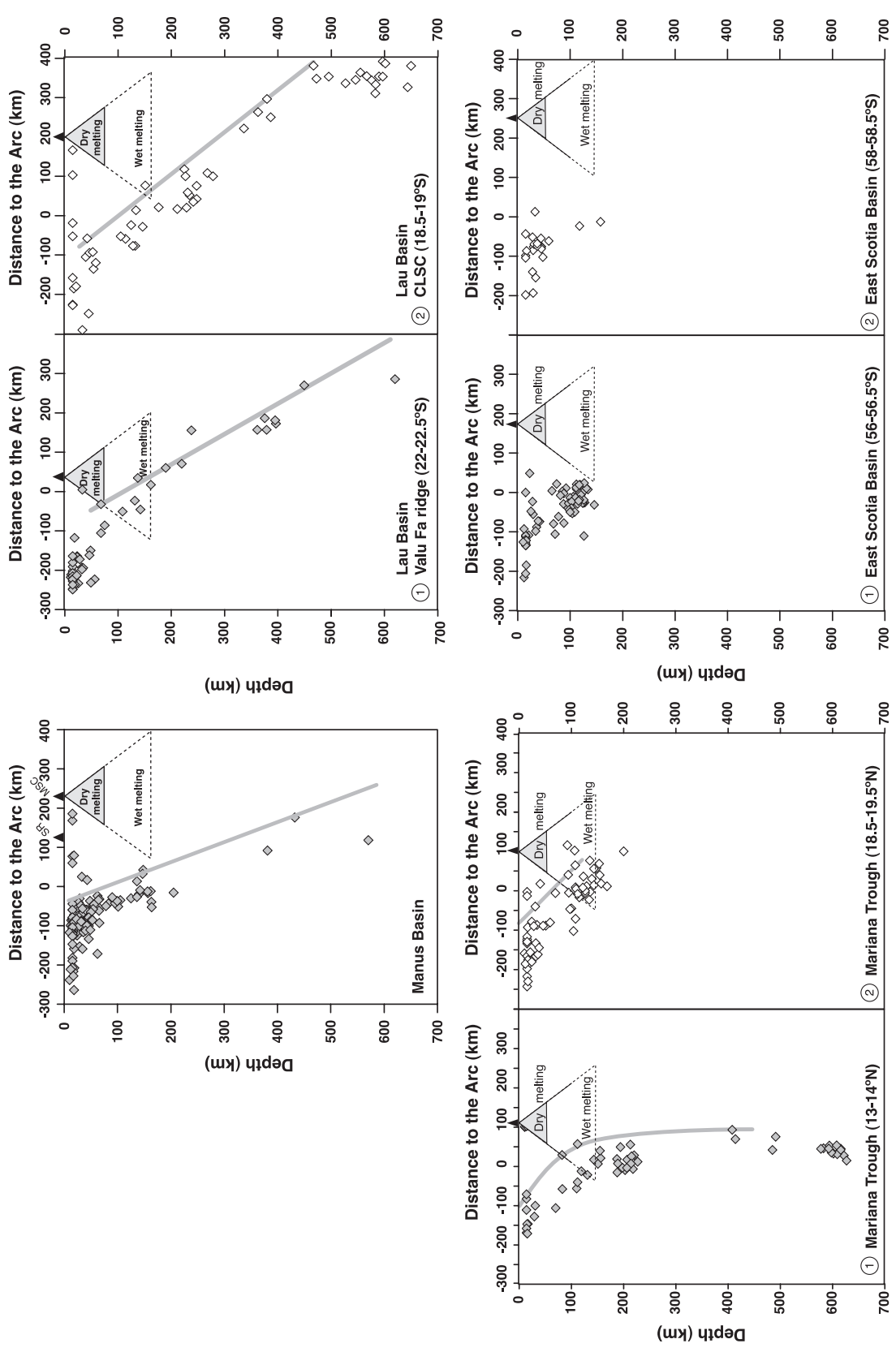

Figure 46. Placement of schematic open ocean melting regimes onto the tectonic environment of the various back-arc basins. Note that open ocean melting regimes are not possible in the back-arc setting. Seismic activity is shown to approximate the location of the slabs. Cross sections for the seismic activity are shown on the maps of Figure 7. Except for the Manus basin, two cross-sections are reported for each back-arc basin, using the seismic data from the Harvard catalogue having an epicenter located within the fields indicated in Figure 7. For each area, the location of the back-arc spreading center is indicated by a triangle. The shape of the dry and wet melting regimes are adjusted according to the mantle temperatures calculated to account for the major element data (Manus Basin and Lau Basin: 1450°C; Mariana Trough and East Scotia Basin: 1350°C). The necessary absence of wings is due not only to the presence of the slab but also to the inverted thermal gradient that extends a considerable distance above the slab.

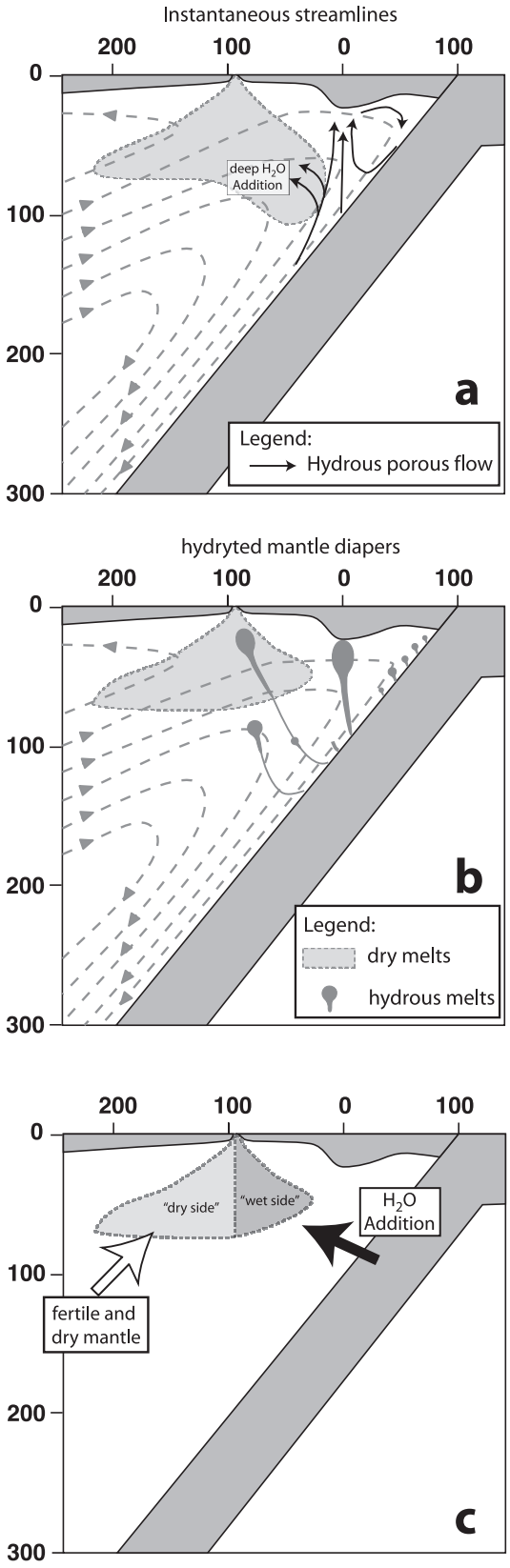

low levels and undergo final equilibration of the melt at shallow depths, akin to what was suggested by *Hall and Kincaid* [2001] for subduction zones (Figure 47b). This would generate the high-water, low-Ti, low-Fe end member. At the same time fractional melts must also be produced from the melting regime to generate the low-water, high-Fe melt. Mixtures of these two would produce the BABB data arrays.

Conceptually, this model could relate to the asymmetry of the back-arc basin melting regime, in contrast to the open ocean melting regime (Figure 47c). In the open ocean, beneath stationary ridges, both halves of the melting regime are equivalent, and sample melts from the "wings." This leads to the effect of lower extents of melting caused by increased water contents of the source. At back-arc basins, the melting regime has an asymmetry caused by both the lateral mantle flow towards the subduction zone and the water flux that is predominantly on the subduction side of the ridge. The back side of the melting regime could give rise to the less hydrous fractional melts. The arc side receives a high water flux associated with rising diapirs (or possibly lateral flow of water), which would produce low-pressure equilibrium melts. The arc side may also be a slightly cooler thermal environment. Melts from these two melting processes then are erupted at the ridge and may mix together, creating the spectrum from high-Ti, high-Fe, low-H_2O melts to low-Ti, low-Fe, high-H_2O melts.

Finally, we note the importance of considering in more detail the mechanisms of melt transport in the back-arc setting. Deep channelized flow might melt out garnet at great depth, permitting transport of water without a garnet signature. If these channels could deliver water-rich melts to shallow levels, where they equilibrate with surrounding

Figure 47. Schematic models for back-arc melting regimes. The overall constraint from the successful models of Figures 42–44 is that mixing of low water, fractional melts with hydrous low-pressure equilibrium melts is able to account for back-arc data. The lack of garnet signature suggests hydrous melts cannot move from depth independently from their solid residue. (a) Model for water rising from depth, leading to deep melting below the pressure of garnet stability. This model does not appear to be consistent with constraints from Dy/Yb for lack of garnet, and the low-Fe contents of hydrous melts, as discussed in the text. (b) Model with deep water that is transported to shallow levels by rising diapirs, following *Hall and Kincaid* [2001] (#23}. The diapirs would need to retain their melt as they ascend and undergo final equilibration at shallow depth. (c) Generic concept of two halves of the back-arc melting regime. The wet side would be the source of the low-pressure equilibrium melts. The dry side would be the source of the low-water, fractional melts. Mixing of melts from the two sides of the melting regime would lead to the mixing arrays that are characteristic of back-arc basin data.

peridotite, that might be another mechanism to create the systematics that are observed.

9. CONCLUSIONS

This work confirms much previous work on back-arc basins and supports previous conclusions of the fundamental role of water in controlling many aspects of the petrogenesis of basalt erupted in such tectonic settings [*Gill*, 1976; *Sinton and Fryer*, 1987; *Stolper and Newman*, 1994; *Taylor and Martinez*, 2003]. Water influences the liquid lines of descent of BABB magmas, causing suppression of plagioclase and contributing to the low-FeO and low-TiO_2 contents of BABB relative to open ocean ridges. When we quantitatively correct for these effects of water, we find that the low-FeO and -TiO_2 of BABB does not disappear. It is not only differentiation that leads to the distinctive BABB chemical characteristics; low-FeO and -TiO_2 are inherited from parental magmas. This is very apparent in the positive correlations of $Fe_{8.0}$ vs. $Na_{8.0}$ and $Fe_{8.0}$ vs. $Ti_{8.0}$ for BABB, pointed out by *Taylor and Martinez* [2003], which persist even after hydrous fractionation correction. The low-$Fe_{8.0}$ and -$Ti_{8.0}$ cause back-arc basin mean compositions to be significantly offset from the global MORB data.

We also confirm the positive correlation between water content and extent of melting first pointed out by *Stolper and Newman* [1994] and see that it is a general phenomenon for back-arc basins, as also noted by *Taylor and Martinez* [2003] and *Kelley et al.* [in press]. As pointed out by *Asimow and Langmuir* [2003] and *Kelley et al.* [in press], this behavior is the opposite of what is observed on open ocean ridges.

Previous models for the melting behavior observed in back-arcs have called on isobaric, isothermal effects of water addition [*Hirschmann et al.*, 1999; *Gaetani and Grove*, 2003] or melting at the water-saturated solidus at great depth beneath back-arc basins [*Kelley et al.*, in press]. We find that neither of these models accounts well for the data. The lack of any garnet influence on the trace elements, supported by the lack of Th excess in the existing U-series data for BABB [*Peate et al.*, 2001], poses challenges for models with melt transported from great depth. Isobaric, isothermal models are inconsistent with the physical realities of melting beneath spreading centers, do not account for the large variations in FeO contents that are observed at every back-arc spreading center, and do not reproduce the linear, negative correlations between H_2O and TiO_2.

In addition, previous models of the effects of water on melting that show a large increase in the effects of water with increased temperature are not consistent with experimental data. We do not find that dF / dC_0^{H2O} is sensitive to temperature and suggest there is a curved relationship between water added and extent of melting. These two results mean that dF / dC_0^{H2O} cannot be used reliably to estimate mantle temperature beneath back-arc basins. Furthermore, reasoning and results from isobaric, isothermal models are unlikely to be pertinent to the polybaric environment that exists at spreading centers.

Source enrichment and depletion play an important role at back-arc basins. The Lau and Manus basin basalts are derived from depleted sources with low-TiO_2 contents compared with contents of the Mariana and Scotia basins. Mariana sees an enriched component that does not correlate with isotopes and must have been recently generated, before the addition of water to the source. Depleted sources are also evident in the Mariana and Scotia basins. Thus there is a complex interplay of sources created by the interaction of back-arc spreading and the subduction process. These sources appear to be generated by the removal and addition of very low degree melts. In the Mariana Basin, "OIB-like" sources have been created very recently, arguing for generation of low-F melts and their associated enriched sources in an active subduction environment [*Donnelly et al.*, 2004].

Na_2O–TiO_2 systematics of back-arc basins suggest that, in addition to the depletion event that causes lowered TiO_2 in some basins, Na_2O has been added along with K_2O by the subduction component. The source differences in Na permit the various basins to be created by mantle temperature differences of about 100°C, significantly less than the 150ºC calculated by *Kelley et al.* [in press] from homogeneous source models. *Wiens et al.* [2006] show that seismic data correlate with inferred temperatures from petrology for the Lau, Fiji, Manus, and East Scotia back-arc basins. The smaller temperature differences we infer are more consistent with the modest crust and axial depth differences observed. The Lau Basin appears to have a temperature gradient within it, since temperatures for the Mangatou triple junction in the north appear to be lower than the temperatures in the south.

In our view a fundamental observation that has not been explained previously is the low-FeO (and generally high-SiO_2) contents of hydrous BABB magmas and the very large range of Fe contents. To account for such differences, models that include fractional melting and pooling of melts at the surface need to be combined with some mechanism that is able to generate hydrous melts equilibrated at low pressures. These hydrous melts were not generated at depth and delivered to the bottom of the melting regime or to the surface—their FeO contents are too low and their trace elements show no evidence of a garnet effect.

Mixing of melts produced by two distinct processes is able to account quantitatively for the back-arc basin systematics. The high-FeO melts can be produced by fractional melting of water-poor sources, analogous to open ocean ridges. The

low-FeO, hydrous melts are generated by equilibrium melting at shallow pressures. Mixing of these two classes of melt produces the characteristic linear arrays of back-arc basin data. We conceive of a generic model for the generation of these two types of melt in a two-sided back-arc melting regime. The arc side generates the hydrous, low-pressure melts. The distal side is water-poor and melts in a manner similar to open ocean ridges. As the ridge gets increasingly distant from the arc, the hydrous influence decreases. A mechanism to produce the hydrous, low-pressure melts could be a modified diapiric model as proposed by *Hall and Kincaid* [2001] for the volcanic front, or possibly channelized flow that is able to deliver hydrous melts from depth to low pressures in dunite channels, where they reequilibrate with peridotite prior to eruption. Another promising possibility is the preexisting arc lithosphere, which could provide a ready-made shallow, hydrous source that could be activated by the incipient back-arc spreading.

The contrast in the effects of water on open ocean ridges and on back-arc basins can be understood from the effects discussed above and from the geometric constraint that the "wings" of the melting regime that contribute low-degree melts beneath open ocean ridges simply cannot exist in the back-arc basin setting. The distal side of the ridge is water-poor, and the arc side is truncated by the inverted thermal gradient of the mantle wedge, and even the subducting plate. Thus the melting regime and methods of water delivery differ fundamentally in the back-arc and open ocean settings.

This paper represents the third review of back-arc basins published recently. *Taylor and Martinez* [2003] summarized back-arc basin data and developed a model of progressive change in wedge composition. *Kelley et al.* [in press] have presented a rather different quantitative interpretation of back-arc data than that presented here. All these papers agree on major conclusions: BABB differ from open ocean MORB in consistent ways; back-arc basins exist over a range of mantle temperatures (as pointed out by *Klein and Langmuir* [1987]); and back-arc basins show striking positive correlations between water contents and extent of melting, as first documented by *Stolper and Newman* [1994]. The contributions of this paper are the reassessment of the effects of water on melting, the emphasis on the constraints from FeO on back-arc melting models, and the suggestion of mixing of melts created under two different melting conditions for the origin of BABB systematics. We also raise the possibility of shallow rather than deep sources of the hydrous component. *Kelley et al.* [in press] emphasize dF / dC_0^{H2O} as a measure of mantle temperature and call on deep melting at the hydrous solidus as an important factor. We argue that dF / dC_0^{H2O} does not change with temperature, and that there is no evidence for deep hydrous melts in the BABB data. This leads to contrasting mantle flow and melting models for the back-arc melting regime. These differences are healthy. We are still at the early stages of understanding the effects of water on mantle melting. Three-dimensional physical models of mantle flow and melt segregation in the back-arc system, a better understanding of lithospheric source contributions during back-arc rifting, and improved experimental constraints will lead to far greater understanding of these problems.

10. APPENDIX: GEOLOGY AND DATA DOCUMENTATION FOR THE FOUR MAJOR BACK-ARC BASINS

10.1. Manus Basin

The Manus Basin is located north of the New Britain island arc in the eastern Bismarck Sea (Figure 7a). The Manus spreading center (MSC) forms the northwestern boundary of the Manus microplate and displays an extreme range of spreading rates, from 92 mm/yr at the southwestern end to near zero at the northern extremity [*Martinez and Taylor*, 1996]. The along-axis depth varies from 2 to 2.6 km, and the morphology of the ridge also changes markedly with the decrease in spreading rate to the north. At its western limit, the MSC is extended by the extensional transform zone (ETZ), a volcanically active zone where oblique spreading occurs. Two rifting areas with localized volcanism are also present within the Manus basin. The Southern Rift (SR), forming the southern boundary of the Manus microplate, consists of a series of grabens (average depth, 2.4 km) with volcanism but no apparent spreading history. The Southeastern Manus Rift (ER), separated from the SR by the Djaul Fault, is a shallow pull-apart basin with a depth of about 2 km. The ER consists of a series of grabens and volcanic ridges that may be precursors of spreading segments [*Martinez and Taylor*, 1996]. The volcanism in this region is somewhat dispersed and not clearly organized into recognizable spreading segments [*Kamenetsky et al.*, 2001]. The initiation of rifting can lead to quite different major and trace element systematics compared with systematics in mature spreading and also to the possibility of interaction with preexisting lithosphere. Since this region has a complex history influenced by multiple subduction zones, changes in the polarity of subduction, and plate reorganization, lithospheric sources are likely to be complex.

Sinton et al. [2003], carrying out a major study of 34 dredges from this region, thoroughly discussed the diverse sources and complex processes that give rise to the large variety of magma compositions observed. They point out that both prior mantle depletion and various types of source enrichment are neces-

sary to account for the data. While the correspondence is not perfect, much of the diversity appears to relate to the distinct tectonic settings of the various volcanic regions.

Application of the screens for MgO and SiO_2 eliminates the fractionated and high- silica magmas that are an important part of the recovered sample suite, but for which estimates of primitive compositions are less reliable. We base our analysis only on the relatively mafic compositions that survive the screens. This eliminates one of the important magma types identified by *Sinton et al.* [2003] as XBABB, for which only very fractionated representatives were recovered.

To present the data from this back-arc basin [*Kamenetsky et al.*, 2001; *Sinton et al.*, 2003], we have divided the samples along the lines presented by *Sinton et al.* [2003], with only slight modifications. *Sinton et al.* [2003] point out that the Manus spreading center can be divided into two distinct provinces, which we call MSC-N and MSC-S. In addition, we define as a separate group the lavas from the ETZ and combine into a single group the samples from the volcanic rifts that are not spreading centers along with the single seamount dredge from the same region.

10.2. Mariana Trough

The Mariana Trough is an active spreading back-arc basin located west of the Mariana arc (Figure 7c). It converges toward the arc at its southern and northern extremities and has a maximum distance from the arc of about 100 km at 18ºN. The spreading rate increases southward from 16 mm/yr at 18.75ºN to 45 mm/yr at 13.5ºN [*Kato et al.*, 2003]. The Mariana Trough consists of 21 segments in addition to the volcano-tectonic zone (VTZ), which can be regrouped into the Southern, Central, and Northern sections (see *Pearce et al.* [2005] for further details). The southernmost and northernmost parts of the ridge are relatively shallow (<3 km) while the central segments reach depths of about 4.5 km.

The Mariana Basin has the largest number of samples and most complete data set of all back-arc basins, numbering several hundred analyses [*Fryer et al.*, 1981; *Fine and Stolper*, 1985; *Hawkins and Melchior*, 1985; *Poreda*, 1985; *Sinton and Fryer*, 1987; *Volpe et al.*, 1987; *Hawkins et al.*, 1990; *Volpe et al.*, 1990; *Alt et al.*, 1993; *Masuda et al.*, 1993; *Stolper and Newman*, 1994; *Gribble et al.*, 1996, 1998; *Ikeda et al.*, 1998; *McPherson et al.*, 2000; *Newman et al.*, 2000; *Yi et al.*, 2000; *Pearce et al.*, 2005]. Early classic work by *Hawkins et al.* [1990] established important aspects of the geochemistry of BABB from the Mariana. *Sinton and Fryer* [1987], using samples from the Mariana, were the first to identify the distinctive major element signature of BABB and noted the importance of water in the their petrogenesis. Recent studies by *Pearce et al.* [2005] and *Gribble et al.* [1996, 1998] provide a coherent set of high-quality data that can be used for a careful evaluation of source and process. Earlier data (e.g., *Volpe et al.* [1987]; *Hawkins et al.* [1990]) are less complete and were obtained by analytical methods that have been superceded by high-quality ICP-MS data, but they also provide useful results. The extensive sample coverage in the basin is well documented by the figures in the recent *Pearce et al.* publication [2005], which also reviews earlier literature and presents an analysis of source variations in trace elements throughout the basin. The Mariana Basin was also the location of the classic study of *Stolper and Newman* [1994] in their initial investigations of the role of water on source and melting in a back-arc basin. The relatively straightforward tectonic setting, the systematic geochemical results, and the extensive data combine to make the Mariana by far the best studied back-arc basin to date.

Except for the segments closer to the arc, the southern section lavas have MORB-like composition—low K_2O content associated with relatively high FeO and TiO_2 contents. The segments closer to the arc present differentiated lavas with MgO < 5%, and high SiO_2 > 55%, and K_2O content increasing with the arc proximity. A similar arc signature is also found in the lavas from the Northern section, especially in the VTZ merging with the arc. The Central section, located farther away from the arc, shows important major element variation, ranging from MORB-like composition to arc-like composition, possibly within a single segment [*Gribble et al.*, 1996, 1998; *Pearce et al.*, 2005].

To present the data, the samples have been divided into separate groups on the basis of the relative enrichment in incompatible elements that are not strongly influenced by the subduction component. Samples with Nb/Zr > 0.06 are classified as "highly enriched", 0.045–0.06 "enriched", 0.03–0.045 "normal", and <0.03 "depleted". As illustrated in Figure 18, the entire range of source compositions reflected in the Nb/Zr ratio is present over very short spatial distances.

10.3. East Scotia Basin

The East Scotia back-arc basin extends from about 55°S to 60°S behind the South Sandwich trench (Figure 7d) [*Livermore*, 2003]. Like the Mariana Trough, the East Scotia spreading axis converges toward the arc at its southern and northern extremities, but the central segments of the ridge are significantly farther from the arc than is the case for the Mariana, attaining a maximum distance from the arc of about 250 km at 59.5ºS. The spreading rate displays little variation, ranging between 60 and 70 mm/yr along the axis [*Taylor and Martinez*, 2003]. The spreading center is divided into nine segments, from E1 in the north to E9 in the south [*Leat et al.*, 2000]. Segments E3 to E8 have the morphology of an axial rift with a rift floor at about 4 km depth while segments E2 and E9

have axial highs rising up to 2.5 km. Segment E1 has depths ranging from 4 to 5.5 km where it joins the trench.

Thanks to the work of *Fretzdorff et al.* [2002] and *Leat et al.* [2000] and the additional analyses of water by *Muenow* [1980] and *Newman* (unpublished data), the data set for the Scotia back-arc basin is also reasonably complete with a large number of recent ICP-MS analyses. The earlier work defined the chemical systematics of the basin and showed the importance of both subduction components and an ocean–island-like component. The segments at the northern and southern ends of the basin show both these signatures. They receive the arc signature because they are closest to the arc volcanic front. Earlier workers also suggest that mantle flow around the edges of the slab provides ancient enriched material from the Bouvet plume in the Atlantic. These features lead to the systematic distribution of chemical compositions seen in Figure 20.

To present the data, the samples have been divided into separate groups on the basis of the Nb/Zr ratio, as described above for the Mariana Basin.

10.4. Lau Basin

The Lau Basin, located behind the Tofua arc, has a substantial number of spreading centers distributed over a basin that extends 600 km in length and some 500 km in maximum width (Figure 7b). In the southern part of the basin, the Eastern Lau spreading center (ELSC) and Valu Fa Ridge (VFR) occupy a single first-order ridge segment, divided into smaller segments by multiple small offsets. The VFR is the southernmost and shallowest (<2 km) spreading center, extended northward by the ELSC, where depths reach as much as 3000 m at the northern extremity. The spreading rate increases northward from 40 to 95 mm/yr along the VFR and the ELSC [*Taylor and Martinez*, 2003]. A complex overlap zone, named the Intermediate Lau spreading center (ILSC), separates the continuous ELSC-VFR from the Central Lau spreading center (CLSC) to the north, which is offset from the ELSC-VFR by some 50 km to the west, farther from the volcanic front of the arc. Spreading rate varies little along the CLSC, with a northward decrease from 92 to 85 mm/yr [*Taylor and Martinez*, 2003].

In the far northern reaches of the Lau Basin are a number of spreading centers, three of which join at the Mangatolu triple junction (MTJ). These ridge segments, some 400 km to the northeast of the ELSC, are not contiguous with the southern Lau spreading centers. Those spreading centers are not only geographically distant but also entirely separate spreading centers with distinct tectonic history; because the data define separate trends, they are best considered separately. In this we differ with the approach of *Kelley et al.*, [in press], who merged the data from the CLSC with those from the MTJ into a single "N. Lau Basin" group.

To present the data [*Hawkins and Melchior*, 1985; *Jambon and Zimmermann*, 1990; *Sunkel*, 1990; *Falloon et al.*, 1992; *Danyushevsky et al.*, 1993; *Pearce et al.*, 1995; *Kamenetsky et al.*, 1997; *Kent et al.*, 2002], we use a geographical separation based on the ridge segmentation as well as an on- and off-axis distinction.

Studies have shown that there are a diversity of source components in the basin, caused not only by the substantial changes in distance of the spreading centers from the volcanic front, but also by the presence of distinct mantle wedge compositions and an apparent influence in the north from the Samoan hot spot [*Volpe et al.*, 1988; *Sunkel*, 1990; *Falloon et al.*, 1992; *Hawkins and Allan*, 1994; *Pearce et al.*, 1995; *Turner and Hawkesworth*, 1997; *Wendt et al.*, 1997; *Ewart et al.*, 1998; *Turner and Hawkesworth*, 1998].

Acknowledgements. This paper benefited from substantive reviews by Terry Plank and Julian Pearce, editing by David Christie, and discussions with Mac Hirschmann, Paul Asimow, Peter Michael, Cyril Aubaud and Katie Kelley. Sally Newman and Ed Stolper graciously provided unpublished water data. This work was supported by the National Science Foundation.

REFERENCES

Alt, J.C., W.C. Shanks, and M.C. Jackson, Cycling of sulfur in subduction zones - The geochemistry of sulfur in the Mariana island arc and back-arc Trough. Earth Planet. Sci. Lett., 119, 477-494, 1993.

Asimow, P.D., J.E. Dixon, and C.H. Langmuir, A hydrous melting and fractionation model for mid-ocean ridge basalts: Application to the Mid-Atlantic Ridge near the Azores. Geochem. Geophys. Geosyst., 5, 2004.

Asimow, P.D., M.M. Hirschmann, and E.M. Stolper, Calculation of peridotite partial melting from thermodynamic models of minerals and melts, IV. Adiabatic decompression and the composition and mean properties of mid-ocean ridge basalts. J. Petrol., 42, 963-998, 2001.

Asimow, P.D,. and C.H. Langmuir, The importance of water to oceanic mantle melting regimes. Nature, 421, 815-820, 2003.

Aubaud, C., E.H. Hauri, and M.M. Hirschmann, Hydrogen partition coefficients between nominally anhydrous minerals and basaltic melts. Geophys. Res. Lett., 31, 2004.

Baker, M.B., M.M. Hirschmann, M.S. Ghiorso, and E.M. Stolper, Compositions of near-solidus peridotite melts from experiments and thermodynamic calculations. Nature, 375, 308-311, 1995.

Baker, M.B., and E.M. Stolper, Determining the composition of high-pressure mantle melts using diamond aggregates. Geochim. Cosmochim. Acta, 58, 2811-2827, 1994.

Bell, D.R., and G.R. Rossman, Water in the earth's mantle; the role of nominally anhydrous minerals. Science, 255, 1391-1397, 1992.

Bezos, A., S. Escrig, and C.H. Langmuir, Empirical calibration of olivine, plagioclase and clinopyroxene mineral-melt partition coefficients in presence of water: an improved fractionation model. In prep.

Bezos, A., and E. Humler, The Fe3+/Sigma Fe ratios of MORB glasses and their implications for mantle melting. Geochim. Cosmochim. Acta, 69, 711-725, 2005.

Burnham, C.W., and N.F. Davis, The role of H_2O in silicate melts: pt.1, P-V-T relatons in the system $NaAlSi_3O_8$-H_2O to 10 kilobars and 1000ºC. American Journal of Science, 270, 54-79, 1971.

Burnham, C.W., and N.F. Davis, Role of H_2O in silicate melts.2. Thermodynamic and phase relations in system $NaAlSi_3O_8$-H_2O to 10

Kilobars, 700ºC to 1100ºC. American Journal Of Science, 274, 902-940, 1974.

Chesley, J., J. Ruiz, K. Righter, L. Ferrari, and A. Gomez-Tuena, Source contamination versus assimilation: an example from the Trans-Mexican Volcanic Arc. Earth Planet. Sci. Lett., 195, 211-221, 2002.

Class, C., D.M. Miller, S. Goldstein, and C. Langmuir, Distinguishing melt and fluid subduction components in Umnak Volcanics, Aleutian Arc. Geochem. Geophys. Geosyst., 1, 2000.

Cushman, B., J. Sinton, G. Ito, and J.E. Dixon, Glass compositions, plume-ridge interaction, and hydrous melting along the Galapagos Spreading Center, 90.5ºW to 98ºW. Geochem. Geophys. Geosyst., 5, 2004.

Danyushevsky, L.V., The effect of small amounts of H_2O crystallisation of mid-ocean ridge and backarc basin magmas. J. Volcanol. Geotherm. Res., 110, 265-280, 2001.

Danyushevsky, L.V., T.J. Falloon, A.V. Sobolev, A.J. Crawford, M. Carroll, and R.C. Price, The H_2O content of basalt glasses from southwest Pacific back-arc basins. Earth Planet. Sci. Lett., 117, 347-362, 1993.

Davidson, J.P., Crustal contamination versus subduction zone enrichment—Examples from the Lesser Antilles and imlications for mantle source compositions of island-arc volcanic-rocks. Geochim. Cosmochim. Acta, 51, 1987.

Davidson, J.P., N.J. McMillan, S. Moorbath, G. Worner, R.S. Harmon, and L. L., The Nevados de Payachata volcanic region (18ºS 69ºW, N Chile). 2. Evidence for widespread crustal involvement in Andean magmatism. Contrib. Mineral. Petrol., 105, 412-432, 1990.

Dixon, J.E., L. Leist, and C.H. Langmuir, Recycled dehydrated lithosphere observed in plume-influenced midocean-ridge basalts. Nature, 420, 385-389, 2002.

Dixon, J.E., E.M. Stolper, and J.R. Holloway, An experimental study of water and carbon dioxide solubilities in mid ocean ridge basaltic liquids.1. Calibration and solubility models. J. Petrol., 36, 1607-1631, 1995.

Donnelly, K.E., S.L. Goldstein, C.H. Langmuir, and M. Spiegelman, Origin of enriched ocean ridge basalts and implications for mantle dynamics. Earth Planet. Sci. Lett., 226, 347-366, 2004.

Elliott, T., T. Plank, A. Zindler, W. White, and B. Bourdon, Element transport from slab to volcanic front at the Mariana arc. J. Geophys. Res., 102, 14991-15019, 1997.

Ewart, A., K.D. Collerson, M. Regelous, J.I. Wendt, and Y. Niu, Geochemical evolution within the Tonga-Kermadec Lau arc back-arc systems: the role of varying mantle wedge composition in space and time. J. Petrol., 39, 331-368, 1998.

Falloon, T.J., A. Malahoff, L.P. Zonenshain, and Y. Bogdanov, Petrology and geochemistry of back-arc basin basalts from Lau Basin spreading ridges at 15, 18, and 19ºS. Mineral. Petrol., 47, 1-35, 1992.

Fine, G., and E. Stolper, Dissolved carbon dioxide in basaltic glasses: concentrations and speciation. Earth Planet. Sci. Lett., 76, 263-278, 1985.

Frenzel, G., R. Muhe, and P. Stoffers, Petrology of the volcanic rocks from the Lau Basin, southwest Pacific. Geol. Jb., 92, 395-479, 1990.

Fretzdorff, S., R.A. Livermore, C.W. Devey, P.T. Leat, and P. Stoffers, Petrogenesis of the back-arc east Scotia Ridge, South Atlantic Ocean. J. Petrol., 43, 1435-1467, 2002.

Fryer, P., J.M. Sinton, and J.A. Philpotts, Basaltic glasses from the Mariana Trough. DSDP Init. Reports, 60, 601-609, 1981.

Gaetani, G.A., and T.L. Grove, The influence of water on melting of mantle peridotite. Contrib. Mineral. Petrol., 131, 323-346, 1998.

Gaetani, G.A., and T.L. Grove, Experimental constraints on melt generation in the mantle wedge. In Inside the Subduction Factory, edited by J.M. Eiler, pp. 107-134, AGU, Washington, D.C., 2003.

Garcia, M.O., N.W.K. Liu, and D.W. Muenow, Volatiles in submarine volcanic rocks from the Mariana Island arc and Trough. Geochim. Cosmochim. Acta, 43, 305-312, 1979.

Gill, J.B., Composition and age of Lau Basin and ridge volcanic-rocks: implications for evolution of an interarc basin and remnant arc. Geol. Soc. Am. Bull., 87, 1384-1395, 1976.

Gill, J.B., Orogenic Andesites and Plate Tectonics, 390 pp. Springer-Verlag, New York, 1981.

Green, D.H., and A.E. Ringwood, The genesis of basaltic magmas. Contrib. Mineral. Petrol., 15, 103-190, 1967.

Gribble, R.F., R.J. Stern, S.H. Bloomer, D. Stuben, T. O'Hearn, and S. Newman, MORB mantle and subduction components interact to generate basalts in the southern Mariana Trough back-arc basin. Geochim. Cosmochim. Acta, 60, 2153-2166, 1996.

Gribble, R.F., R.J. Stern, S. Newman, S.H. Bloomer, and T. O'Hearn, Chemical and isotopic composition of lavas from the Northern Mariana Trough: Implications for magmagenesis in back-arc basins. J. Petrol., 39, 125-154, 1998.

Grove, T.L., S.W. Parman, S.A. Bowring, R.C. Price, and M.B. Baker, The role of an H2O-rich fluid component in the generation of primitive basaltic andesites and andesites from the Mt. Shasta region, N California. Contrib. Mineral. Petrol., 142, 375-396, 2002.

Hall, P.S., and C. Kincaid, Diapiric flow at subduction zones: A recipe for rapid transport. Science, 292, 2472-2475, 2001.

Hanson, G.N., and C.H. Langmuir, Modeling of major elements in mantle-melt systems using trace element approaches. Geochim. Cosmochim. Acta, 42, 725-741, 1978.

Hawkins, J.W., and J.F. Allan, Petrologic evolution of the Lau Basin, sites 834-839. Proc. ODP Sci. Results, 135, 427-470, 1994.

Hawkins, J.W., P.F. Lonsdale, J.D. Macdougall, and A.M. Volpe, Petrology of the axial ridge of the Mariana Trough backarc spreading center. Earth Planet. Sci. Lett., 100, 226-250, 1990.

Hawkins, J.W., and J.T. Melchior, Petrology of Mariana Trough and Lau basin basalts. J. Geophys. Res., 90, 1431-1468, 1985.

Hildreth, W., and S. Moorbath, Crustal contributions to arc magma in the Andes of central Chile. Contrib. Mineral. Petrol., 98, 455-489, 1988.

Hirose, K., and T. Kawamoto, Hydrous partial melting of Iherzolite at 1 Gpa - The effect of H2O on the genesis of basaltic magmas. Earth Planet. Sci. Lett., 133, 463-473, 1995.

Hirose, K., and I. Kushiro, Partial melting of dry peridotites at high pressures: determination of compositions of melts segregated from peridotite using aggregates of diamond. Earth Planet. Sci. Lett., 114, 477-489, 1993.

Hirschmann, M.M., P.D. Asimow, M.S. Ghiorso, and E.M. Stolper, Calculation of peridotite partial melting from thermodynamic models of minerals and melts. III. Controls on isobaric melt production and the effect of water on melt production. J. Petrol., 40, 831-851, 1999.

Hirschmann, M.M., M.B. Baker, and E.M. Stolper, The effect of alkalis on the silica content of mantle-derived melts. Geochim. Cosmochim. Acta, 62, 883-902, 1998.

Hirth, G., and D.L. Kohlstedt, Water in the oceanic upper mantle: Implications for rheology, melt extraction and the evolution of the lithosphere. Earth Planet. Sci. Lett., 144, 93-108, 1996.

Hochstaedter, A.G., J.B. Gill, B. Taylor, O. Ishizuka, M. Yuasa, and S. Morita, Across-arc geochemical trends in the Izu-Bonin arc: Constraints on source composition and mantle melting. J. Geophys. Res., 105, 495-512, 2000.

Hofmann, A.W., and W.M. White, Mantle plumes from ancient oceanic crust. Earth Planet. Sci. Lett., 57, 421-436, 1982.

Ikeda, Y., K. Nagao, R.J. Stern, M. Yuasa, and S. Newman, Noble gases in pillow basalt glasses from the northern Mariana Trough back-arc basin. Island Arc, 7, 471-478, 1998.

Jambon, A., and J.L. Zimmermann, Water in oceanic basalts—Evidence for dehydration of recycled crust. Earth Planet. Sci. Lett., 101, 323-331, 1990.

Kamenetsky, V.S., R.A. Binns, J.B. Gemmell, A.J. Crawford, T.P. Mernagh, R. Maas, and D. Steele, Parental basaltic melts and fluids in eastern Manus backarc Basin: implications for hydrothermal mineralisation. Earth Planet. Sci. Lett., 184, 685-702, 2001.

Kamenetsky, V.S., A.J. Crawford, S. Eggins, and R. Muhe, Phenocryst and melt inclusion chemistry of near-axis seamounts, Valu Fa Ridge, Lau Basin: insight into mantle wedge melting and the addition of subduction components. Earth Planet. Sci. Lett., 151, 205-223, 1997.

Kato, T., J. Beavan, T. Matsushima, Y. Kotake, and J. Camacho, Geodetic evidence of back arc spreading in the Mariana Through. Geophys. Res. Lett., 2003.

Katz, R.F., M. Spiegelman, and C.H. Langmuir, A new parameterization of hydrous mantle melting. Geochem. Geophys. Geosyst., 4, 2003.

Kay, R.W., Aleutian magnesian andesites: Melts from subducted Pacific ocean crust. J. Volcanol. Geotherm. Res., 4, 117-132, 1978.

Kelley, K.A., T. Planck, T.L. Grove, E.M. Stolper, S. Newman, and E.H. Hauri, Mantle melting as a function of water content beneath back-arc basins. J. Geophys. Res., in press.

Kent, A.J.R., D.W. Peate, S. Newman, E.M. Stolper, and J.A. Pearce, Chlorine in submarine glasses from the Lau Basin: seawater contamination and constraints on the composition of slab-derived fluids. Earth Planet. Sci. Lett., 202, 361-377, 2002.

Klein, E.M., and C.H. Langmuir, Global correlations of ocean ridge basalt chemistry with axial depth and crustal thickness. J. Geophys. Res., 92, 8089-8115, 1987.

Klein, E., and C.H. Langmuir, Local versus global variations in ocean ridge basalt composition: a reply, J. Geophys. Res., 84, 4241–4252, 1989.

Langmuir, C.H., 2003. A new upper mantle composition and the origin of mantle heterogeneity, EGS-AGU-EUG Joint Assembly, Nice, France.

Langmuir, C.H., E.M. Klein, and T. Planck, Petrological systematics of mid-ocean ridge basalts: Constraints on melt generation beneath ocean ridges. In Mantle Flow and Melt generation at Mid-Ocean Ridges, edited by P.M. J., D.K. Blackman and J.M. Sinton, pp. 183-280, American Geophysical Union, Washington DC, 1992.

Leat, P.T., R.A. Livermore, I.L. Millar, and J.A. Pearce, Magma supply in back-arc spreading centre segment E2, east Scotia Ridge. J. Petrol., 41, 845-866, 2000.

Livermore, R.A., Back-arc spreading and mantle flow in the East Scotia Sea. In Intra-oceanic subduction systems: Tectonics and magmatic processes, edited by R.D. Larter and P.T. Leat, Geol. Soc. London Spec. Publ., 2003.

Martinez, F., and B. Taylor, Backarc spreading, rifting, and microplate rotation between transform faults in the Manus Basin. Mar. Geophys. Res., 18, 203-224, 1996.

Masuda, A., T. Gamo, P. Fryer, T. Ishii, L.E. Johnson, H. Tanaka, U. Tsunogai, S. Matsumoto, and K. Fujioka, The major element chemistry of submarine volcanic rocks from the Southern Mariana Trough and its relation to the topography. Proc. JAMSTEC Symp. Deep. Sea. Res., 182-189, 1993.

McKenzie, D., and M.J. Bickle, The volume and composition of melt generated by extension of the lithosphere. J. Petrol., 29, 625-679, 1988.

McPherson, C.G., D.R. Hilton, D.P. Mattey, and C.W. Sinton, Evidence for an ^{18}O-depleted mantle plume from contrasting $^{18}O/^{16}O$ ratios of back-arc lavas from the Manus Basin and Mariana Trough. Earth Planet. Sci. Lett., 176, 2000.

Michael, P.J., The concentration, behavior and storage of H_2O In the suboceanic upper mantle—Implications for mantle metasomatism. Geochim. Cosmochim. Acta, 52, 555-566, 1988.

Michael, P.J., and R.L. Chase, The influence of primary magma composition, H_2O and pressure on midocean ridge basalt differentiation. Contrib. Mineral. Petrol., 96, 245-263, 1987.

Miller, D.M., S.L. Goldstein, and C.H. Langmuir, Cerium/lead and lead-isotope ratios in arc magmas and the enrichment of lead in the continents. Nature, 368, 514-520, 1994.

Muenow, D.W., N.W.K. Liu, M.O. Garcia, and A.D. Saunders, Volatiles in submarine volcanic-rocks from the spreading axis of the East Scotia sea back-arc basin. Earth Planet. Sci. Lett., 47, 272-278, 1980.

Mysen, B.O., and A.L. Boetcher, Melting of a hydrous mantle: I. Phase relations of a neutral peridotite at high pressures and temperatures with controlled activities of water, cabon dioxde and hydrogen. J. Petrol., 16, 520-548, 1975.

Mysen, B.O., and K. Wheeler, Solubility behavior of water in haploandesitic melts at high pressure and high temperature. American Mineralogist, 85, 1128-1142, 2000.

Newman, S., and J.B. Lowenstern, VolatileCalc: a silicate melt-H_2O-CO_2 solution model written in Visual Basic for excel. Computers and Geosciences, 28, 567-604, 2002.

Newman, S., E. Stolper, and R.J. Stern, H_2O and CO_2 in magmas from the Mariana arc and back-arc system. Geochem. Geophys. Geosyst., 1, 2000.

Niu, Y.L., and R. Batiza, Trace element evidence from seamounts for recycled oceanic crust in the eastern Pacific mantle. Earth Planet. Sci. Lett., 148, 471-483, 1997.

Pearce, J.A., Mantle preconditioning by melt extraction during flow: Theory and petrogenetic implications. J. Petrol., 46, 973-997, 2005.

Pearce, J.A., P.E. Baker, P.K. Harvey, and I.W. Luff, Geochemical evidence for subduction fluxes, mantle melting and fractional crystallization beneath the south Sandwich island arc. J. Petrol., 36, 1073-1109, 1995.

Pearce, J.A., P.T. Leat, P.F. Barker, and I.L. Millar, Geochemical tracing of Pacific-to-Atlantic upper-mantle flow through the Drake passage. Nature, 410, 457-461, 2001.

Pearce, J.A., and I.J. Parkinson, Trace element models for mantle melting: application to volcanic arc petrogenesis. In Magmatic Processes and Plate Tectonics., edited by H.M. Pritchard, T. Alabaster, N.N.W. Harris, and C.R. Neary, pp. 373-403, Geological Society, London, 1993.

Pearce, J.A., R.J. Stern, S.H. Bloomer, and P. Fryer, Geochemical mapping of the Mariana arc-basin system: Implications for the nature and distribution of subduction components. Geochem. Geophys. Geosyst., 6, 2005.

Peate, D.W., T.F. Kokfelt, C.J. Hawkesworth, P.W. Van Calsteren, J.M. Hergt, and J.A. Pearce, U-series isotope data on Lau Basin glasses: The role of subduction-related fluids during melt generation in back-arc basins. J. Petrol., 42, 1449-1470, 2001.

Pickering-Witter, J., and A.D. Johnston, The effect of variable composition on the melting systematics of fertile peridotitic assemblages. Contrib. Mineral. Petrol., 140, 190-211, 2000.

Plank, T., 1993. Mantle melting and crustal recycling at subduction zones, Columbia University, New York.

Plank, T., and C.H. Langmuir, Effects of the melting regime on the composition of the oceanic crust. J. Geophys. Res., 97, 19749-19770, 1992.

Plank, T., M. Spiegelman, C.H. Langmuir, and D.W. Forsyth, The meaning of "mean F": Clarifying the mean extent of melting at ocean ridges. J. Geophys. Res., 100, 15045-15052, 1995.

Poreda, R., ^3He and deuterium in back-arc basalts—Lau Basin and the Mariana Trough. Earth Planet. Sci. Lett., 73, 244-254, 1985.

Salters, V.J.M., and A. Stracke, Composition of the depleted mantle. Geochem. Geophys. Geosyst., 5, 2004.

Schilling, J.G., Azore mantle blob—Rare-Earth evidence. Earth Planet. Sci. Lett., 25, 93-102, 1975.

Schilling, J.G., M.B. Bergeron, and R. Evans, Halogens in the mantle beneath the North-Atlantic. Philos. Trans. R. Soc. Lond. Ser. A: Math. Phys. Sci., 297, 147-178, 1980.

Schilling, J.G., R.H. Kingsley, and J.D. Devine, Galapagos hot spot - spreading center system. 1. Spatial petrological and geochemical variations (83ºW - 101ºW). J. Geophys. Res., 87, 5593-5610, 1982.

Schwab, B.E., and A.D. Johnston, Melting systematics of modally variable, compositionally intermediate peridotites and the effects of mineral fertility. J. Petrol., 42, 1798-1811, 2001.

Simons, K., J. Dixon, J.G. Schilling, R. Kingsley, and R. Poreda, Volatiles in basaltic glasses from the Easter-Salas y Gomez Seamount Chain and Easter Microplate: Implications for geochemical cycling of volatile elements. Geochem. Geophys. Geosyst., 3, 2002.

Sinton, J.M., L.L. Ford, B. Chappell, and M.T. McCulloch, Magma genesis and mantle heterogeneity in the Manus back-arc basin, Papua New Guinea. J. Petrol., 44, 159-195, 2003.

Sinton, J.M., and P. Fryer, Mariana Trough lavas from 18ºN: Implications for the origin of back arc basin basalts. J. Geophys. Res., 92, 12782-12802, 1987.

Sisson, T.W., and S. Bronto, Evidence for pressure-release melting beneath magmatic arcs from basalt at Galunggung, Indonesia. Nature, 391, 883-886, 1998.

Sisson, T.W., and T.L. Grove, Experimental investigations of the role of H_2O in calc-alkaline differentiation and subduction zone magmatism. Contrib. Mineral. Petrol., 113, 143-166, 1993.

Smith, P.M., and P.D. Asimow, Adiabat_1ph: A new public front-end to the MELTS, pMELTS, and pHMELTS models. Geochem. Geophys. Geosyst., 6, 2006.

Stolper, E., The speciation of water in silicate melts. Geochim. Cosmochim. Acta, 46, 2609-2620, 1982.

Stolper, E., and S. Newman, The role of water in the petrogenesis of Mariana Trough magmas. Earth Planet. Sci. Lett., 121, 293-325, 1994.

Su, Y.J., 2002. Mid-ocean ridge basalts trace element systematics: Constraints from database management, ICP-MS analyses, global data compilation, and petrologic modeling, Columbia University, New York.

Sunkel, G., Origin of petrological and geochemical variations of Lau Basin lavas (SW Pacific). Mar. Min., 9, 205-234, 1990.

Taylor, B., and F. Martinez, Back-arc basin basalt systematics. Earth Planet. Sci. Lett., 210, 481-497, 2003.

Turner, S.P., and C.J. Hawkesworth, Constraints on flux rates and mantle dynamics beneath island arcs from Tonga-Kermadec lava geochemistry. Nature, 389, 568-573, 1997.

Turner, S.P., and C.J. Hawkesworth, Using geochemistry to map mantle flow beneath the Lau Basin. Geology, 26, 1019-1022, 1998.

Volpe, A.M., J.D. Macdougall, and J.W. Hawkins, Mariana Trough Basalts (Mtb) - Trace element and Sr-Nd isotopic evidence for mixing between Morb-like and arc-like melts. Earth Planet. Sci. Lett., 82, 241-254, 1987.

Volpe, A.M., J.D. Macdougall, and J.W. Hawkins, Lau Basin basalts (LBB): Trace element and Sr-Nd isotopic evidence for heterogeneity in back-arc basin mantle. Earth Planet. Sci. Lett., 90, 174-186, 1988.

Volpe, A.M., J.D. Macdougall, G.W. Lugmair, J.W. Hawkins, and P. Lonsdale, Fine-scale isotopic variation In Mariana Trough basalts: Evidence for heterogeneity and a recycled component in backarc basin mantle. Earth Planet. Sci. Lett., 100, 251-264, 1990.

Wallace, P.J., Volatiles in subduction zone magmas: concentrations and fluxes based on melt inclusion and volcanic gas data. J. Volcanol. Geotherm. Res., 140, 217-240, 2005.

Weaver, J., and C.H. Langmuir, Calculation of phase equilibrium in mineral-melt systems. Chem. Geol., 16, 1-19, 1990.

Wendt, J.I., M. Regelous, K.D. Collerson, and A. Ewart, Evidence for a contribution from two mantle plumes to island-arc lavas from northern Tonga. Geology, 25, 611-614, 1997.

Wiens, D.A., K.A. Kelley, and T. Plank, Mantle temperature variations beneath back-arc spreading centers inferred from seismology, petrology, and bathymetry. Earth Planet. Sci. Lett., 248, 16-27, 2006.

Wood, D.A., N.G. Marsh, J. Tarney, J.L. Joron, P. Fryer, and M. Treuil, Geochemistry of igneous rocks recovered from a transect across the Mariana Trough, arc, fore-arc, and trench Site-453-461. DSDP Init. Reports, 60, 611-645, 1982.

Woodhead, J., S. Eggins, and J. Gamble, High-field strength and transition element systematics in island-arc and back-arc basin basalts—Evidence for multiphase melt extraction and a depleted mantle wedge. Earth Planet. Sci. Lett., 114, 491-504, 1993.

Woodhead, J.D., S.M. Eggins, and R.W. Johnson, Magma genesis in the New Britain island arc: Further insights into melting and mass transfer processes. J. Petrol., 39, 1641-1668, 1998.

Yi, W., A.N. Halliday, J.C. Alt, D.C. Lee, M. Rehkamper, M.O. Garcia, and Y.J. Su, Cadmium, indium, tin, tellurium, and sulfur in oceanic basalts: Implications for chalcophile element fractionation in the Earth. J. Geophys. Res., 105, 18927-18948, 2000.

Yoder, H.S., and C.E. Tilley, Origin of basaltic magmas: an experimental study of natural and synthetic rock systems. J. Petrol., 3, 342-532, 1962.

A. Bézos, S. Escrig, and C.H. Langmuir, Department of Earth and Planetary Sciences, Harvard University, 20 Oxford Street, Cambridge, Massachusetts 02138, USA. (langmuir@eps.harvard.edu)

S.W. Parman, Department of Earth Sciences, Durham University, Durham DH1 3LE, UK.